MYTorus Compton-thick X-ray Reprocessor Model: The Manual

Tahir Yaqoob & Kendrah D. Murphy

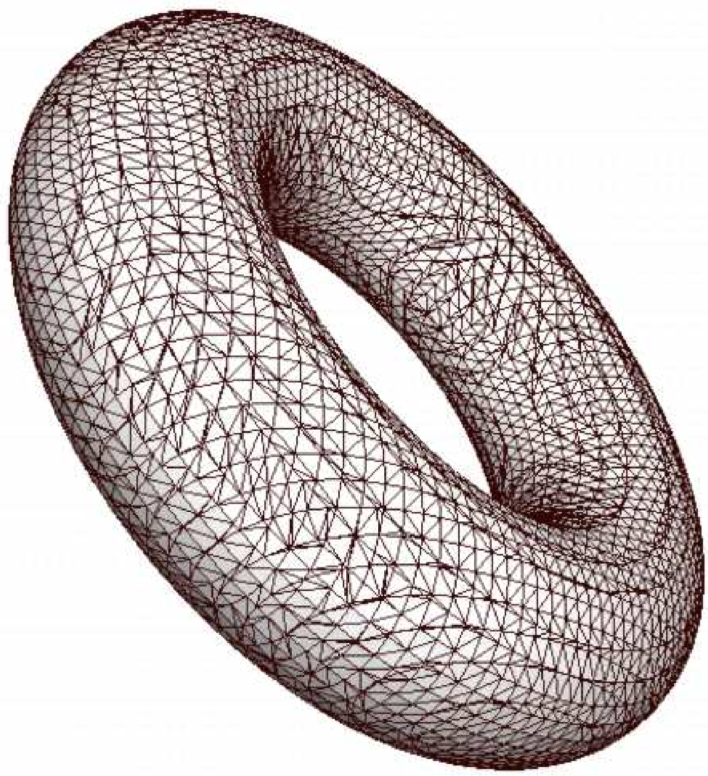

Version 0.0, July 2010
The latest version of this manual can be found at
`http://www.mytorus.com/manual/`

Contents

List of Tables

LIST OF TABLES

List of Figures

LIST OF FIGURES

LIST OF FIGURES

Chapter 1

Introduction

1.1 Modeling absorption and scattering in X-ray spectra: challenges for spectral fitting

Welcome to the manual for MYTORUS, a spectral-fitting suite for modeling X-ray spectra from a toroidal reprocessor that is valid in the Compton-thick regime. The basic model has been described in Murphy & Yaqoob (2009) but the results in this manual have superior accuracy and supersede those in that paper (details will be given as appropriate).

Constructing a model of Compton-thick obscuration and reprocessing that is suitable for spectral fitting to real data is extremely challenging for several reasons. One is that the scattering of X-rays is energy-dependent and geometry-dependent, and the correct treatment of the radiative transfer does not lend itself to fast and accurate calculation "on the fly" as is required for spectral fitting. Model spectra must be pre-calculated using, for example, Monte Carlo techniques, and the calculations are highly cpu-intensive if adequate spectral resolution and statistical accuracy is to be achieved. The calculation time is increased even further when fluorescent emission lines are included in the emerging spectra. Another reason is that the statistical errors on the final model must be sufficiently small (compared to the expected systematic and statistical errors on the data) for a spectral-fitting application. We have performed extensive Monte Carlo simulations and expended much effort to quantitatively assess, analyze, and benchmark our results in order to produce a model that has adequate statistical quality, especially at low energies. In particular, we have found that previous Monte Carlo studies of obscuration in AGN are not available with a statistical accuracy that is high enough for spectral fitting in the most challenging physical regime. That is, along directions in which the *line-of-sight passes through* a column density greater than $\sim 5 \times 10^{24}\ \mathrm{cm}^{-2}$, at energies for which the scattering optical depth is $\sim 10 - 50\%$ of the total optical depth. This regime requires numbers of rays injected into the medium to be two orders of magnitude higher than the "easiest" case, for which the line-of-sight column density to the observer is *zero* (i.e. pure Compton-thick reflection).

Our model has an energy range, statistical quality, and spectral resolution that is suitable for current X-ray data as well as that expected from *NuSTAR* and *Astro-H*. In particular, the spectral detail and resolution for the Fe Kα and Fe Kβ emission lines in our model is good enough for calorimeter data from *Astro-H*. The MYTORUS model is valid for column densities in the range 10^{22}–$10^{25}\ \mathrm{cm}^{-2}$ so it provides *continuous* coverage from the Compton-thin to Compton-thick regimes.

The MYTORUS model was designed specifically for modeling the X-ray spectra of active galaxies with a reprocessor that has a toroidal geometry. The fact that AGN "type classification" is in general related to orientation of the structure in the central engine, along with a large body of additional evidence, supports a geometry that is in some general sense, toroidal. Gaskell *et al.* (2008) argue that there is considerable observational evidence that the broad-line region itself has a toroidal structure, and that there may be no distinct boundary between the broad-line region and the classical parsec-scale torus. Gaskell *et al.* (2008) also argue that there may even be no distinction between the outer accretion disk and the BLR. A toroidal distribution of matter may exist anywhere from the outer accretion disk to parsec-scale distances from the central black hole. Throughout this manual we shall refer to *ANY* toroidal distribution of matter in the central engine as "the torus", regardless of it's actual size or physical location in the central engine. The MYTORUS model is not restricted to any absolute size scale so it can be applied to *any* toroidal distribution of matter that is centrally-illuminated by X-rays.

It may be possible to apply components of the MYTORUS model to sources other than AGN and/or other situations, albeit in restricted ways. Although there should be sufficient information in this manual to adapt the model for a different purpose, detailed discussion of such applications is beyond the scope of this manual.

It is of course possible to use the spectral-fitting model for the purpose of simply making spectral files (for plots, or other purposes), and/or deriving various numerical quantities such as observed to intrinsic luminosity ratios. Even for these applications we urge you to read the entire manual.

In order to apply the MYTORUS model you *must* understand the physics. Otherwise you may misinterpret the results of applying the MYTORUS model, or else you may apply the model incorrectly (both are easy to do). In particular, the MYTORUS model necessarily comes in several "bits and pieces" because that is required by the physics. However, different components of the model need to be set up correctly with respect to each other and making a mistake here could be critical. The model is sufficiently complex, especially when additional model components are included, that you may not even be able to find a valid good fit to your data if you start the model far away from a solution. This manual will take you through a step-by-step process to learn the essentials of using the MYTORUS model. Applying the model will also require changing your approach to the spectral-fitting process itself compared to what you may be used to, and this aspect is also covered in the manual.

1.2 Outline of the manual and how to use it

In order to apply the MYTORUS model you have to invest some time in studying this manual before firing up a spectral-fitting package (such as XSPEC – Arnaud 1996). It is important that you thoroughly understand the model first before attempting any spectral fitting because it is easy to apply the model incorrectly. Also, there are different ways of implementing different components of the model, so more than one option may be available for particular purposes and different implementations will have different characteristics. The suitability of different implementations may vary with the particular application that it would be used for.

This manual is organized as follows. In Chapter 2 we describe some basic concepts with respect to absorption and scattering of X-rays that will be important for fully understanding the MYTORUS model. In Chapter 3 we set up the basic geometry and physics of the MYTORUS model. In Chapter 4 we summarize the essential assumptions that the MYTORUS model is based on so that the regimes of validity of the model can be fully appreciated. In the next three Chapters (5–7) we describe the three principal components of the MYTORUS model in considerable detail (namely the zeroth-order continuum, the scattered continuum, and the fluorescent emission-line spectrum). In Chapter 8 we describe the practical aspects of fitting real data using the MYTORUS model, illustrating the procedures with specific examples. Also discussed are details of how to include model components that are not part of MYTORUS. Finally, in Chapter 9, we briefly discuss some of the effects of covering factor, elements abundances, and geometry, compared to the assumptions made for the MYTORUS model.

1.3 Updates and future enhancements

As will be explained in this manual we expect to further update the capabilities and range of applicability of the MYTORUS model. The latest enhancements to the model and to this manual can be found at

`http://www.mytorus.com`

You may subscribe to an e-mail distribution list in order to keep informed about updates to the model and to this manual, as well as any issues that may arise with the model, by sending a request to `model@mytorus.com`. Note that you are not automatically subscribed even if you received an e-mail notification about the release of MYTORUS – you must explicitly send a request to `model@mytorus.com`. Unfortunately we do not have the resources to provide user support. Nevertheless, you may send an e-mail to `model@mytorus.com` with a problem or question, with the understanding that a reply is not guaranteed. General feedback *is* encouraged as it has the potential to eventually provide justification for requesting funding for user support and further development.

Finally, we emphasize that the current release of MYTORUS is a *beta version (0.0)*. Whilst we have gone to great effort to test, benchmark, and validate the results that were used to construct the model, it is to be understood that you will be using the model and the associated documentation at your own risk. We are not responsible for errors, or for the validity or accuracy of any results that you might obtain using the MYTORUS model. Especially in view of the fact that is is quite easy to apply the model incorrectly (a property that is certainly not unique to MYTORUS), it is *your* responsibility to apply the model correctly. If you do find any errors in this manual please report them to `model@mytorus.com`.

Chapter 2

Basic Concepts

Throughout this manual, we will refer to various concepts and terminology related to the interaction of X-rays with matter. Here we define and clarify the most important of these. This discussion is minimal and geared towards a practical working knowledge that is required to apply the MYTORUS model. We give only limited background physics but you are strongly encouraged to pursue these topics in greater detail.

2.1 Compton-thin versus Compton-thick

There is some confusion in the literature with respect to whether an obscured X-ray source is Compton-thick or not. Strictly speaking, the Compton-thickness (more appropriately, the Compton optical depth) of a medium depends on the electron-scattering column density *angle-averaged over the source photon distribution over* 4π. The electron-scattering column density itself depends on the photon energy (which *changes* upon each scattering of the photon in the medium). Suppose the X-ray source emits $P(E_0, \theta, \phi)$ photons per unit solid angle with an initial energy of E_0. Here, θ and ϕ specify the direction of a photon in spherical polar coordinates. If the equivalent column density of neutral Hydrogen in the specified direction is $N_{\theta,\phi}$, the Compton optical depth *with respect to the incident photons* is then

$$\tau_{\rm s}(E_0) \quad = \quad x\sigma_{\rm KN}(E_0) \left[\frac{\int_0^{2\pi} \int_0^{\pi} P(E_0,\theta,\phi)\; N_{\theta,\phi} \sin\theta \; d\theta \; d\phi}{\int_0^{2\pi} \int_0^{\pi} P(E_0,\theta,\phi) \sin\theta \; d\theta \; d\phi} \right] \tag{2.1}$$

where x is the mean number of electrons per H atom and is equal to $\frac{1}{2}(1+\mu)$, where μ is the mean molecular weight. In Eq. 2.1, $\sigma_{\rm KN}(E_0)$, is the total Klein-Nishina Compton cross-section at an energy E_0. Thus, the Compton depth of the medium is not a simple quantity. It depends on the geometry of the medium, the angular distribution of obscuring matter, the angular distribution of the incident X-ray photons and their initial energy. Moreover, as E_0 becomes comparable to $m_e c^2$, the Compton depth for a given photon can change *significantly* (compared to the initial value) as it scatters in the medium.

If one has a *spectrum* of photons that is incident on the medium, then how can the Compton depth be defined? Clearly, there are a large number of possible choices for such a definition. We are, unfortunately, stuck with the conventional definition, that the Compton depth is defined as the *Thomson depth* of the medium *regardless of the energy spectrum of the incident photons*, with the additional assumptions that the X-ray source is isotropic and that the column-density distribution is spherically-symmetric. Neither of the latter two assumptions may be true. This definition of course does not accommodate the fact that the optical depth for a photon evolves as it scatters in the medium and it is equivalent to the assumption that $E_0 \ll m_e c^2$. With the assumptions of the conventional definition, Eq. 2.1 reduces to

$$\tau_{\rm s} \quad \sim \quad x\;\sigma_T\;N_{\rm H} \tag{2.2}$$

because $\sigma_{\rm KN} \sim \sigma_T$ if $E_0 \ll m_e c^2$. For the cosmic abundances of Anders & Grevesse (1989), Eq. 2.2 is

$$\tau_{\rm s} \quad \sim \quad 0.8090\;N_{24} \tag{2.3}$$

where N_{24} is the column density in units of $10^{24}\ {\rm cm}^{-2}$. According to the conventional definition then, a source is Compton-thick if $\tau_{\rm s} > 1$, or $N_{24} > 1.24$.

Confusion in the literature arises because the line-of-sight column density may be very different to the column density in directions out of the line-of-sight and often no distinction is made between the two quantities. The column density in Eq. 2.2 and Eq. 2.3 in the context of the conventional definition should really be the column density angle-averaged over all directions but it is incorrectly assigned to the line-of-sight column density in the literature. The angle-averaged column density out of the line-of-sight cannot be measured with ad hoc models of the X-ray spectrum. It must be derived indirectly, either using a self-consistent model such as MYTORUS, or using other indicators of the column density out of the line-of-sight. The latter indicators, such as the infra-red to X-ray luminosity ratio, or the O III to Fe Kα line ratio *do not* give unique, unambiguous estimates of the required column density. Therefore, if a source is said to be Compton-thick in the literature, you must first scrutinize precisely how that classification was arrived at, given the discussion of the complex assumptions above. Ultimately, of course, the classification is *arbitrary and is not in fact important*. What *is* important is to derive physical parameters from the observables. When you apply the MYTORUS model for this purpose, it does not matter whether you define the source to be Compton-thick or Compton-thin *because there is no requirement to make a distinction*. The MYTORUS model smoothly handles the range of equatorial column densities from $10^{22}\ \mathrm{cm}^{-2}$ to $10^{25}\ \mathrm{cm}^{-2}$.

On the other hand, the simple quantities in Eq. 2.2 and Eq. 2.3 do have a limited physical significance in the sense that they might, *under some circumstances*, roughly indicate certain properties of the source that you might expect if the Thomson depth is much less than or much greater than unity. However, it must be remembered that the conventional definition refers only to the line-of-sight Thomson depth, which may be completely different to the angle-averaged Thomson depth. For average Thomson depths much less than unity, the scattered X-ray spectrum will be dominated by the first scattering. The greater the Thomson depth compared to unity, the greater the mean number of scatterings will be *and* the greater the effects of X-ray absorption. In this manual we will use the conventional definition of Compton-thin to mean $\tau_{\mathrm{s}} = x\sigma_T N_{\mathrm{H}} \ll 1$ and Compton-thick to mean $\tau_{\mathrm{s}} = x\sigma_T N_{\mathrm{H}} > 1$, unless otherwise specified. Whenever either term is used we will specify what we mean by N_{H}.

2.2 The zeroth-order (or unscattered) continuum

There is a finite probability that a photon entering a medium will leave without interacting with it at all, (i.e., the photon is neither absorbed nor scattered). The zeroth-order continuum is the collection of all such photons.

In Fig. 2.1, we show a typical zeroth-order continuum photon path in a very generalized manner to illustrate the concept.

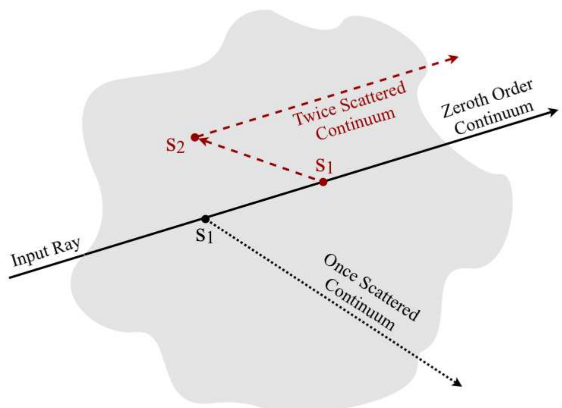

Figure 2.1: A very generalized illustration of the concept of the zeroth-order continuum, showing a typical photon path. Examples of rays that have undergone one and two scatterings are also shown (S_1 and S_2 denote sites for the first and second scattering respectively). Not all rays will of course reach an observer.

The zeroth-order continuum is simply

$$N_{0^{\rm th}} \quad = \quad N_{\rm in} e^{-(\tau_{\rm a}+\tau_{\rm s})}, \tag{2.4}$$

where $\tau_{\rm a}$ and $\tau_{\rm s}$ are the absorption and scattering optical depths along the line-of-sight, respectively, and $N_{\rm in}$ is the number of input photons per unit solid angle. *Both the absorption and scattering optical depths are energy dependent.*

In Fig. 2.1, we show a typical zeroth-order continuum photon path.

Since the zeroth-order continuum is purely a line-of-sight quantity, it *does not* depend on the geometry or covering factor of the material out of the line-of-sight. This component is simply a fraction of the input spectrum at a given energy, and that fraction depends only on the optical depth at that energy. The zeroth-order photons experience no time delay with respect to any unabsorbed continuum from the same source. The zeroth-order continuum is commonly referred to as the "direct" or "transmitted" continuum, but we only use the term "zeroth-order" throughout this manual.

Monte-Carlo simulations are not required to calculate the zeroth-order continuum for any geometry, since it can be calculated numerically. Although our Monte Carlo simulations produce zeroth-order continua, our spectral-fitting models utilize numerical zeroth-order continuum calculations.

2.3 The scattered continuum

For a photon incident upon a reprocessing medium, there is a finite probability that it will interact with the medium through Compton scattering or absorption, which is determined by the respective optical depths in the direction of photon propagation. At each interaction with the medium, the photon may be scattered with a probability equal to the ratio of the scattering cross-section to the total (scattering plus absorption) cross section. To this end, it is useful to define the (energy-dependent) single-scattering albedo:

$$s = \frac{\sigma_{\rm s}}{\sigma_{\rm a} + \sigma_{\rm s}} \tag{2.5}$$

.

The scattered continuum is the collection of all escaping photons that have been scattered in the medium at least once. It is sometimes referred to as the "reflection spectrum", but this implies that the escaping photons are always scattered "back" towards the observer. However, these photons may also be scattered forward towards the observer with respect to the initial direction of propagation.

Compton scattering shifts the energy of a photon. Therefore, the photons that contribute to the scattered continuum at a given energy can have a wide range of initial energies. For a cold medium (one in which the photon energy in the electron rest-frame is much less than $m_e c^2$), photons lose energy to electrons because Compton scatterings always transfers energy from photons to electrons in the electron rest frame. The net scattered spectrum for a cold medium at a given energy then depends on the input spectrum at all higher energies.

The fractional energy shift due to Compton scattering depends on the initial energy of the photon itself and is larger for higher energies (e.g. Murphy & Yaqoob 2009). For example, 500 keV photons can be down-scattered in energy to ~ 170 keV after a single scattering, whereas 5 keV photons are down-scattered by less than 100 eV in a single scattering. The total scattered continuum is therefore a complex function of the input spectrum, the reprocessor geometry, orientation, optical depth distribution, element abundances, and covering factor.

Due to the extra path lengths involved, the scattered continuum will be subject to time delays with respect to the zeroth-order continuum. For an obscured X-ray source, the observed spectrum will be composed of both scattered and zeroth-order continua, and therefore their relative normalizations may vary in time in response to intrinsic continuum variations. Calculation of the time response function is complex, but the time delays of the scattered component *could be* much longer than the typical intrinsic variability timescales. In Fig. 2.2 , we show examples of typical scattered photon paths to illustrate how scattered photons are affected by time delays.

2.4 The zeroth-order (or unscattered) fluorescent emission lines

If photons are absorbed above the K-edge threshold energy of an atom or ion, a K-shell electron can be removed. Subsequently, auger decay may follow, or a fluorescent line may be emitted if the K-shell vacancy is filled by an electron from an upper level. The probability that the absorption of a continuum photon above the K-edge threshold results in fluorescent line emission (the fluorescence yield) increases with the atomic number of the element.

A certain fraction of the line photons that are created will escape the medium with-

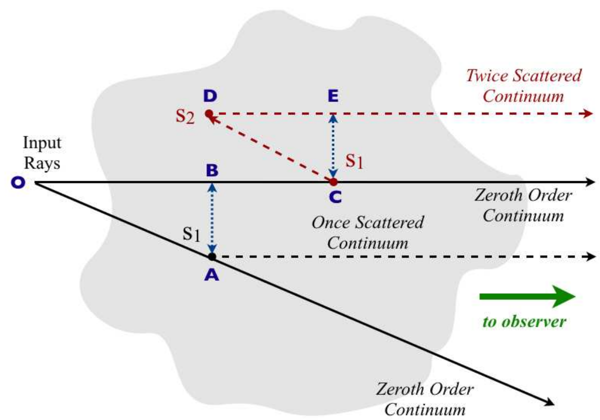

Figure 2.2: A very generalized illustration of the time delays between photon paths for the zeroth-order continuum and the scattered continuum (S_1 and S_2 denote sites for the first and second scattering respectively). In this example, the once-scattered ray will be delayed (with respect to the zeroth-order array) by the difference in the travel time between OA and OB. The twice-scattered ray will likewise be delayed by the sum of the travel times between CD and DE, with respect to the zeroth-order ray. Not all rays shown reach the observer (e.g. the zeroth-order ray along OA does not). The overall temporal response function of the scattered continuum is therefore a very complex quantity that can be obtained by accumulating the time delays for every ray over all scattering orders.

out being scattered. These are the zeroth-order emission-line photons, which constitute the "core" of the line. All of these zeroth-order line photons have an energy that is *not* affected by Compton scattering. Only Doppler and gravitational energy shifts would affect the zeroth-order line photons (which can be implemented in the MYTORUS model by other functions in the spectral-fitting package). The observed zeroth-order line flux and equivalent width (EW) depend on the input spectrum and the reprocessor geometry, orientation, column density distribution, element abundances, and covering factor.

Note that the zeroth-order line emission is *not* polarized, since the emission is isotropic. Fig. 2.3 illustrates the creation and escape of zeroth-order Fe Kα line photons. These emission-line photons may be created after multiple scatterings of higher-energy continuum photons and therefore will be subject to similar (but not identical) time delays as the scattered continuum with respect to the zeroth-order continuum.

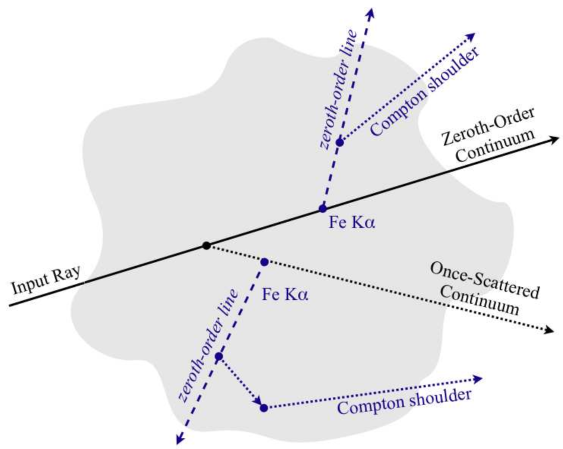

Figure 2.3: A very generalized illustration of some typical photon paths relevant for the creation of the zeroth-order and scattered fluorescent emission-line spectrum. The zeroth-order fluorescent line photons will appear to have time delays with respect to the zeroth-order continuum that are of the same order as the time delays between the scattered continuum and the zeroth-order continuum.

2.5 The scattered components of the fluorescent emission lines

Emission-line photons may be scattered before they escape the medium (see Fig. 2.3). The scattered photons constitute the "Compton shoulder" of the observed emission line. Typically, the largest contribution to the Compton shoulder comes from line photons that have been scattered once before escape. The flux in the Compton shoulder relative to the zeroth-order emission-line component depends mainly on the column density distribution, element abundances, orientation, and geometry of the reprocessor. Since the spatial distribution of the origin of the zeroth-order and scattered components of the emission line is similar, we don't expect time delays between these components to be significant and they are neglected in our implementation of the MYTORUS model.

2.6 Relative normalizations of the model components

It is clear from the above discussion that separation of the zeroth-order continuum, scattered continuum, and emission-line spectrum must be maintained in order to allow for time delays and deviations from model assumptions. As described above, there may be time delays between the scattered continuum and the zeroth-order continuum and, possibly different, time delays between the line emission and the zeroth-order continuum. In reality, the reprocessor will not have the same geometry, covering factor, and element abundances assumed in our model. Allowing the three groups of model components to have variable relative normalizations is therefore necessary. The total spectrum is the sum of the three groups of model components, weighted by their relative cross-normalizations. However, relative normalizations cannot correctly account for differences in the spectrum for different geometries, covering factors, and element abundances (see Chapter 9). Future implementations, based on additional Monte Carlo simulations, will include more choices in covering factor and element abundances.

Chapter 3

Toroidal Model

3.1 Toroidal reprocessor model

Our model adopts a tube-like, azimuthally-symmetric torus (see Fig. 3.1). Here c is the distance from the center of the torus (located at the origin of coordinates) to the center of the "tube", and a is the radius of the tube, but note that only the *ratio*, c/a, is important for our calculations. This corresponds to the classic "doughnut" type of geometry for the obscuring torus in AGN.

The inclination angle between the observer's line-of-sight and the symmetry axis of the torus is given by $\theta_{\rm obs}$, where $\theta_{\rm obs} = 0^\circ$ corresponds to a face-on observing angle and $\theta_{\rm obs} = 90^\circ$ corresponds to an edge-on observing angle.

The equatorial column density, $N_{\rm H}$, is defined as the equivalent Hydrogen column density through the diameter of the tube of the torus (as indicated in Fig. 3.1). The actual line-of-sight column density is:

$$N_{\rm H,\ l.o.s.} = N_{\rm H} \left[1 - \left(\frac{c}{a} \right)^2 \cos^2 \theta_{\rm obs} \right]^{\frac{1}{2}}. \qquad (3.1)$$

The mean column density, integrated over all lines-of-sight through the torus, is $(\pi/4)N_{\rm H}$ (assuming an X-ray source that emits isotropically and is located at the

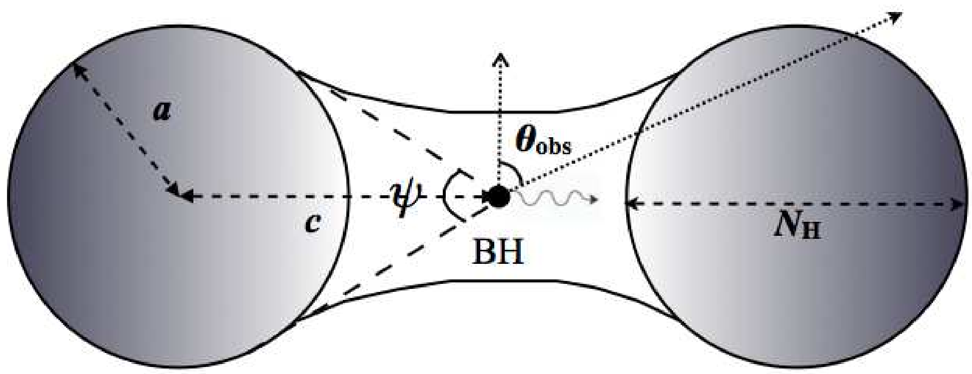

Figure 3.1: Assumed model geometry. The half-opening angle is given by $(\pi - \psi)/2$ and the inclination angle of the observer's line-of-sight with respect to the symmetry axis of the torus is given by $\theta_{\rm obs}$. The equatorial column density, $N_{\rm H}$, of the torus is defined by the diameter of the tube of the "doughnut". The illuminating X-ray continuum source is located at the origin (filled circle, marked "BH" for "black hole").

origin of the torus). The column density may also be expressed in terms of the Thomson depth: $\tau_{\rm T} = \frac{1}{2}(1+\mu)N_{\rm H}\sigma_{\rm T}$, where μ is the mean molecular weight (see Murphy & Yaqoob 2009). For the cosmic abundances of Anders & Grevesse (1989) this quantity is $\sim 0.809 N_{24}$, where N_{24} is the column density in units of 10^{24} cm^{-2}.

The half-opening angle of the torus is given by $(\pi - \psi)/2$ (see Fig. 3.1). The covering factor, $\Delta\Omega/(4\pi)$, is given by a/c, where a and c are the lengths illustrated in Fig. 3.1. In the current implementation, the half-opening angle is 60° (equivalent to $[\Delta\Omega/(4\pi)] = 0.5$, or $(c/a) = 2$).

We assume that the the reprocessing material is uniform and essentially neutral and cold (see §4.5). Dynamics are not included in the Monte Carlo code. Kinematic information can be approximated by convolving the final output spectrum with a velocity function.

We utilize photoelectric absorption cross sections for 30 elements as described in Verner & Yakovlev (1995) and Verner *et al.* (1996). Although these cross section parameterizations are only valid up to 100 keV, the absorption cross sections near 100 keV and at higher energies can be approximated by a simple power-law form and they are orders of magnitude less than the values at the threshold energies (all < 10 keV). Therefore, we extrapolate the total cross section for energies above 100 keV using a power law with a slope equal to that in the $90 - 100$ keV interval. We currently use Anders and Grevesse (1989) elemental cosmic abundances in our calculations.

We included $K\alpha$ fluorescent line emission in our Monte Carlo code for Fe and Ni, as well as the $K\beta$ line for Fe. Fluorescent lines from other cosmically-abundant elements (such as C, O, Ne, Mg, Si, and S) are less observationally relevant than those from Fe and Ni due to their small fluorescence yield and because lower-energy line photons have a greater probability of being absorbed before escaping the medium than higher-energy photons. Currently, only the Fe Kα and Fe Kβ emission lines are included in the actual spectral-fitting model (see Chapter 7 for details).

3.1.1 Inclination angle bins

The spectra are stored in 10 $\theta_{\rm obs}$ bins between $0°$ and $90°$ that cover equal intervals in solid angle (see Table 3.1). Because of the symmetry of the torus and the isotropy of the illuminating X-ray radiation, these solid-angle bins cover the entire sky. The angle bins are illustrated in Fig. 3.2. For the current geometry with a half-opening angle of $60°$, this corresponds to 5 angle bins that intercept the torus (with $\theta_{\rm obs}$ between $60°$ and $90°$) and 5 that do not intercept the torus (with $\theta_{\rm obs}$ between $0°$ and $60°$). Note that the first angle bin is actually a cone centered on $0°$. For this bin, $0°$ can be interpreted as a bin center, as opposed to a bin boundary. Likewise, the last angle bin includes emission from the $\theta_{\rm obs}$ interval $84.26°$ to $95.74°$, centered on $90°$ due to the symmetry. Thus, interpolation of physical quantities for an arbitrary value of $\theta_{\rm obs}$ is not straightforward if $\theta_{\rm obs}$ lies in one the "end-bin" intervals. Our method is to interpolate quantities at the mid-point of each angle bin, except that if the specified value of $\theta_{\rm obs}$ lies in the first half of the first bin or the second half of the last bin, the value of the physical quantity is simply set equal to the literal value of the quantity for that angle bin (which is equal to the mid-point value).

Table 3.1: Bin boundaries for $\theta_{\rm obs}$. Bins 1–5 correspond to lines-of-sight that do not intercept the torus for the opening angle discussed here. Bins 6–10 correspond to lines-of-sight that intercept the torus.

Bin	$\cos(\theta_{\rm obs,max})$	$\cos(\theta_{\rm obs,min})$	$\theta_{\rm obs,min}$ (degrees)	$\theta_{\rm obs,max}$ (degrees)
1	0.9	1.0	0.00	25.84
2	0.8	0.9	25.84	36.87
3	0.7	0.8	36.87	45.57
4	0.6	0.7	45.57	53.13
5	0.5	0.6	53.13	60.00
6	0.4	0.5	60.00	66.42
7	0.3	0.4	66.42	72.54
8	0.2	0.3	72.54	78.46
9	0.1	0.2	78.46	84.26
10	0.0	0.1	84.26	90.00

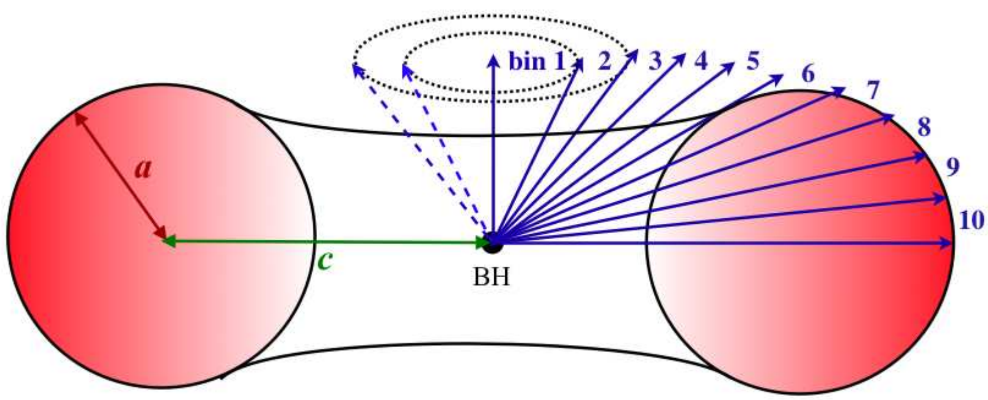

Figure 3.2: Illustration of the physical meaning of the 10 angle bins used in the MYTORUS model (see Table 3.1 and §3.1.1). The torus has azimuthal symmetry, as well as symmetry around the edge-on inclination angle ($\theta_{\rm obs} = 90°$). The latter symmetry allows us to sum rays that have directions $\theta_{\rm obs}$ and $180 - \theta_{\rm obs}$. The angle bin labeled "1" (face-on) actually includes a cone around the pole, centered on $\theta_{\rm obs} = 0°$, and the angle bin labeled "10" includes a "wedge" that is centered on $\theta_{\rm obs} = 90°$. The geometry of the discrete angle bins should be considered carefully when interpreting spectra from MYTORUS.

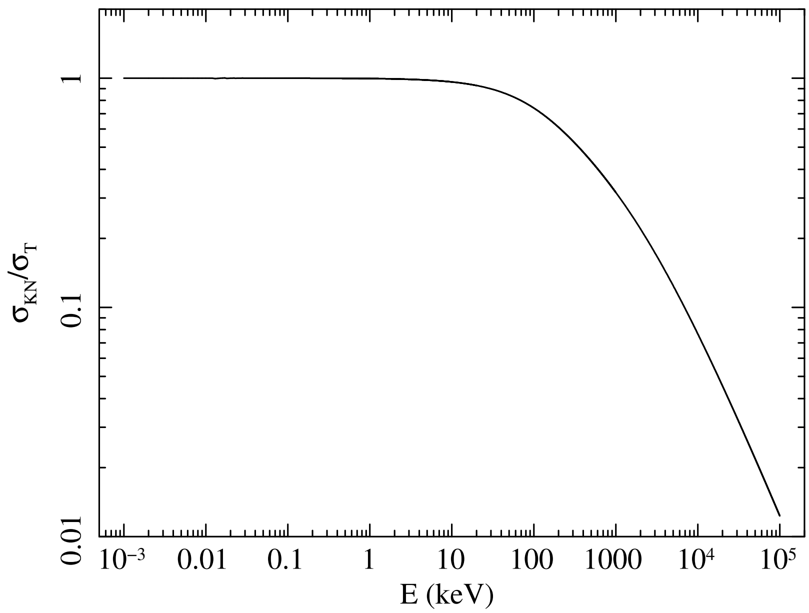

Figure 3.3: Total Klein-Nishina Compton-scattering cross section versus energy, in units of of the Thomson cross section.

3.2 Understanding the energy-dependence of the spectra

3.2.1 Zeroth-order spectrum

The zeroth-order continuum has an energy dependence that is affected by the energy-dependent photoelectric absorption cross sections and the Klein-Nishina Compton-scattering cross section (see Fig. 3.3). The zeroth-order spectrum at each energy is simply the input spectrum multiplied by a factor between 0 and 1 that corresponds to the fraction of photons escaping in the line-of-sight without interacting with the medium.

3.2.2 Scattered spectrum at low energies

The absorption probability for photons becomes increasingly higher as the photon energy decreases and so the fraction of escaping photons decreases significantly. In order to obtain reliable escape fractions, larger input photon numbers must be injected into the torus at low energies. Moreover, the multitude of absorption edges below 10 keV would require carefully selected injection energies in order to achieve the desired energy resolution with sufficient accuracy (even with the method of photon weights that we employ for our latest Monte Carlo results). However, when the energy is low enough that Compton scattering is in the Thomson regime, the total scattering cross section is essentially independent of energy and, if absorption dominates over scattering, most of the escaping photons will be zeroth-order or once-scattered. Under these circumstances, the passage of photons through the torus depends only on the single-scattering albedo (see Eq. 2.5) and not on the initial photon energy.

Using our Monte Carlo code, we can calculate the number of escaping photons for a relatively small set of albedo values and interpolate for any desired, arbitrary value of the albedo. Thus, to obtain the output for a given input photon energy, we can calculate the corresponding albedo for a given set of element absorption cross sections at that energy and use that albedo value to obtain the escape fraction by interpolating the albedo-based Monte Carlo results. We note that if any of the element abundances is changed, the same albedo-based Monte Carlo results can be used since only the correspondence between albedo and energy changes. In practice, we can calculate the zeroth-order photon numbers using Eq. 2.4 and use the interpolated Monte Carlo results for the scattered photons. At 5 keV the maximum energy shift after one scattering is ~ 100 eV, which is comparable to CCD-resolution.

3.2.3 Scattered spectrum at high energies

At any particular energy value, the scattered spectrum includes contributions from Compton downscattered photons that had higher initial energies. In principle, an infinite number of scatterings could contribute to the total spectrum at a given energy. In practice, the intrinsic spectrum of an astrophysical source and the Klein-Nishina cross section decrease with increasing energy. Moreover, the intrinsic source spectrum cuts off at a characteristic energy which is usually unknown. The scattered spectra show an observed high-energy cutoff that occurs at lower energies than the intrinsic cutoff, due to Compton downscattering. Including an additional high-energy cutoff may not be necessary. The functional form of a power-law with an exponential cutoff is not physical; in particular, thermal comptonization models do not predict curvature that can be modeled adequately with an exponential cutoff. Either a physical model of the intrinsic spectrum should be used (which would have a natural high-energy cutoff), or if an empirical model is used, it may be more realistic to assume that it simply terminates at a discrete energy. The range of high-energy cutoffs for the input spectra of AGN is poorly determined, but we note that non-blazar AGNs have rarely been detected above 500 keV (e.g. see Dadina 2008). In the MYTORUS model, spectra are calculated based upon the assumption that the intrinsic power-law continuum terminates at an energy that we will refer to as E_T throughout this manual. Although this termination energy is not implemented as a free parameter, calculations are available for a range of values of E_T up to 500 keV (see §6.1.3 and §6.2).

3.3 Implementation as a spectral-fitting model

There are a variety of possible implementations for transforming the Monte Carlo simulation results to an actual spectral-fitting model. Particular implementations may be optimal for certain applications, but any implementation will inevitably involve some compromise. Two major desirable factors of the spectral-fitting tool are 1) that it should be as fast as possible and 2) that is allows for an arbitrary input spectrum. In practice, there is a trade-off between these two properties. Allowing an arbitrary input spectrum requires "on-the-fly" integration of the Monte Carlo results (Greens functions) and input spectrum, and consequently this can result in impractical run times. Although in the future we will release a version of the tool that can handle arbitrary input spectra, for the current release we choose speed as the most important factor. Thus the first release of the MYTORUS model is in the form of pre-calculated tables for input spectra in the form of a power law, a choice which is suitable for the application of fitting AGN X-ray spectra.

There are other practical aspects to consider in an implementation of the spectral-fitting model. For example, instrument calibration uncertainties demand some freedom in the energy scale of the model spectrum, especially with respect to emission-line features. Energy resolution is also an important practical consideration. The energy resolution in the current model implementation is suitable for current X-ray spectral instrumentation and the spectral resolution for the fluorescent emission lines is suitable for data that will be obtained by calorimeters aboard *Astro-H*.

For the current and future implementations of the model, we will use the albedo-based results (see §3.2.2) to construct the spectra below 5.0 keV. The albedo-based method uses an elastic-scattering approximation. The cross-over energy of 5.0 keV was chosen to give a reliable transition to the regime in which the general Monte Carlo results are used (see Murphy & Yaqoob 2009 for quantitative details).

3.4 The default implementation: power-law table model

The default implementation of the spectral-fitting model is based on tables of spectra calculated from a power-law input spectrum. There are three groups of tables, corresponding to the three groups of model components described in Chapter 2: the zeroth-order continuum, the scattered continuum, and the emission-line spectrum. The components are combined to produce the net spectrum. This includes convolving the line emission with a Gaussian function (that is part of the spectral-fitting package) to model velocity broadening. The current implementation includes only Fe Kα and Fe Kβ line emission. Although our Monte Carlo model calculates the Ni Kα line emission, we have not yet included it in the current spectral-fitting model since the nickel abundance is currently highly uncertain. Furthermore, this line emission is not commonly detected in AGN spectra. However, we plan to include this component in future implementations of the model.

The first release of the spectral-fitting model pertains to fixed element abundances (Anders & Grevesse 1989) and a single opening angle (i.e. a half-angle of 60°, equivalent to a covering factor of $(\Delta\Omega/[4\pi]) = 0.5$).

The current implementation includes different tables that correspond to different termination energies of the input spectrum, up to a maximum energy of 500 keV.

Table 3.2: Summary of parameters for the MYTORUS table model

Parameter	Description	Range
z	Cosmological redshift of the source	0–$[(E_T/E_U) - 1]$ †
Γ_i	Photon index of the intrinsic power-law continuum	1.4–2.6
A_i	Normalization of the intrinsic power-law continuum (photon flux at 1 keV)	...
N_H	Equatorial column density of the torus	0.01–10×10^{24} cm^{-2}
$\theta_{\rm obs}$	Inclination angle between the torus polar axis and the observer's line of sight	0°–90°
A_S	Relative normalization of the scattered continuum	...
A_L	Relative normalization of the Fe Kα and Fe Kβ fluorescent line spectrum	...
σ_L ‡	Gaussian width of fluorescent emission lines	...
E_T	Termination energy of the intrinsic continuum (keV)	$\leq$ 500 keV

† Here E_T is the maximum energy of the intrinsic power-law spectrum (different tables for the scattered continuum will have different values – see Chapter 6), and E_U is the maximum energy of the *observed-frame* data.
‡ Regardless of the centroid energy of an emission line, this parameter is related to the FWHM velocity width, $V_{\rm FHWM}$, by $V_{\rm FHWM} = 2.354c\sigma_L({\rm keV})/[6\ {\rm keV}]$ when the velocity broadening is implemented with the `gsmooth` function in XSPEC, with the energy index, α, frozen at 1.0 (see Eq. 7.4 and Eq. 7.6 in §7.3.5). Here, c is the speed of light.

3.4.1 Model components

The zeroth-order continuum component is in the form of multiplicative tables. The $\theta_{\rm obs}$ dependence on the zeroth-order continuum component is not confined to the 10 solid angle bins that we define for the scattered continuum and line emission (i.e., Table 3.1, Fig. 3.2). Instead, the calculation of the zeroth-order spectrum is interpolated on a finer energy grid (see Chapter 5).

The scattered continuum component is in the form of additive tables. Details of the different available tables, corresponding to different high-energy intrinsic continuum termination energies are given in Chapter 6.

The line emission component combines the zeroth-order and scattered line emission and is in the form of additive tables. Currently these tables include only Fe Kα and Fe Kβ line emission. Different tables are available for different energy offsets and different termination energies of the incident power-law continuum, as described in Chapter 7 (which also describes the implementation of velocity broadening).

3.4.2 Model parameters

Table 3.2 shows a summary of parameters for the XSPEC table model implementation, including their valid ranges where appropriate. The notation for the parameters in Table 3.2 will be used throughout this manual. In practice a model is implemented using three separate tables combined with additional components that are intrinsic to the spectral fitting package. A given parameter may appear in more than of the tables, even though the multiple appearances of a parameter may refer to the same physical quantity. Such parameters will usually be tied to vary together in the actual spectral-fitting procedure. The details of the tables are described in Chapters 5, 6, and 7, whilst Chapter 8 describes the practical aspects of how the tables and intrinsic functions in the spectral-fitting package are combined to set up complete models in preparation for spectral fitting.

Chapter 4

Understanding the Model Assumptions

In this chapter we summarize the various assumptions of the MYTORUS model that are important to understand before applying the model to data. Although some of these may be quite restrictive, applying a physical model can be *less* restrictive than applying ad hoc (non-physical) models since it has the ability to yield a higher scientific return. In this respect, the statistical goodness of fit alone may not decide which is the best model for the data. In other words, adding model components that do not have a sound physical basis, just to get a better fit to the data may not yield any new information about the astrophysics of the source. The MYTORUS model provides a *physical and self-consistent baseline* as a starting point and this is more useful than using ad hoc, non-physical models. Real AGN will not conform to all of the assumptions in the MYTORUS model but the results of starting to fit real data with MYTORUS will serve as quantitative indicators of how the model should be extended in a physical and self-consistent manner. Such an approach is not possible with models that are completely ad hoc.

4.1 Intrinsic, incident spectrum

The X-ray continuum source in the MYTORUS model is located at the center, or origin, of the torus and emits isotropically (see Fig. 3.1). Although in the future we will release a version of the MYTORUS tool that can handle arbitrary input spectra, only a power-law intrinsic continuum is currently supported. For the majority of applications for fitting AGN X-ray spectra this will not be prohibitive.

4.2 High-energy cutoff

In the current implementation, the high-energy cutoff of the intrinsic continuum is not a free parameter. However, tables are available for a discrete set of termination energies of the incident power-law continuum (see §3.2.3 and §6.1.3 for details). We also recommend that you do *not* put in an additional high-energy exponential cutoff, for reasons explained in §8.4.3.

4.3 Opening angle/covering factor

The model assumes a single value for the covering factor of the torus ($[\Delta\Omega/(4\pi)] = 0.5$, or $(c/a) = 2$), corresponding to a half-opening angle of $60°$; see §3.1). Future implementations will include tables for additional values of the covering factor.

4.4 Element abundances

We use Anders & Grevesse (1989) cosmic abundances. In the future there will be a version that utilizes Asplund *et al.* (2009) abundances. Future implementations will allow also freedom in the abundance of iron.

4.5 Ionization state

The observed peak energy of the narrow Fe Kα line at 6.4 keV in many AGN provides overwhelming evidence that the narrow core of the Fe Kα line in AGN originates in cold, neutral matter (see Shu, Yaqoob, & Wang 2010, and references therein). It is *this* circumnuclear matter that MYTORUS models. We know there is evidence from emission and absorption lines in AGN that ionized matter also exists in many AGN. MYTORUS is not a model for the ionized matter, it is a model for the neutral/cold matter. The model is calculated for neutral matter but in practice may be applicable (with careful interpretation) to low-ionization material, with the possibility of H and He being fully ionized, and the existence Fe ions up to Fe XVII. Corresponding temperatures may be of the order of $\sim 10^4$ K or so.

4.6 Kinematics

The table model does not include kinematics and therefore velocity broadening must be applied using an intrinsic function that is part of the spectral-fitting package in use (e.g. a Gaussian convolution). A method of implementing velocity broadening is fully described in Chapters 7 and 8.

4.7 The Ni Kα emission line

The Ni Kα line emission is not yet included in the model since the nickel abundance is currently highly uncertain. Furthermore, this line emission is not commonly detected in AGN spectra. However, we supply calculations of the equivalent width of the Ni Kα emission line in order to aid in the interpretation of empirical fits with a Gaussian model component. We plan to include the Ni Kα line in future implementations of the MYTORUS model.

4.8 Emission-line fluxes and equivalent widths

Due to the nature of the implementation of table models in XSPEC, it is not possible to directly obtain line equivalent widths and fluxes. Instead, the line flux is calculated using the regular "flux" command, and the EWs must be calculated manually (for details, see §7.1.4, §7.3.5.3, and §7.3.5.4).

4.9 Statistical uncertainties

Since the MYTORUS model is based on Monte Carlo simulations, it is has statistical errors that are a complex function of the model parameters and the desired energy resolution (see §6.2.5.1). It is important not to forget this because you will not notice statistical noise in the spectra for most of the parameter because the statistical errors are so small. However, for the regime of very high column density ($N_{\rm H}$ greater than $\sim 7 \times 10^{24}\ {\rm cm}^{-2}$) and high inclination angles (edge-on) you will notice some noise in the 5–10 keV band at the $\pm 3\%$ level. This level of statistical noise is still unprecedented for model calculations of a toroidal distribution of matter in the edge-on, high column-density regime when *both* the absorption and scattering optical depths are significantly greater than unity. It is unlikely that the statistical errors on the model will be larger than the statistical errors associated with your data and the effective area calibration of the instrument that your data were obtained with. In particular, the statistical precision of the MYTORUS model is still high enough in the edge-on, high column-density regime to capture some effects associated with the Fe K edge and Fe Kα and Fe Kβ emission lines that could not be previously studied in a spectral-fitting context. The statistical errors improve for smaller column densities and smaller inclination angles and can be more than an order of magnitude smaller than the worst case. Even the highest column density (10^{25} cm^{-2}) has statistical errors that are more than an order of magnitude better than the edge-on inclination angle for the same column density. Note that the Monte Carlo results upon which the MYTORUS model is based have a higher accuracy than those in Murphy & Yaqoob (2009) due to several improvements. More accurate algorithms for the calculation of escape distances were developed, photon rays with weights were employed instead of using single, discrete photons, and the the statistical errors on the emergent spectra are smaller.

4.10 What the model does not include

Our model does not include, for example, the following components commonly used to fit AGN spectra:

- Photoionized absorbers
- Continuum emission that does not originate in the central X-ray source (e.g. optically-thin scattered and/or thermal emission)
- Relativistic emission lines
- Disk-reflection continuum emission

While such components can be used in combination with our model, you should be aware of the many related caveats (see Chapter 8 and Chapter 9 for details).

Chapter 5

MYTorus Zeroth-order Continuum

5.1 General Properties

The zeroth-order continuum is comprised of those incident continuum photons that escape the torus without any interaction with it. The detailed meaning of the zeroth-order continuum has been discussed in §2.2 and §3.2.1.

In this chapter we discuss important practical aspects of the implementation of the zeroth-order continuum component of the MYTORUS spectral-fitting model.

The zeroth-order continuum is obtained by applying an *energy-dependent multiplicative factor, or attenuation*, to the intrinsic X-ray continuum that is incident on the torus *along the line-of-sight*. It is important to realize each of the following points.

- The zeroth-order multiplicative component of MYTORUS can be applied to *arbitrary incident continuum spectral shapes*, regardless of *how* the zeroth-order continuum is implemented in MYTORUS. However, in most cases you will need to set up the zeroth-order continuum to be self-consistent with the scattered continuum and fluorescent emission-line components of MYTORUS, in which case the incident continuum is currently restricted to have a power-law form (but see §5.1.1 and §8.4.3).

- The zeroth-order multiplicative component of MYTORUS is *not* generated using Monte Carlo calculations, and therefore it is not subject to statistical errors (unlike the scattered continuum and fluorescent emission-line components of MYTORUS).

- Since the zeroth-order continuum is not generated by Monte Carlo calculations, it is not restricted to the finite angle bins that the scattered continuum and fluorescent emission-line components are (see Fig. 3.2 and the related discussion in Chapter 3). In principle the zeroth-order continuum can be calculated for arbitrary inclination angles (values of $\theta_{\rm obs}$) of the torus. The zeroth-order continuum can also be calculated at arbitrary energies.

- The zeroth-order continuum does *not* depend on covering factor (or opening angle of the torus) because it is a line-of-sight quantity. It *does* depend on element abundances, however.

- The zeroth-order multiplicative component distorts the incident continuum at all energies, not just those that are affected by absorption (see §5.2).

There are two principal ways in which the zeroth-order continuum could be implemented in MYTORUS. The first is by means of a numerical code that calculates the photoelectric absorption and Compton scattering attenuation "on the fly", and the second is by means of pre-calculated optical depths or attenuation factors in a table. The former method has the advantage that arbitrary element abundances can be employed (and therefore allowed to be free parameters). However, the table-model implementation has the advantage of higher run-time speed because the calculation of photoelectric and Klein-Nishina cross sections is much slower than interpolation of pre-calculated table values. We plan to implement both methods for MYTORUS but currently only the table model implementation is available (for the cosmic abundances of Anders & Grevesse 1989).

5.1.1 When and how to use the zeroth-order spectrum

For most applications, the zeroth-order continuum will be used in conjunction with the other components of the MYTORUS model (i.e. the scattered continuum and the fluorescent emission-line spectrum). The three components work together to form a self-consistent model and Chapter 8 describes in detail how this is done in practice.

One situation in which you might want to use *only* the zeroth-order continuum by itself corresponds to the case when the X-ray reprocessor subtends such a small solid angle at the X-ray source that the scattered continuum and fluorescent line emission can be neglected. Physically, this could represent a "ring" (or torus with $c/a \gg 1$), or even a cloud in the line-of-sight. In the latter case, the entire *distribution* of clouds must subtend a small enough solid angle at the X-ray source that their contribution to the scattered continuum can be neglected. It is *your* responsibility to determine whether the approximation is tolerable for your particular application.

It is also worth bearing in mind that since the zeroth-order continuum multiplicative component is simply equivalent to a line-of-sight absorber with additional attenuation due to Compton scattering, it can replace any "regular" neutral absorption model component with cosmic abundances (see also §8.4.6).

5.2 Distortion of the intrinsic spectrum

It is important to understand that the zeroth-order continuum multiplicative factor distorts the incident intrinsic X-ray continuum over a wide energy band. The distortion is NOT due to Compton downscattering because the zeroth-order continuum photons have not interacted with the medium. At energies below ~ 20 keV the spectral shape is determined principally by photoelectric absorption and above ~ 20 keV it is determined principally by the form of the Klein-Nishina (total) Compton scattering cross section (see §3.2.1 and Fig. 3.3). The effect of the latter is to produce an effective hardening of the intrinsic spectrum at high energies, and this is illustrated in Fig. 5.1 for an intrinsic power-law continuum with a photon index of $\Gamma = 1.9$, for $N_{\rm H} = 10^{24}\ {\rm cm}^{-2}$ and $10^{25}\ {\rm cm}^{-2}$.

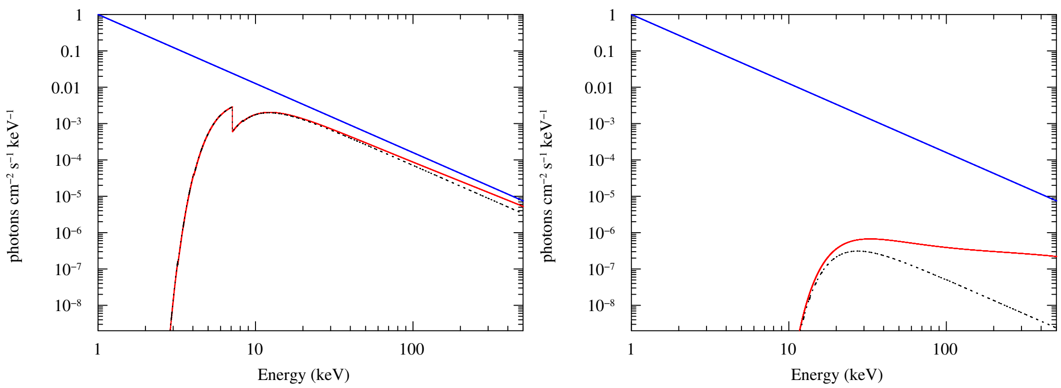

Figure 5.1: The zeroth-order continuum (red, solid curves) for an incident, intrinsic power-law continuum (blue, solid lines) with a photon index of $\Gamma = 1.9$, for $N_{\rm H} = 10^{24}$ cm^{-2} *(left)* and 10^{25} cm^{-2} *(right)*. Also shown for comparison are the results of applying the CABS model in XSPEC (black, dotted lines) to the same incident continuum. The CABS model does not capture the spectral hardening because the Compton scattering cross section used by CABS is an inadequate approximation (see §5.3).

5.3 Comparison with the XSPEC "CABS" model

Results in the literature that model the line-of-sight attenuation in Compton-thick AGN with only simple absorption completely miss the spectral hardening effect discussed above. Even the XSPEC model CABS does not capture the effect (even though the "C" in CABS stands for Compton scattering). This is because the CABS model simply assumes a constant Compton scattering cross section equal to the Thomson cross section. However, this approximation is only valid below ~ 10 keV (see Fig. 3.3). For a direct comparison with the MYTORUS model, Fig. 5.1 shows the CABS model (dotted curves) applied to the same incident, intrinsic continuum.

5.4 Table-model implementation

In this section we describe the table-model implementation of the zeroth-order continuum multiplicative factor (currently the only implementation). The implementation is in the form an XSPEC `etable` or `mtable` which contain pre-calculated optical depths or transmission factors respectively (the transmission factors having numerical values in the range 0–1). An XSPEC `etable` is similar to an `mtable` except that for the former, XSPEC negates and exponentiates the table values in order to produce a multiplicative factor. The practical usage for the two types of table is the same. The `etable` is the preferred default for reasons explained in §5.4.2. There is no velocity broadening included in the zeroth-order tables, although it could be included using a convolution function intrinsic to the spectral-fitting package. For most applications however, velocity broadening will not be necessary. The available default table-model file name is `mytorus_Ezero_v00.fits` and pertains specifically to a torus half-opening angle of 60° (corresponding to $(c/a) = 2$; see §3), and the cosmic abundances of Anders & Grevesse (1989).

Symbolically, the zeroth-order model component of MYTORUS will be represented throughout this manual as

$$\mathrm{MYTZ}(z, N_{\mathrm{H}}, \theta_{\mathrm{obs}}, E) \tag{5.1}$$

where z is the cosmological redshift, N_{H} is the equatorial column density, θ_{obs} is the inclination angle, and E is the energy (in keV). Recall that the actual line-of-sight column density, $N_{\mathrm{H,los}}$, can be calculated for a given N_{H} and θ_{obs} using Eq. 3.1.

The tables cover the range $N_{\mathrm{H}} = 10^{22}\ \mathrm{cm}^{-2}$ to $10^{25}\ \mathrm{cm}^{-2}$ and the energy range 0.5–500 keV. It is important to understand why the value of the the inclination angle, θ_{obs}, covers the range 0° to 90°. Values of θ_{obs} that lie in the range 0° to 60° *do not intercept the torus*. The multiplicative factor for this range of θ_{obs}, regardless of the value of N_{H} or E, is equal to unity. In other words, the zeroth-order continuum for lines-of-sight that do not intercept the torus is simply equal to the intrinsic, unobscured, X-ray continuum. This is physically what would be required for most scenarios and allows the θ_{obs} parameter of the zeroth-order component to be set equal to the θ_{obs} parameter in the scattered continuum and fluorescent line components of MYTORUS.

The practical details of how to use the zeroth-order table in conjunction with other model components are given in Chapter 8.

5.4.1 Energy resolution

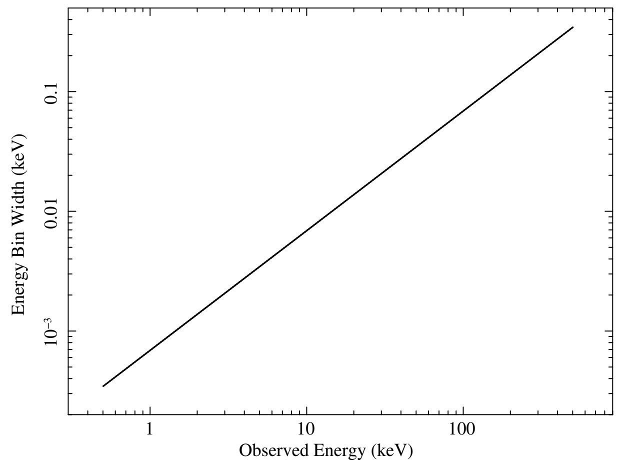

Figure 5.2: The energy bin widths versus the corresponding energy bin centers in the zeroth-order continuum component in the `etable` `mytorus_Ezero_v00.fits` and `mtable` `mytorus_Mzero_v00.fits` (see §5.4.1).

Since the zeroth-order continuum component of MYTORUS can in principle be calculated for arbitrary energies, the energy resolution of the table-model implementation is simply given by the energy bin widths. For reference, the energy bin widths are plotted against the corresponding energy bin centers in Fig. 5.2. Below 10 keV the energy resolution is better than 7 eV.

5.4.2 WARNING: etable and mtable anomalies

The `etable` implementation for the zeroth-order continuum is the default but it is important to be aware of the fact that if an energy is specified that lies outside the valid range of the `etable`, XSPEC assigns an optical depth of zero. The data should never extend beyond the valid energy range of the table (see §5.4.3) but the "plot model" command in XSPEC may plot the model beyond the specified energy range, resulting in a plot that may be incorrect *even in the valid energy range* (see §8.5). Moreover, we know of at least one version of XSPEC that does not correctly handle the `etable` (XSPEC version 12.3.1x that was released with `ftools 6.3.2`), in that it treated the `etable` as an `mtable`. If you are unsure

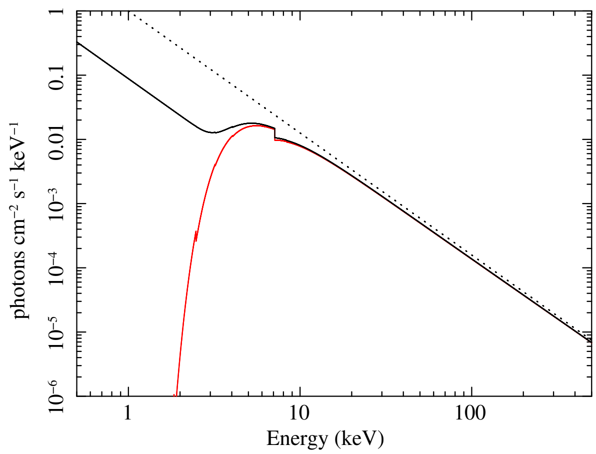

Figure 5.3: The anomalous zeroth-order continuum spectrum (black, solid curve) obtained from interpolation of the `mtable` values in `mytorus_Mzero_v00.fits` when the specified inclination angle, $\theta_{\rm obs}$, lies in the $\theta_{\rm obs}$ interval that has a boundary at the surface of the torus. In this example, the intrinsic X-ray continuum is a power law with a photon index, $\Gamma = 1.9$ (dotted line), $\theta_{\rm obs} = 61^\circ$ and $N_{\rm H} = 10^{24}$ cm^{-2}. For comparison the spectrum obtained from interpolation of the `etable` values in (`mytorus_Ezero_v00.fits`) for this inclination angle is shown in red. The bin boundary is at 61.09° so any value of $\theta_{\rm obs}$ greater than this will *not* show the anomaly for the `mtable`. See §5.4.2 for details.

of the validity of your results you should cross-check with the `mtable` version of the zeroth-order continuum.

The `mtable` implementation for the zeroth-order continuum itself shows anomalous behavior of a different kind, which we describe in the remainder of this section. In the `mtable` implementation of the zeroth-order continuum, the spectrum for a given value of $\theta_{\rm obs}$ is obtained by interpolation of values between the two $\theta_{\rm obs}$ bin values that bracket the specified value of $\theta_{\rm obs}$. The file `mytorus_Mzero_v00.fits` has 31 $\theta_{\rm obs}$ values between $\theta_{\rm obs} = 60^\circ$ and 90° spaced at equal intervals is $\cos\theta_{\rm obs}$ (actually the file `mytorus_Ezero_v00.fits` also has the same intervals). For the $\theta_{\rm obs}$ interval that has one boundary that corresponds to the "edge" of the torus (i.e. if that boundary value is 60° in the default model), the interpolation is problematic. This is because XSPEC will calculate the zeroth-order spectrum by forming a weighted sum of both obscured and unobscured continua. An example of such a spectrum is shown in Fig. 5.3, for $N_{\rm H} = 10^{24}$ cm^{-2} and $\theta_{\rm obs} = 61.0^\circ$. The black, solid curve shows the anomalous spectrum when the *mtable* is used in XSPEC, and the red curve shows the exact spectrum calculated for $\theta_{\rm obs} = 61.0°$ by interpolating on the line-of-sigh column density *using the etable model file*. The boundaries of the bin at the edge of the torus are at $60°$ and $61.09°$, so any value of $\theta_{\rm obs}$ greater than $61.09°$ will *not* show the anomaly. The *mtable* model file `mytorus_Mzero_v00.fits` has the default "soft" lower limit on $\theta_{\rm obs}$ set at $61.1°$. In some ways the anomalous behavior near the edge of the torus may actually be desirable, since the boundary of a real toroidal reprocessor in an AGN is unlikely to be as clearly defined as that of a mathematical torus. In other words, the spectrum from a "fuzzy" surface may actually be more physically relevant. Note that the form of the anomalous spectrum is similar to partial covering.

5.4.3 WARNING: Respect the valid energy range of the model

It is important to realize that the provided XSPEC tables for the zeroth-order continuum will extend to an energy of 500 keV, *even though some of the tables for the scattered continuum have termination energies lower than 500 keV*. Although this may sound self-evident, it is vitally critical that you do not extend the energy range of a spectral fit to energies above E_T for *any* component of the MYTORUS model, even if it is only for plotting purposes, because the results will not be correct. It is also important to manually restrict the lower energy bound of the data because XSPEC will assign incorrect values to the model outside the valid energy range. Currently the lower bound for which the MYTORUS model is valid is 0.5 keV. Even if you have correctly set the energy bounds for your data, the "plot model" command in XSPEC may plot the model outside the valid energy range, resulting in spectral plots that are incorrect (see §8.5).

Chapter 6

MYTorus Scattered Continuum

6.1 General Properties

In this chapter we describe the scattered continuum component of the MYTORUS model. We begin with the basic definitions and terminology, summarizing the main features of the scattered continuum spectrum. We also discuss some general issues pertaining to the application of a self-consistent model of X-ray reprocessing to real data. In this section we summarize the salient Monte Carlo results. In §6.2 we discuss some more practical issues involved in turning the Monte Carlo results into a useable spectral-fitting model. We also describe the specific details of the implementation of the spectral-fitting model.

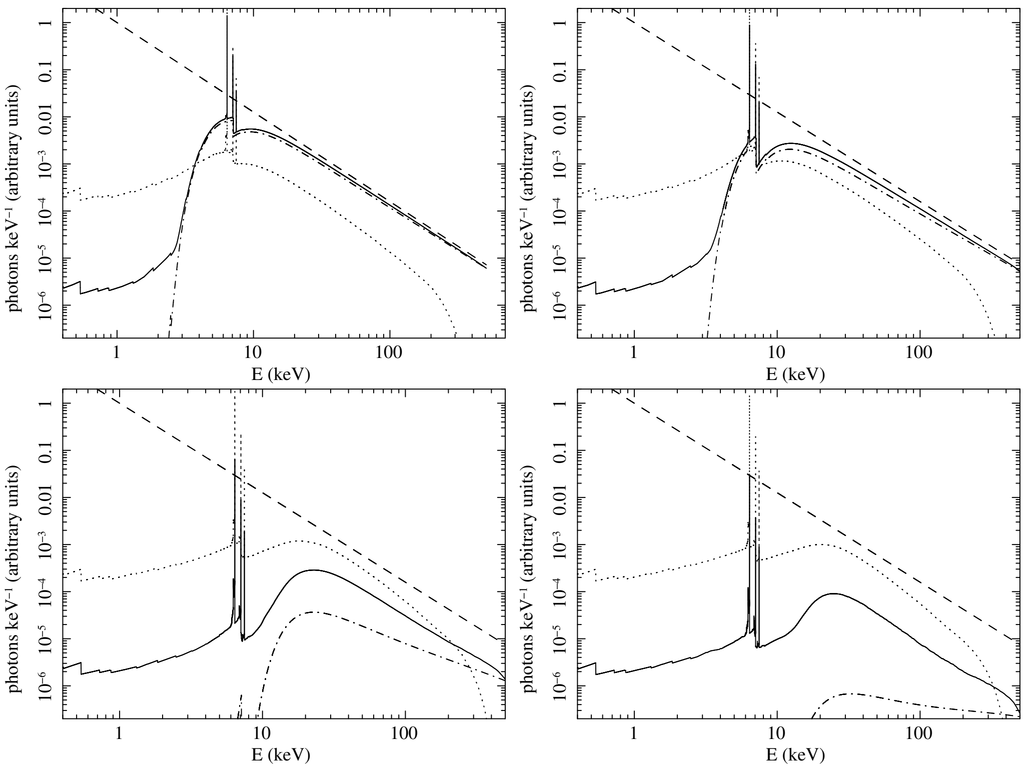

Figure 6.1: Scattered spectra for an input power-law continuum with $\Gamma = 1.9$ (*dashed line*). Spectra for the face-on $\theta_{\rm obs}$ bin (bin 1 – *dotted curves*; see Table 3.1) and edge-on $\theta_{\rm obs}$ bin (bin 10 – *solid curves*; see Table 3.1) are shown for $N_{\rm H} = 5 \times 10^{23}$ cm^{-2} (*top left*), 10^{24} cm^{-2} (*top right*), 5×10^{24} cm^{-2} (*bottom left*), and 10^{25} cm^{-2} (*bottom right*). The zeroth-order spectrum for the edge-on $\theta_{\rm obs}$ bin is shown (*dot-dashed curves*) for each $N_{\rm H}$.

6.1.1 Dependence on model parameters

The scattered continuum depends primarily on $N_{\rm H}$, $\theta_{\rm obs}$, the shape of the intrinsic continuum, the torus opening angle (and therefore covering factor), and element abundances. For the MYTORUS model with a half-opening angle of 60° ($[\Delta\Omega/(4\pi)] = 0.5$) and the cosmic abundances of Anders & Grevesse (1989), we show just a few of the scattered spectra for illustration in Fig. 6.1. The spectra for the face-on $\theta_{\rm obs}$ bin (bin 1 – *dotted curves*; see Table 3.1) and edge-on $\theta_{\rm obs}$ bin (bin 10 – *solid curves*; see Table 3.1) for $N_{\rm H} = 5 \times 10^{23}$ cm^{-2} (*top left*), 10^{24} cm^{-2} (*top right*), $5 \times$

10^{24} cm^{-2} (*bottom left*), and 10^{25} cm^{-2} (*bottom right*) for an input power-law continuum with $\Gamma = 1.9$ (*dashed line*) are shown. The zeroth-order spectrum for the edge-on $\theta_{\rm obs}$ bin is also shown (*dot-dashed curves*) for each $N_{\rm H}$. From Fig. 6.1 we see that the Compton hump, as expected, begins to appear for column densities of $\sim 10^{24}$ cm^{-2} and higher and is stronger for the edge-on spectra (solid curves) since the photons that are scattered into the edge-on angle bin in general pass through a larger Compton depth than those that are scattered into the face-on angle bin (dotted). The relative magnitude of the Compton hump depends on Γ as well as $N_{\rm H}$, the hump being stronger for flatter incident spectra. The relative magnitude of the Compton hump also depends on the inclination angle of the torus, but for lines of sight that do not intercept the structure, the dependence is weak.

At low energies, although the continuum is diminished, we do not see a complete extinction of the spectrum. At high energies, we find that the spectra for the face-on angle bin cut off at lower energies than those for the edge-on angle bin. In our particular geometry, photons emerging in the face-on angle bins are dominated by back-scattering (which incurs the largest Compton energy shifts). There is also a diluting effect due to the zeroth-order contribution to the reprocessed spectra in the angle bins that intercept the torus. For $N_{\rm H}$ less than $\sim 5 \times 10^{24}$ cm^{-2}, the edge-on reprocessed spectra are dominated by the zeroth-order photons above a few keV. However, we find that, for high $N_{\rm H}$ values (greater than $\sim 5 \times 10^{24}$ cm^{-2}) even the edge-on high-energy spectra are cut off below E_T (since the zeroth-order photons no longer dominate).

The scattered spectrum contains imprints of the atomic absorption cross sections in terms of discontinuities at the K and L absorption-edge threshold energies. For the abundant elements these "edge depths" may be measurable. However, *the absorption-edge depths cannot be trivially related to the element abundances*. This is because the edge depth in the emergent spectrum depends on the detailed radiative transfer, and therefore on the geometry, inclination angle, and column density (amongst other factors). Further discussion of the dependence of the scattered continuum on covering factor and element abundances can be found in Chapter 9.

The Fe K absorption edge can be a very prominent feature of the scattered and zeroth-order spectrum, especially for a Compton-thick X-ray reprocessor. The observed Fe K edge shape (as a function of energy) in the scattered continuum is affected by Compton scattering (this is not of course not true of the zeroth-order continuum). Compton scattering broadens the Fe K edge feature and gives it additional structure. Moreover, when the column density of the torus is much larger than $\sim 5 \times 10^{24}\,\mathrm{cm}^{-2}$, edge-on inclination angles give a scattered continuum spectrum that is strongly biased for the escape of back-scattered photons, so that the *apparent* discontinuity in the Fe K edge is shifted *down* in energy by $\sim 0.1 - 0.2$ keV.

6.1.2 The low-energy scattered continuum

As described in §3.2.2, the scattered spectrum below a certain energy is calculated using an elastic scattering approximation and therefore does not contain any energy shifts. In our implementation, we utilize a cross-over energy between the elastic approximation and the full Monte Carlo results of 5.0 keV. The scattered spectra in Fig. 6.1 illustrate the continuity between calculations in the two energy ranges (see Murphy & Yaqoob 2009 for more details).

6.1.3 The high-energy scattered spectrum

As described in §3.2.3, the scattered spectra show an observed high-energy cutoff that occurs at lower energies than the termination energy of the intrinsic power law continuum, due to Compton downscattering (see Fig. 6.1). Green's functions must be calculated for incident energies that are higher than the highest energy that we require for the final spectra since photons are always down-shifted in energy in the electron rest-frame. Recall that the zeroth-order spectrum also imparts additional curvature to the high-energy spectrum (see Chapter 5). The current implementation of the MYTORUS model assumes an intrinsic power-law continuum that terminates at a particular energy, E_T. Although this is an approximation, it is likely to be more physical than an exponentially-decaying power law (see §3.2.3). For the current table model implementation, there are several tables that are available for the scattered continuum, each with a different power-law termination energy (see §6.2.5). You should not introduce an additional, ad hoc, exponential cutoff to the model because it is not physical and it does not preserve the self-consistency of the MYTORUS model.

You may notice some "kinks" or "waviness' in parts of the scattered continuum at the highest energies. This is partly due to the abrupt termination energy of the incident continuum (E_T) but it is also partly due to physics and to that extent, the features are *not* artifacts. The absolute shift in the energy of a photon undergoing Compton scattering, when its energy is comparable to $m_e c^2$, can be a large fraction of $m_e c^2$. For example, a photon with initial energy 500 keV can be shifted in energy by 0 to 331 keV *in a single scattering*, depending on the scattering angle. Contrast this with a maximum shift of ~ 0.1 keV for a photon with an initial energy of 5 keV. This means that a large energy band from E_T, down to $E_T/[1 + (2E_T/511)]$, may be dominated by the first Compton scattering, even for Compton-thick matter. At lower energies, the spectrum may be "smoothed out" by multiple scatterings but at the highest energies there are no photons from higher energies to smooth out the spectrum in that way. To some extent, a more gradual cutoff in the incident spectrum would give a smoother scattered spectrum, but the highest energy portion will *still* be dominated by the first scattering, simply because the energy shifts are such a large fraction of $m_e c^2$ in that regime.

6.2 Implementation as a spectral-fitting model

In this section we describe specific choices and methods employed to implement the MYTORUS scattered continuum Monte Carlo results as part of a spectral-fitting model. The first major decision is whether the spectral-fitting implementation should calculate integrated spectra "on the fly" from the "raw" Monte Carlo results or whether it should interpolate on pre-calculated spectra. The former would allow the use of arbitrary input spectra but the latter would not. However, calculation of integrated spectra "on the fly" is much slower than interpolation of pre-calculated spectra. Eventually, the MYTORUS model will be implemented with both options but for the current release we chose the method of interpolation of pre-calculated spectra for the sake of fast run-times for spectral-fitting and error analysis.

The interpolation of pre-calculated spectra could be implemented either as a code or directly as an interpolation table, such as an XSPEC "`atable`" model. The latter has faster run times and this is the form of the implementation in the current release of MYTORUS.

No matter which of the above methods is actually used in the implementation, there are several important issues that are common to any method and these are discussed in turn below.

6.2.1 Energy offset

No instrument has a perfectly calibrated energy scale. The Fe K absorption edge in the MYTORUS can be a significant feature of the spectrum and this can make a spectral fit very sensitive to errors in the energy scale calibration. It is not only sharp absorption features that are sensitive to the energy scale calibration but the shape of the broadband spectrum itself can also be sensitive to the calibration.

An energy offset parameter for the scattered continuum could in principle be included in implementations of MYTORUS for spectral fitting applications. If the spectral-fitting model is implemented as a code the energy offset can be applied as a function of one or more additional model parameters. However, if the model is implemented as an interpolation of pre-calculated spectra then an energy offset has to be included as another dimension of the interpolation table, or else different tables must be made for different offsets.

There are other reasons why an energy offset might be needed. That is, the absorption edge energies in the actual data for an astrophysical source may not in fact correspond to the rest-frame energies used in the Monte Carlo calculations. Our Monte Carlo results were calculated assuming strictly neutral material. In reality the material may be mildly ionized, resulting in slightly different energies for atomic features such as absorption edges or emission lines. Doppler and/or gravitational shifts can also change the edge energies. Obviously, in any of these scenarios, the physics in the model will no longer be correct and the allowance of an energy shift in the spectrum would simply be an empirical compensation. Currently, there is not yet a provision in the MYTORUS model to include an energy offset for the scattered continuum (although it is included for the fluorescent-line spectrum – see Chapter 7). In the meantime, one can adjust the cosmological redshift parameter to mimic an energy offset, although this is not a satisfactory solution. It is *your* responsibility to determine whether the errors incurred in the process of applying an empirical energy shift are tolerable, given the statistical quality of the data, the particular application, and any other relevant factors.

6.2.2 Velocity broadening

As already mentioned, the Monte Carlo results do not include kinematic information but this can be implemented in an empirical fashion by convolving the emission-line spectrum with a velocity-broadening function. This is of course not physical but this does not compromise the application for which MYTORUS is designed. In fact, for most applications it may be possible to neglect velocity broadening of the scattered continuum altogether (but in general it cannot be neglected for the fluorescent emission-line spectrum– see Chapter 7). It is your responsibility to determine whether the errors incurred in neglecting velocity broadening of the scattered continuum are tolerable, given the statistical quality of the data, the particular application, and any other relevant factors.

If the spectral-fitting model is implemented as a code, the velocity-broadening could be calculated "on the fly" with a suitable function included in the code. If the spectral-fitting model is implemented as an interpolation on pre-calculated spectra, the velocity-broadening could either be included in the pre-calculated spectra, or it could be applied using a convolution function that is intrinsic to the spectral-fitting package.

6.2.3 Relative normalization of the scattered spectrum

The scattered continuum in the MYTORUS model is calculated on the basis of a specific set of assumptions (see Chapter 3 for details). In particular, the current calculations pertain only to a toroidal half-opening opening angle of $60°$ and the cosmic element abundances of Anders & Grevesse (1989). In practice real data from a real source of course will not correspond to the exact assumptions that went into the model, including the exact toroidal geometry (see also §2.6). In particular, literal use of our Monte Carlo results implicitly assumes a steady-state situation so that there are no time lags affecting the magnitude of the scattered continuum relative to the incident continuum normalization *and* relative to the zeroth-order continuum. Therefore an extra degree of freedom is needed to fit real data. For this purpose, we use a free parameter which is a scalar that is a multiplicative factor applied to the scattered continuum. Throughout this manual we refer to this relative normalization factor for the scattered spectrum as A_S. This parameter, A_S, changes the normalization of the scattered continuum relative to the intrinsic continuum and the zeroth-order continuum, compared to the steady-state value calculated with all of the model assumptions described in Chapter 3. Future enhancements to MYTORUS will include extension of the parameter space for the toroidal opening angle and element abundances. However, even with such extensions, time delays between the scattered continuum and intrinsic continuum variations in real data may affect the relative normalization, A_S. Such time delays are not known *a priori* and cannot be determined from a single time-averaged spectrum. Time delays between the scattered continuum and intrinsic continuum variations can only be determined by time-resolved spectroscopy of extensive data sets from targeted monitoring campaigns, and these are extremely rare. Complicating matters further is the fact that the zeroth-order continuum does *not* suffer the time delays that the scattered continuum does, but rather follows variations in the intrinsic continuum. Direct spectral deconvolution of the scattered and zeroth-order continua may in practice be difficult or impossible.

In summary, the relative normalization parameter A_S embodies a wealth of unknown and degenerate information in a single scalar value. The interpretation of any derived range for A_S from spectral-fitting to real data is therefore highly non-trivial. It is your responsibility to carefully interpret the meaning of A_S taking due consideration of all relevant information pertaining to the data and to the astrophysics of the source in question. In particular, *under no circumstances should the parameter A_S be interpreted directly as a measure of the covering factor or relative element abundance*. In most cases a unique interpretation of A_S will not be possible without other supporting evidence and you should not hesitate to say so in a paper.

As tempting as it may be, *do not try to derive a relationship or correspondence between A_S and the standard "reflection fraction" (R) of the disk-reflection model*. Such a comparison is devoid of physical meaning. Also note that R is *not* a covering factor either, contrary to statements in hundreds of papers in the literature. You cannot simply scale the reflection spectrum up and down and call the scaling factor a covering factor. The magnitude and shape of the scattered spectrum depends on many factors, including geometry, abundances, angular distribution of the illuminating continuum, and the inclination angle of the system. In fact the disk-reflection spectrum itself depends on the disk-inclination angle, so R itself depends on the inclination angle. However, the disk inclination angle has no meaning in the context of modeling obscuration in AGN, yet it is usually fixed at some arbitrary value and hidden from view. In such a scenario the column density in the model cannot be related to R, even though R is supposed to model scattering in the absorber, because the model is not physical. Therefore, there is absolutely no value in trying to relate A_S to R.

6.2.4 Watch out for "wild normalization" situations

It is important to understand that if the data do not have any signature of the intrinsic continuum, no model can ever constrain the normalization of the scattered continuum relative to the intrinsic continuum. This can happen in a variety of situations. For example, if the observed spectrum of an astrophysical source is dominated by reflection in the bandpass of the instrument, the intrinsic continuum may not be observable anywhere in the bandpass. In such situations, there will be too many normalizations in the model, leading to severe degeneracy and ultimately a lack of convergence of spectral fits. One of the normalization parameters of the model will then have to be frozen. In general it is not possible to know *a priori* if the scattered to intrinsic continuum normalization ratio cannot be constrained by the data so several iterations of examining the behavior of the various fit parameters may be necessary.

6.2.5 Table-model implementation (power-law continuum)

In this section we describe the table-model implementation of the scattered continuum (currently the only implementation). The implementation is in the form of XSPEC "`atables`" which contain pre-calculated spectra for a power-law incident continuum. There is no velocity broadening included in the scattered continuum, although it could be included using a convolution function intrinsic to the spectral-fitting package. For most applications however, velocity broadening will not be necessary for the scattered continuum. The relative normalization parameter, A_S, is implemented using the XSPEC model component CONSTANT, applied as a multiplicative factor. It is important to realize that for the purpose of interpolation of the spectra, the midpoints of the cosines of the $\theta_{\rm obs}$ angle bins are used, and this involves special treatment of the boundaries of the first and last angle bins (see §3.1.1). The full set of scattered continuum tables currently available is given in Table 6.1.

Table 6.1: Scattered continuum XSPEC tables

Name	Termination Energy $(E_T)^a$ (keV)
`mytorus_scatteredH500_v00.fits`	500
`mytorus_scatteredH400_v00.fits`	400
`mytorus_scatteredH300_v00.fits`	300
`mytorus_scatteredH200_v00.fits`	200
`mytorus_scatteredH160_v00.fits`	160
`mytorus_scatteredH100_v00.fits`	100

[a] The termination energy of the incident power-law continuum.

Symbolically, the scattered spectrum in the tables will be represented throughout this manual as

$$\mathrm{MYTS}(z, A_i, \Gamma_i, N_{\mathrm{H}}, \theta_{\mathrm{obs}}, E) \tag{6.1}$$

where z is the cosmological redshift, N_{H} is the equatorial column density, θ_{obs} is the inclination angle, and E is the energy (in keV). The incident continuum could in principle be composed of more than one power-law spectrum and $A_i E^{-\Gamma_i}$ is the $i\mathrm{th}$ continuum component. If A_i is in units of $\mathrm{photons\ cm^{-2}\ s^{-1}\ keV^{-1}}$ the scattered spectrum will have the same units. In other words, if A_i in the scattered spectrum is forced to be the same parameter as the normalization of the incident power-law continuum component, MYTS (i.e. the model table spectrum) will be correctly normalized for that continuum. In XSPEC language, the parameter A_i in the incident continuum model component must be tied together with the parameter A_i that is the scattered continuum table model normalization.

The table model for the scattered continuum, plus the relative normalization of the scattered continuum (A_S) can be set in XSPEC as follows.

```
XSPEC>mo constant*( atable{mytorus_scatteredH500_v00.fits} )
```

Here the XSPEC `atable` `mytorus_scatteredH500_v00.fits` is used an example (see Table 6.1). A more detailed and practical description of how to set up the model with other model components is given in Chapter 8.

6.2.5.1 Energy resolution and statistical accuracy

The energy resolution of the scattered continuum is not simply a matter of examining the energy bin widths in the `atables`. Rather, the energy resolution depends on the details of the original Monte Carlo calculations that were used to make the tables. The effective energy resolution trades off against the desired statistical accuracy and is a complex relationship. Obviously, one could increase statistical accuracy by sacrificing energy resolution. The worst-case scenario for both energy resolution and statistical accuracy is that of a torus with an edge-on inclination, with a column density of $10^{25}\ \mathrm{cm}^{-2}$, below 10 keV. In that case the statistical accuracy is 3% or better for an energy resolution in the range 1–100 eV. The energy resolution is variable in order to treat absorption edges, especially those due to the Fe and Ni K-shells, for which the resolution is ~ 10 eV. However, recall that below 5.0 keV and elastic scattering approximation is used, which limits the energy resolution to $\Delta E \sim 2[E(\ \mathrm{keV})]^2$ eV (i.e. $\sim 0.5 - 50$ eV in the 0.5–5.0 keV band). The absorption edges below 5.0 keV should be more smeared than they are in the model, over an energy interval of ΔE. At high energies the effective energy resolution in our model becomes increasingly more coarse, being ~ 20 keV at 500 keV. We point out that for column densities less than $10^{25}\ \mathrm{cm}^{-2}$ and lower inclination angles, the statistical accuracy of MYTORUS can be an order of magnitude or more *better* than the worst-case scenario outlined above. In addition, the energy-resolution of the fluorescent emission-line spectrum in the MYTORUS model is even better than that of the scattered continuum (see §7.3.5.1). We have ensured that below 10 keV the energy resolution of MYTORUS is suitable for the calorimeters to be flown on *Astro-H*, and that above 10 keV the energy resolution is sufficiently good for data from past and current high-energy X-ray detectors, as well as those planned for the foreseeable future.

6.2.6 WARNING: Respect the valid energy range of the model

We repeat the warning from §5.4.3 since it is so critical. That is, the provided XSPEC tables for the zeroth-order continuum will extend to an energy of 500 keV, *even though some of the tables for the scattered continuum have termination energies lower than 500 keV*. Although this may sound self-evident, it is vitally critical that you do not extend the energy range of a spectral fit to energies above E_T for *any* component of the MYTORUS model, even if it is only for plotting purposes, because the results will not be correct. It is also important to manually restrict the lower energy bound of the data because XSPEC will assign incorrect values to the model outside the valid energy range. Currently the lower bound for which the MYTORUS model is valid is 0.5 keV. Even if you have correctly set the energy bounds for your data, the "plot model" command in XSPEC may plot the model outside the valid energy range, resulting in spectral plots that are incorrect (see §8.5).

Chapter 7

MYTorus Fluorescent Emission-Line Model

7.1 General Issues

In this chapter we describe the fluorescent emission-line components of the MYTORUS model. We begin with the basic definitions and terminology, summarizing the main features of the fluorescent emission-line spectrum. We also discuss some general issues pertaining to the application of a self-consistent model of X-ray reprocessing to real data, when line emission is included. In §7.2 we summarize the salient Monte Carlo results, giving some key plots of EW and flux of the emission lines as a function of the other model parameters. In §7.3 we discuss some more practical issues involved in turning the Monte Carlo results into a useable spectral-fitting model. We then describe the specific details of the implementation of the spectral-fitting model.

7.1.1 The zeroth-order emission-line components

The zeroth-order components of the fluorescent emission lines refer to line photons that escape without any interaction with the medium that they were created in. Although they are emitted by atoms/ions isotropically, the angular distribution of the emerging zeroth-order line photons in general depends on the geometry, unless the medium is optically-thin to the line photons. The zeroth-order line photons constitute the majority of photons in an emergent emission line (see §7.1.3), and they all have the same energy in the Monte Carlo results because they have not interacted with the medium. When velocity broadening is applied to the zeroth-order line emission the photon energies are of course modified to reflect the distribution of the broadening function. Most of the fluorescent X-ray emission line measurements in the literature that have been modeled with simple Gaussian functions correspond to the zeroth-order of the emission line. However, depending on the spectral resolution of the instrument, some of the measured flux of this line core may include a contribution from the Compton-scattered line photons (or Compton shoulder) since the scattered line component consists of photons with a range of energies going all the way up to the zeroth-order line energy. In most cases the latter energy corresponds to the centroid energy of the line core. In the MYTORUS spectral-fitting model the zeroth-order and scattered components of the emission lines are strictly tied to the other parameters of the model ($N_{\rm H}$, $\theta_{\rm obs}$, Γ) so there is no need for an extra parameter as is the case for ad hoc models. If you compare the results of applying the MYTORUS to results in the literature that were obtained using ad hoc models you must scrutinize precisely which components of a line were actually measured with the ad hoc model.

7.1.2 The scattered components of the emission lines (Compton shoulders)

We refer to fluorescent emission-line photons that escape the medium after at least one interaction as the scattered component of the line. Compton scattering shapes the energy distribution of the scattered line photons. However, the final scattered line profile depends on the geometry, orientation, and column density distribution of the medium because the escape probabilities after scattering may be highly directional. Some details of the scattered line profiles as a function of other parameters in the MYTORUS model are discussed further in §7.1.4.3 and §7.2.6. In cold matter, the scattered photon distribution resulting from the nth scattering has a spread in energy from E_0 (the rest-frame zeroth-order line energy), down to $511/[(511/E_0\ {\rm keV})+2n]$. The number of photons in each scattering is diminished compared to the number in the previous scattering. The exact dependence of the relative number of photons in each scattering, and therefore of the measurable width of the scattered distribution, is a function of the other model parameters. If the optical depth to absorption of the line photons is much greater or much less than unity, only the first scattering may dominate. Even for intermediate optical depths the third scattering is negligible in flux compared to the first scattering.

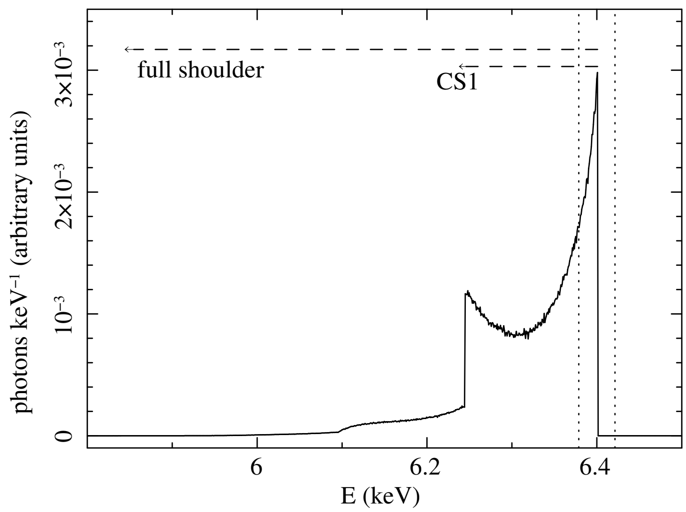

Figure 7.1: Illustration of our definition of the Compton shoulder for an emission line, compared with the definition "CS1". Our definition ("full shoulder" in the figure) includes ALL of the scattered line flux, but "CS1" includes all of the flux only in the energy interval of the first scattering. Note that no velocity broadening has been applied. When velocity broadening is applied, ad hoc models will confuse line flux from the zeroth-order and the Compton shoulder (regardless of definition). The vertical dotted lines in the figure illustrate this by showing the energy width corresponding to $\pm 1000 \text{ km s}^{-1}$ either side of the zeroth-order line energy. See §7.1.2 and §7.1.3 for further details.

The scattered component of the emission line is often referred to as the "Compton shoulder". However, this term has been used in the literature in more than one way, which could be confusing if you are not aware of the distinctions. The most common usage refers to the line flux between the energy extrema of the first scattering, *which includes some contributions from all scatterings*. This is because the contributions from different scattering orders cannot be measured separately. This is referred to as "CS1" (e.g. see Matt 2002), and is illustrated in Fig. 7.1. Some literature may refer to only the first scattering as the Compton shoulder, but this of course can only have a theoretical context. A third definition, which is the one we use here and throughout this manual, is that the Compton shoulder includes *all* of the scattered line flux, for all scatterings (see Fig. 7.1). This is the most appropriate definition for a model such as MYTORUS which self-consistently calculates the zeroth-order and the entire scattered line profile and does not allow the relative fluxes of the two components to vary in an ad hoc fashion. Definitions such as CS1 are not necessary because there is no need to fit the scattered component of an emission line separately. You should *not* attempt to compare fits with MYTORUS with results in the literature that were obtained by fitting Gaussian model components to the Compton shoulder. The Compton shoulder is not Gaussian and for most of the parameter space it is not even approximately Gaussian.

7.1.3 Ratio of the Compton shoulder flux to the zeroth-order line flux

The relative magnitude of the zeroth-order and scattered line components is fixed by the physics and geometry and you will not be able to vary it in the MYTORUS model. Nevertheless, in order for you to see at a glance whether the Compton shoulder is going to be important for your particular data set, in Fig. 7.2 we show that ratio of the Compton shoulder flux to the zeroth-order line flux as a function of N_H for two different values of $\theta_{\rm obs}$ (corresponding to the face-on and edge-on inclination angle bins –see Table 3.1). The calculations in Fig. 7.2 were made for an incident power-law continuum with a photon index of 1.9. It can seen that the ratio peaks at $N_H \sim 2 - 3\ \times 10^{24}\ {\rm cm}^{-2}$, reaching a maximum of ~ 0.29 (face-on), and ~ 0.37 (edge-on). See Matt (2002) for discussion and details concerning other geometries.

Note that the relative strength of the Compton shoulder compared to the zeroth-order emission line and the shape of the Compton shoulder *do* depend on the shape of the incident continuum spectrum. For a power-law continuum, this means that the scattered to zeroth-order flux ratio and the shape of the Compton shoulder depend on the power-law photon index, Γ (see §7.1.4.3).

In practice it may not actually be possible to observationally distinguish the zeroth-order component of an emission line from its Compton shoulder. The finite energy resolution of the instrument and/or the velocity broadening (of all the emission-line components) may confuse the two components of a line. This is illustrated in Fig. 7.1 with dotted lines placed at energies corresponding to $\pm 1000\ {\rm km\ s}^{-1}$ either side of the zeroth-order line energy. Having said that, you will never need to observationally distinguish between the zeroth-order component of an emission line from its Compton shoulder with the MYTORUS model because it is a self-consistent model. However, it is important to be aware of the "mixing" for the interpretation of spectral-fitting results.

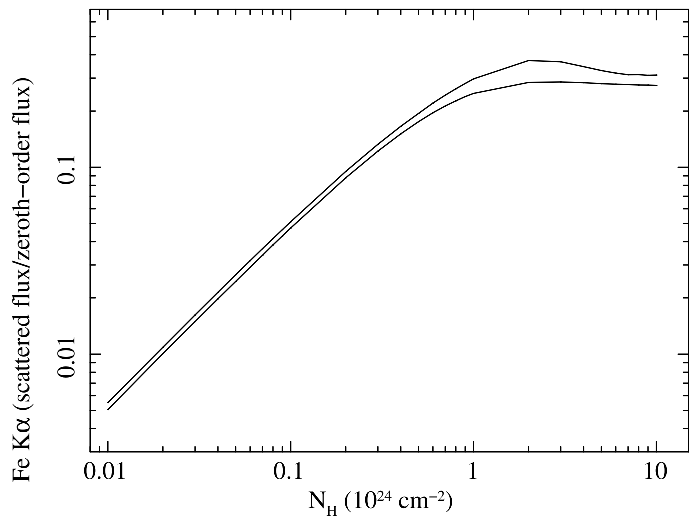

Figure 7.2: The ratio of the scattered flux to the zeroth-order flux in Fe Kα line from the MYTORUS model, as a function of $N_{\rm H}$ (for $\Gamma = 1.9$). Shown are curves for the face-on (lower curve) and edge-on (upper curve) inclination-angle bins. See text in §7.1.3 for further details.

7.1.4 The fluorescent line EW and flux

7.1.4.1 The line EW and flux in ad hoc models

When modeling emission lines with ad hoc model components such as Gaussian functions, the line intensity and EW are free parameters, independent of any model parameters that pertain to the continuum or obscuring matter that produces the line. Aside from the fact that one loses physical information when the emission-line components are ad hoc, great care must be exercised in obtaining the correct EW and flux of the emission lines. This is partly because one is forced to place an emission-line model component either "behind" or "in front of" the absorbing matter (that presumably produces the line). For example, in the language of XSPEC, one could have:

```
phabs(1) * ( zpo(2) + zga(2) )
```

or

```
( phabs(1) * zpo(2) ) + zga(2) .
```

The second expression above gives the *observed* line EW and flux. However, neither of the two expressions reflect that fact that the emission line is produced *in* the absorber. Moreover, the absorber component in the expressions above refers only to the line-of-sight to the line-emitting matter. Although the second expression does give a measure of the observed line flux, it is not possible to relate it to the absorber component in the same expression without invoking some assumptions (which may not be true). It should also be clear that the term "intrinsic line flux" or "absorption-corrected line flux" is entirely an artifact of applying an ad hoc model because it has no physical meaning. *Only the observed line flux has a physical meaning*. Therefore, the first expression above does not give a line flux that is physical. It may not give the correct EW either because, in a physical context, the X-ray continuum is attenuated by all of the column density in the line-of-sight, but if the line is created in the absorber, the line should not be simply attenuated by the line-of-sight column density.

Self-consistent models such as MYTORUS do not, by definition, suffer from the problem described above. The reason why we have explained the problem with ad hoc models is that you should be aware of it if you attempt to compare line EWs and fluxes from MYTORUS with measurements in the literature because the latter will most likely have been derived using ad hoc model components. The EWs and fluxes of emission lines in sources that are Compton-thin in the *line-of-sight* may not necessarily be comparable between ad hoc models and MYTORUS either, because the material *out of the line-of-sight* may be Compton-thick (see discussion in §2.1).

7.1.4.2 The line EW and flux in self-consistent models

In an X-ray reprocessing model in which the fluorescent emission lines are produced self-consistently, the line EWs and fluxes are completely determined by the other parameters of the model. Therefore in a spectral-fitting context there is, strictly speaking, no need for the emission-line fluxes to be free parameters. However, in many situations, one may need to know the values of the EW and flux explicitly for a particular line. The spectral-fitting model would then have to be able to calculate the line EW and flux using the other model parameters and display the values to the screen. If the spectral-fitting model is implemented as a set of interpolation tables, it may be problematic for the spectral-fitting package. In §7.3.5 we describe the table-model implementation of the MYTORUS emission-line spectrum in more detail and explain how the line EW and flux can be calculated.

7.1.4.3 Dependence of the line EW, flux, and Compton shoulder on other model parameters

The dependence of the fluorescent emission-line EWs and fluxes on the system geometry, orientation, column density, covering factor, and element abundances may be easily appreciated but it may not be so obvious that the EWs and fluxes also depend on the *shape of the incident X-ray spectrum*. This is because high-energy photons in the continuum can down-scatter many times and eventually be absorbed by an inner shell and produce a fluorescent emission line. A hard continuum will have a greater proportion of high-energy photons that are available for this than a steeper continuum. Therefore a hard spectrum will produce a fluorescent line with a larger flux than a steeper spectrum. In addition, since high-energy photons will penetrate deeper into the medium than lower energy photons, the fluorescent lines produced by hard spectra will have contributions from deeper in the medium. This affects the relative strength (compared to the zeroth-order line) and shape of the Compton shoulder.

The dependence of the zeroth-order Fe Kα emission-line flux on the incident continuum photon energy is illustrated in Fig. 7.3 which shows, for several column densities, the number of Fe Kα emission-line photons resulting from continuum photons centrally injected into the toroidal medium at an energy E, as a fraction of the number of line photons resulting from continuum photons injected at 7.2 keV (just above the Fe K absorption edge). It can be seen that the $N_H = 5 \times 10^{24}$ cm^{-2} (dotted line, Fig. 7.3), and $N_H = 10^{25}$ cm^{-2} (upper solid line, Fig. 7.3) curves break and become flatter above ~ 50 keV. In fact, at 50 keV the contribution to the Fe Kα line flux is still as high as 10% of the contribution at the energy of 7.2 keV. Further discussion can be found in Yaqoob *et al.* (2010).

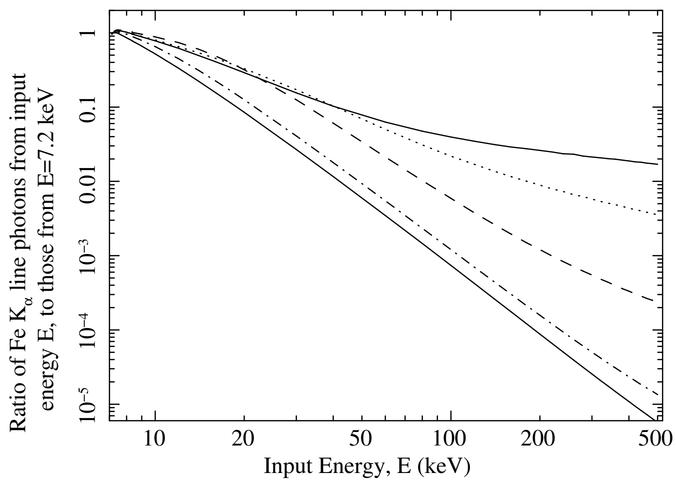

Figure 7.3: Monte-Carlo results for the number of escaping Fe Kα emission-line photons resulting from monoenergetic continuum photons injected into the toroidal X-ray reprocessor of Murphy & Yaqoob (2009) at an energy E, as a fraction of the number of line photons resulting from continuum photons injected at 7.2 keV. Results are shown for five equatorial column densities: 2×10^{23} cm^{-2} (lower solid curve), 5×10^{23} cm^{-2} (dot-dashed curve), 2×10^{24} cm^{-2} (dashed curve), 5×10^{24} cm^{-2} (dotted curve), and 10^{25} cm^{-2} (upper solid curve). For each column density, the Fe Kα line photons that escape the medium are summed over all escape directions. As the reprocessor becomes more and more Compton-thick, the relative contribution to the Fe Kα line from high-energy continuum photons increases significantly.

If the incident spectrum is a power-law continuum the emission-line EW, flux, and shape of the Compton shoulder will have a dependence on the power-law photon index, Γ. This dependence, and the dependence on the other model parameters mentioned above, will be discussed in more detail in §7.2. We caution that the dependence of the fluorescent emission-line parameters and Compton shoulder on Γ should not be neglected for the Fe Kα line and lines at higher energies. Fluorescent lines with lower energies than the Fe Kα line are not yet included in MYTORUS. The dependence of lower energy lines on Γ is less severe because the fractional energy shift per scattering of continuum photons is less.

7.2 Monte Carlo results

In this section we give some graphical results from the Monte Carlo simulations that will be useful for understanding the general behavior of the EWs and fluxes of the fluorescent emission lines as a function of inclination angle, and column density for an incident power-law continuum with a photon index of Γ. Note that all of the results here correspond to the default model with a half-opening angle of 60° (or $[\Delta\Omega/(4\pi)] = 0.5$), and the cosmic abundances of Anders & Grevesse (1989). The effects of variations in the latter two assumptions will be discussed in Chapter 9. It is also important to realize that the EW versus $N_{\rm H}$ curves give the line EW with respect to the sum of the scattered continuum from the torus and the zeroth-order continuum (for non-intercepting angle bins the latter is just the intrinsic continuum). If you include additional continuum components in a spectral-fitting model (i.e. not from MYTORUS), the observed EW will change.

Finally, we do not give extensive discussions of the graphical results in this section–see Murphy & Yaqoob (2009) and Yaqoob *et al.* (2010) for further details.

7.2.1 The fluorescent emission lines

The MYTORUS model is based on Monte Carlo simulations that currently include three fluorescent emission lines (more will be added in the future). The included emission lines are shown in Table 7.1.

Note that for neutral Fe, the Kα emission consists of two lines, Kα_1 at 6.404 keV and Kα_2 at 6.391 keV, with a branching ratio of 2:1 (e.g. see Bambynek *et al.* 1972). In the Monte Carlo simulations these were treated as a single line with an energy of 6.4008 keV (corresponding to the weighted mean energies of the Fe Kα_1 and Fe Kα_2 lines). For the MYTORUS spectral-fitting model, the two components of the Fe Kα line are *reconstructed* using the above branching ratio and line energies (see §7.3). The energy difference between the two components is small enough to neglect the differences in opacities and the error incurred in this procedure is too small to impact fitting even *Astro-H* data. The ratio of Fe Kβ/ Fe Kα assumed in the model is 0.135 (see Murphy & Yaqoob 2009, and references therein). This ratio cannot be changed in the MYTORUS spectral-fitting model, although in the table model implementation (§7.3.5), tables with different Fe Kβ/

Fe Kα ratios may be available in the future.

Further details on the atomic data used for the emission lines can be found in Murphy & Yaqoob (2009) and references therein.

Table 7.1: Fluorescent emission lines in the Monte Carlo code.

Element	Line	K-edge energy (keV)	Line Energy (keV)
Fe	Kα	7.1240	6.4008
Fe	Kβ	7.1240	7.0580
Ni	Kα	8.3480	7.4720

Note that the emission-line spectra produced by the Monte Carlo code do not include velocity broadening. Kinematic effects must be applied to the Monte Carlo results. The particular approximations and methods employed will be discussed in §7.3.

7.2.2 Fe Kα line EW and flux

In Fig. 7.4, we show the zeroth-order EWs of the Fe Kα line as a function of the column density of the torus, N_{H}. The lower curves show the results for the non-intercepting angle bins, with ascending θ_{obs} bins from top to bottom, and the upper curves show the results for the intercepting angle bins, with ascending θ_{obs} bins from bottom to top (see Table 3.1).

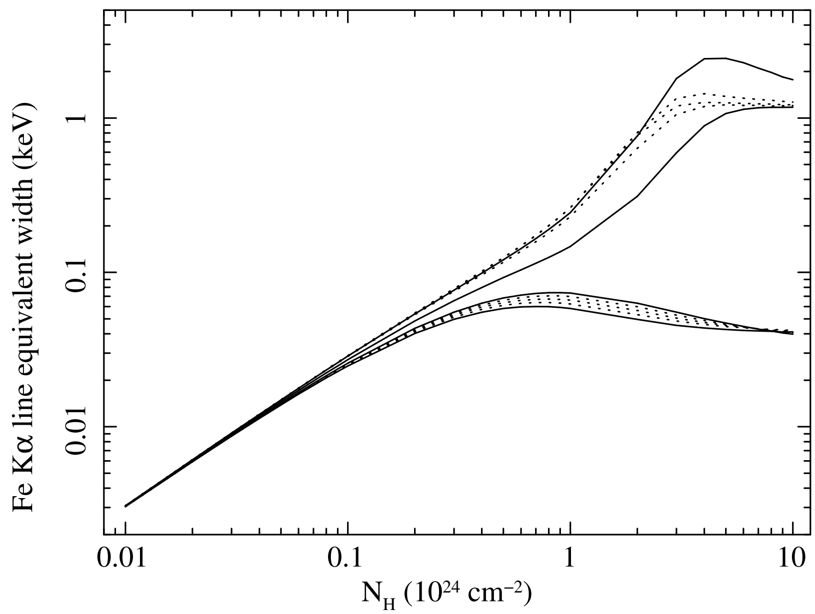

Figure 7.4: The Fe Kα line equivalent width (EW) versus N_{H} for $\Gamma = 1.9$ as calculated from the Monte Carlo code. Curves are shown for each of the 10 θ_{obs} bins (see Table 3.1). The lower set of curves corresponds to bins 1–5 (lines-of-sight that do not intercept the torus) and the upper set of curves corresponds to bins 6–10 (lines-of-sight that intercept the torus). The *solid* curves correspond to the two boundary θ_{obs} bins (bins 1, 5, 6, and 10; see Table 3.1) for both intercepting and non-intercepting cases.

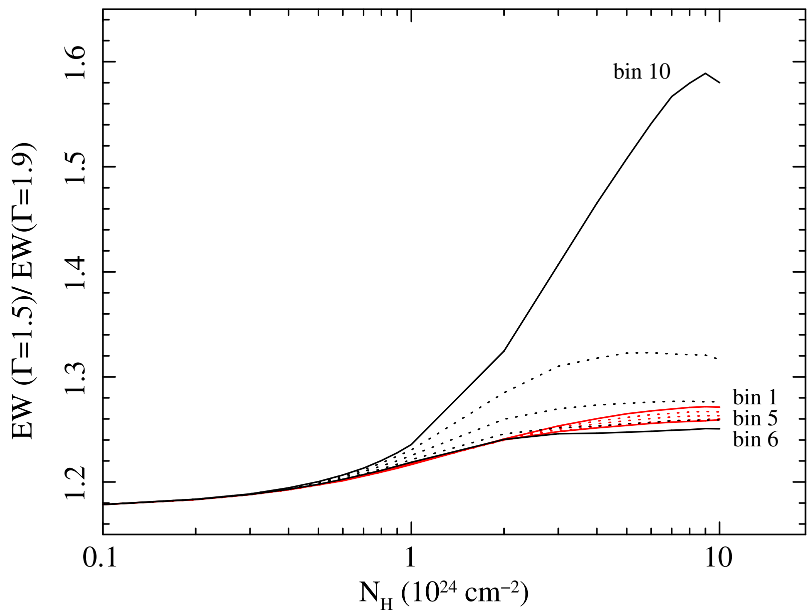

Figure 7.5: Ratio of the Fe Kα line equivalent width (EW) for $\Gamma = 1.5$ to the corresponding EW for $\Gamma = 1.9$, versus $N_{\rm H}$. Curves are shown for each of the 10 $\theta_{\rm obs}$ bins (see Table 3.1). The set of red curves corresponds to bins 1–5 (lines-of-sight that do not intercept the torus) and the set of black curves corresponds to bins 6–10 (lines-of-sight that intercept the torus). The *solid* curves correspond to the two boundary $\theta_{\rm obs}$ bins (bins 1, 5, 6, and 10; see Table 3.1) for both intercepting and non-intercepting cases.

Fig. 7.5 shows the ratio of the Fe Kα line EW for $\Gamma = 1.5$ to the corresponding EW for $\Gamma = 1.9$, versus $N_{\rm H}$, for each of the inclination-angle bins (see Table 3.1). In the Compton-thick regime, the ratio of the EWs for the non-intercepting angle bins can be as large as ~ 1.3 and for the intercepting bins it can be as large as ~ 1.6.

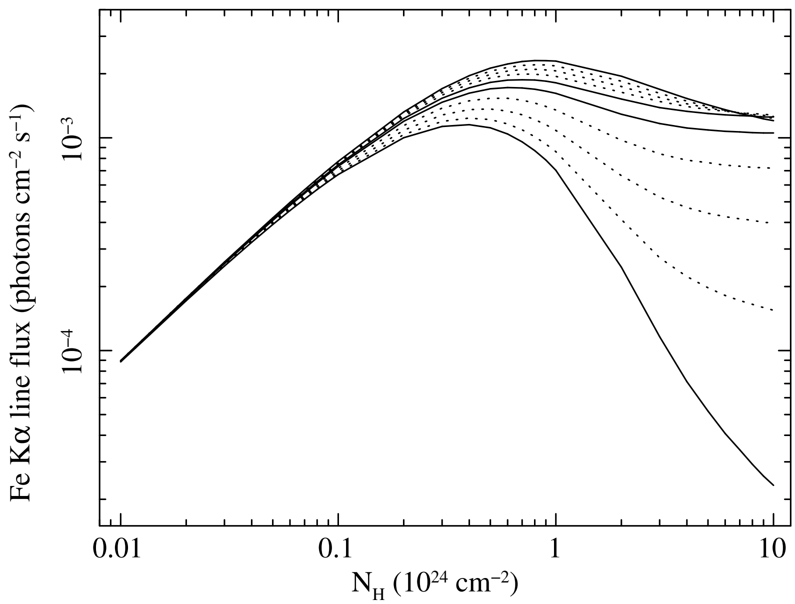

Figure 7.6: The Fe Kα line flux versus $N_{\rm H}$ for $\Gamma = 1.9$ as calculated from the Monte Carlo code. Curves are shown for each of the 10 $\theta_{\rm obs}$ bins (see Table 3.1). The upper set of curves corresponds to bins 1–5 (lines-of-sight that do not intercept the torus) and the lower set of curves corresponds to bins 6–10 (lines-of-sight that intercept the torus). The *solid* curves correspond to the two boundary $\theta_{\rm obs}$ bins (bins 1, 5, 6, and 10; see Table 3.1) for both intercepting and non-intercepting cases. The normalization of the line flux corresponds to a power-law incident continuum that has a normalization at 1 keV of $1 \ {\rm photon \ s^{-1} \ cm^{-2} \ keV^{-1}}$.

In Fig. 7.6 we show the Fe Kα line flux versus $N_{\rm H}$ for $\Gamma = 1.9$, for each of the 10 inclination angle bins (see Table 3.1). The upper set of curves corresponds to bins 1–5 (lines-of-sight that do not intercept the torus) and the lower set of curves corresponds to bins 6–10 (lines-of-sight that intercept the torus). Further discussion of the Fe Kα line flux can be found in Yaqoob *et al.* (2010).

7.2.3 Fe Kβ line EW and flux

In Fig. 7.7, we show the zeroth-order EWs of the Fe Kβ line as a function of the column density of the torus, $N_{\rm H}$. The lower curves show the results for the non-intercepting angle bins, with ascending $\theta_{\rm obs}$ bins from top to bottom, and the upper curves show the results for the intercepting angle bins, with ascending $\theta_{\rm obs}$ bins from bottom to top (see Table 3.1).

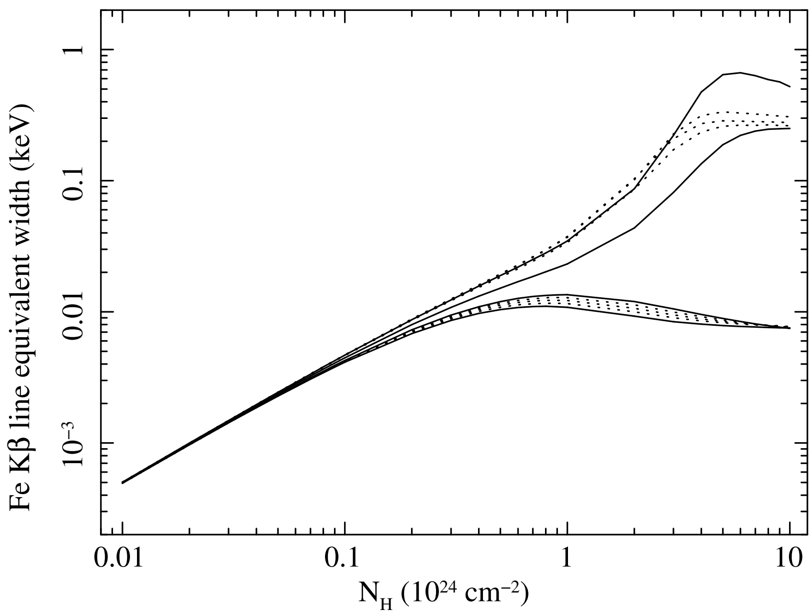

Figure 7.7: The Fe Kβ line equivalent width (EW) versus $N_{\rm H}$ for $\Gamma = 1.9$. Curves are shown for each of the 10 $\theta_{\rm obs}$ bins (see Table 3.1). The lower set of curves corresponds to bins 1–5 (lines-of-sight that do not intercept the torus) and the upper set of curves corresponds to bins 6–10 (lines-of-sight that intercept the torus). The *solid* curves correspond to the two boundary $\theta_{\rm obs}$ bins (bins 1, 5, 6, and 10; see Table 3.1) for both intercepting and non-intercepting cases.

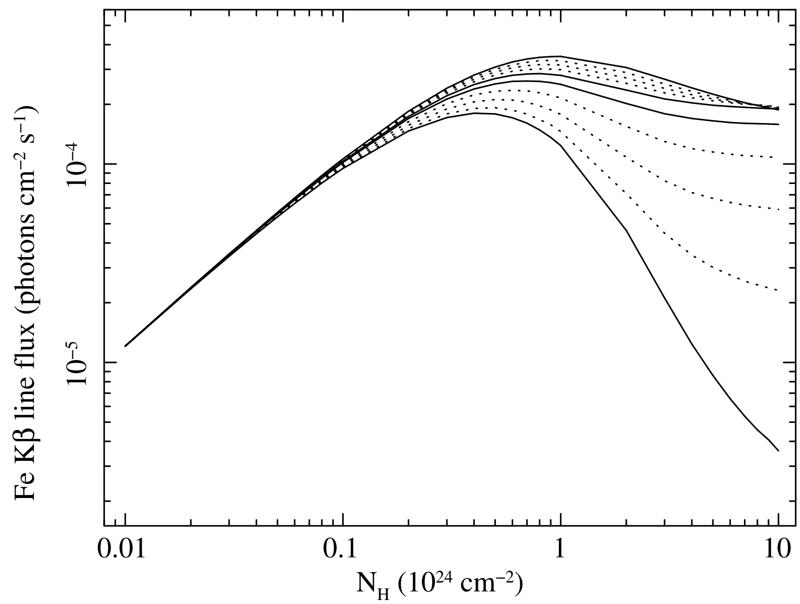

Figure 7.8: The Fe Kβ line flux versus $N_{\rm H}$ for $\Gamma = 1.9$ as calculated from the Monte Carlo code. Curves are shown for each of the 10 $\theta_{\rm obs}$ bins (see Table 3.1). The upper set of curves corresponds to bins 1–5 (lines-of-sight that do not intercept the torus) and the lower set of curves corresponds to bins 6–10 (lines-of-sight that intercept the torus). The *solid* curves correspond to the two boundary $\theta_{\rm obs}$ bins (bins 1, 5, 6, and 10; see Table 3.1) for both intercepting and non-intercepting cases. The normalization of the line flux corresponds to a power-law incident continuum that has a normalization at 1 keV of $1\ \rm photon\ s^{-1}\ cm^{-2}\ keV^{-1}$.

In Fig. 7.8 we show the Fe Kβ line flux versus $N_{\rm H}$ for $\Gamma = 1.9$, for each of the 10 inclination angle bins (see Table 3.1). The upper set of curves corresponds to bins 1–5 (lines-of-sight that do not intercept the torus) and the lower set of curves corresponds to bins 6–10 (lines-of-sight that intercept the torus).

7.2.4 Ni Kα line EW and flux

In Fig. 7.9, we show the zeroth-order EWs of the Ni Kα line as a function of the column density of the torus, $N_{\rm H}$. The lower curves show the results for the non-intercepting angle bins, with ascending $\theta_{\rm obs}$ bins from top to bottom, and the upper curves show the results for the intercepting angle bins, with ascending $\theta_{\rm obs}$ bins from bottom to top (see Table 3.1).

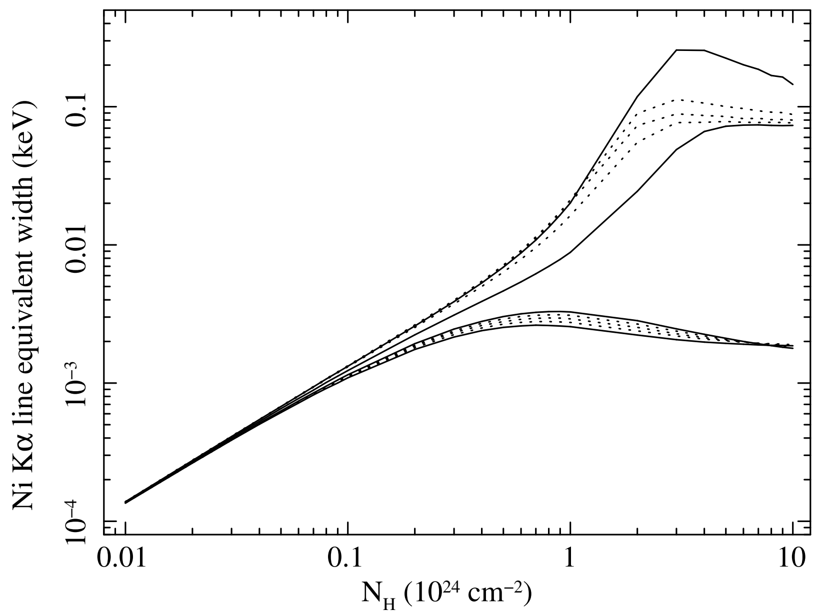

Figure 7.9: The Ni Kα line equivalent width (EW) versus $N_{\rm H}$ for $\Gamma = 1.9$ as calculated from the Monte Carlo code. Curves are shown for each of the 10 $\theta_{\rm obs}$ bins (see Table 3.1). The lower set of curves corresponds to bins 1–5 (lines-of-sight that do not intercept the torus) and the upper set of curves corresponds to bins 6–10 (lines-of-sight that intercept the torus). The *solid* curves correspond to the two boundary $\theta_{\rm obs}$ bins (bins 1, 5, 6, and 10; see Table 3.1) for both intercepting and non-intercepting cases.

In Fig. 7.10 we show the Ni Kα line flux versus $N_{\rm H}$ for $\Gamma = 1.9$, for each of the 10 inclination angle bins (see Table 3.1). The upper set of curves corresponds to bins 1–5 (lines-of-sight that do not intercept the torus) and the lower set of curves corresponds to bins 6–10 (lines-of-sight that intercept the torus).

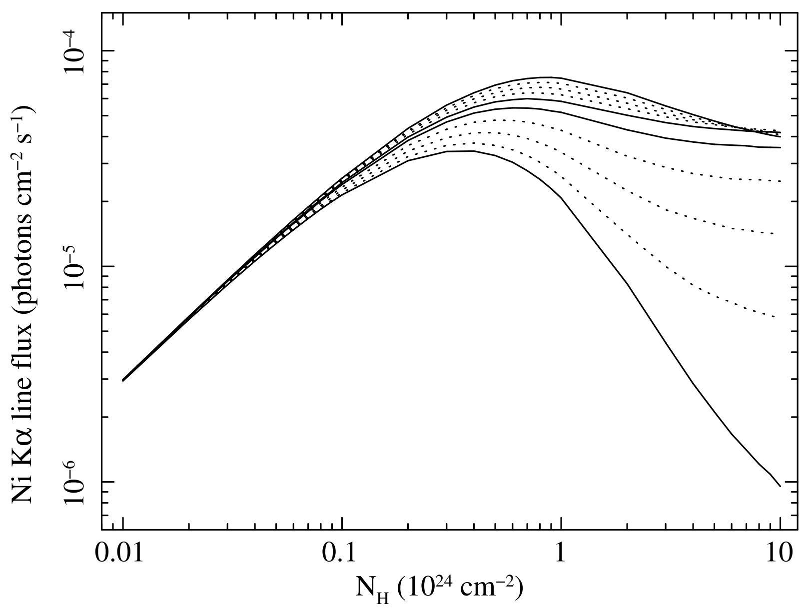

Figure 7.10: The Ni Kα line flux versus $N_{\rm H}$ for $\Gamma = 1.9$ as calculated from the Monte Carlo code. Curves are shown for each of the 10 $\theta_{\rm obs}$ bins (see Table 3.1). The upper set of curves corresponds to bins 1–5 (lines-of-sight that do not intercept the torus) and the lower set of curves corresponds to bins 6–10 (lines-of-sight that intercept the torus). The *solid* curves correspond to the two boundary $\theta_{\rm obs}$ bins (bins 1, 5, 6, and 10; see Table 3.1) for both intercepting and non-intercepting cases. The normalization of the line flux corresponds to a power-law incident continuum that has a normalization at 1 keV of $1~{\rm photon~s^{-1}~cm^{-2}~keV^{-1}}$.

7.2.5 Fe Kβ / Fe Kα EW and flux ratios

Although the Fe Kβ/Fe Kα ratio assumed in the Monte Carlo calculations was 0.135, the Fe Kβ/Fe Kα ratio of emission-line photons that *escape* from the torus may be higher than this when the medium is optically-thick to absorption of either of the two emission lines. This is because of the differential absorption opacities for the Fe Kα and Fe Kβ lines. Fig. 7.11 shows the ratio of the line fluxes, Fe Kβ/Fe Kα, for photons escaping in the face-on and edge-on angle bins, as a function of $N_{\rm H}$. An incident power-law continuum with a photon index of $\Gamma = 1.9$ was used for the plot. Note that the flux ratio is different to the EW ratio of Fe Kβ/Fe Kα, since the continuum opacity at the two line energies is different. There is some dependence of the Fe Kβ/Fe Kα ratio (both in flux and EW) on Γ for high column densities (greater than $\sim 5 \times 10^{24}$ cm^{-2} or so) and high inclination angles.

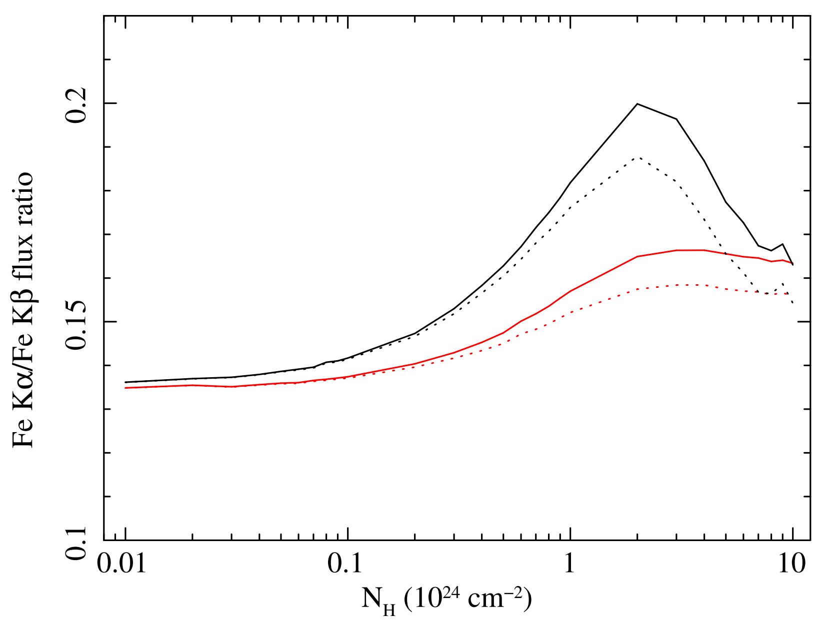

Figure 7.11: The Fe Kβ/Fe Kα *flux* ratio for photons escaping the torus in the face-on (red) and edge-on (black) angle bins as a function of $N_{\rm H}$, for $\Gamma = 1.9$. The dotted curves correspond to the ratio of zeroth-order line components only and the solid curves correspond to the ratio of the total line fluxes including all scatterings.

7.2.6 The shapes of the Compton shoulders

The shape of the Compton shoulder of a fluorescent emission-line escaping from the torus has a dependence on the column density and inclination angle of the torus. It is also affected by the shape of the incident continuum spectrum (including the termination energy), the covering factor (or opening angle), and element abundances. Fig. 7.12 and Fig. 7.13 illustrate the shapes of the Compton shoulder for a power-law incident continuum with $\Gamma = 1.9$, for five column densities (10^{22}, 10^{23}, 10^{24}, 5×10^{24}, and 10^{25} cm^{-2}) and different inclination angles of the torus. The results shown are for the Fe Kα emission line but the Compton-shoulder shapes are similar (for the same set of model parameters) for the Fe Kβ and Ni Kα emission lines. The Compton shoulder shapes shown in Fig. 7.12 and Fig. 7.13 are from the original Monte Carlo results and have no velocity broadening applied to them (***see** §7.3 for the actual, composite, fluorescent-line spectra that are used in the final spectral-fitting model*). The Compton shoulders are shown in wavelength space in units of the dimensionless Compton wavelength shift with respect to the zeroth-order rest-frame energy of the emission line. In other words, if E is the energy of a line photon, and E_0 is the zeroth-order line energy, $\Delta\lambda = (511 \mathrm{~keV}/E) - (511 \mathrm{~keV}/E_0)$.

Fig. 7.14 shows the Compton shoulder for $N_{\mathrm{H}} = 10^{25}$ cm^{-2} for the face-on and edge-on inclination angle bins, for $\Gamma = 1.5$ and $\Gamma = 2.5$. It can be seen that although the dependence is weak for the face-on angle bin, it is not negligible for the edge-on case. The reason for the dependence on the spectral shape of the incident continuum was explained in §7.1.4.3. The dependence of the Compton shoulder shape on the element abundances and the torus covering factor is currently beyond the scope of this manual.

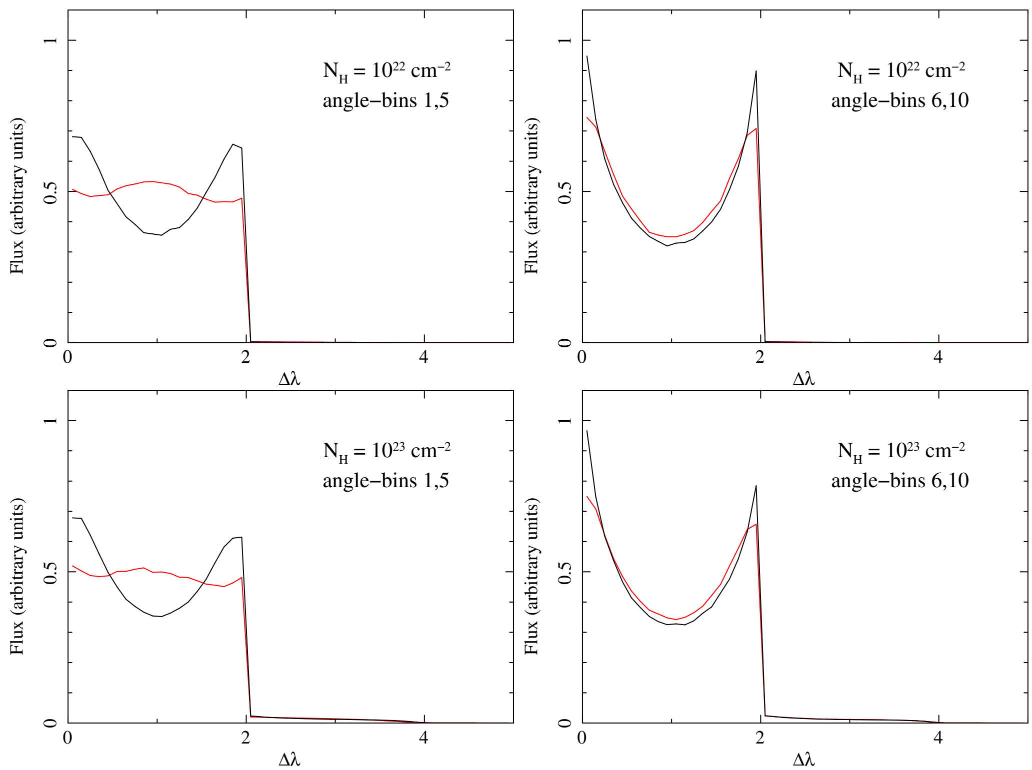

Figure 7.12: The Fe Kα emission-line Compton shoulders for a power-law incident continuum with $\Gamma = 1.9$, for five column densities (from top to bottom, $N_{\rm H} = 10^{22}$, 10^{23}, 10^{24}, 5×10^{24}, and 10^{25} $\rm cm^{-2}$) and different inclination angles of the torus (figure continues on next page). The left-hand panels show the two extreme non-intercepting angle bins #1 (red) and #5 (black), and the right-hand panels show the two extreme intercepting angle bins, #6 (red) and #10 (black)– see Table 3.1. No velocity broadening had been applied. *Note that in order to directly compare the Compton shoulder shapes, the total flux for each shoulder has been renormalized to the same value*. The line flux (in arbitrary units) is plotted against the dimensionless Compton wavelength shift with respect to the zeroth-order rest-frame energy of the emission line, $\Delta\lambda = (511\ {\rm keV}/E) - (511\ {\rm keV}/E_0)$ (see §7.2.6).

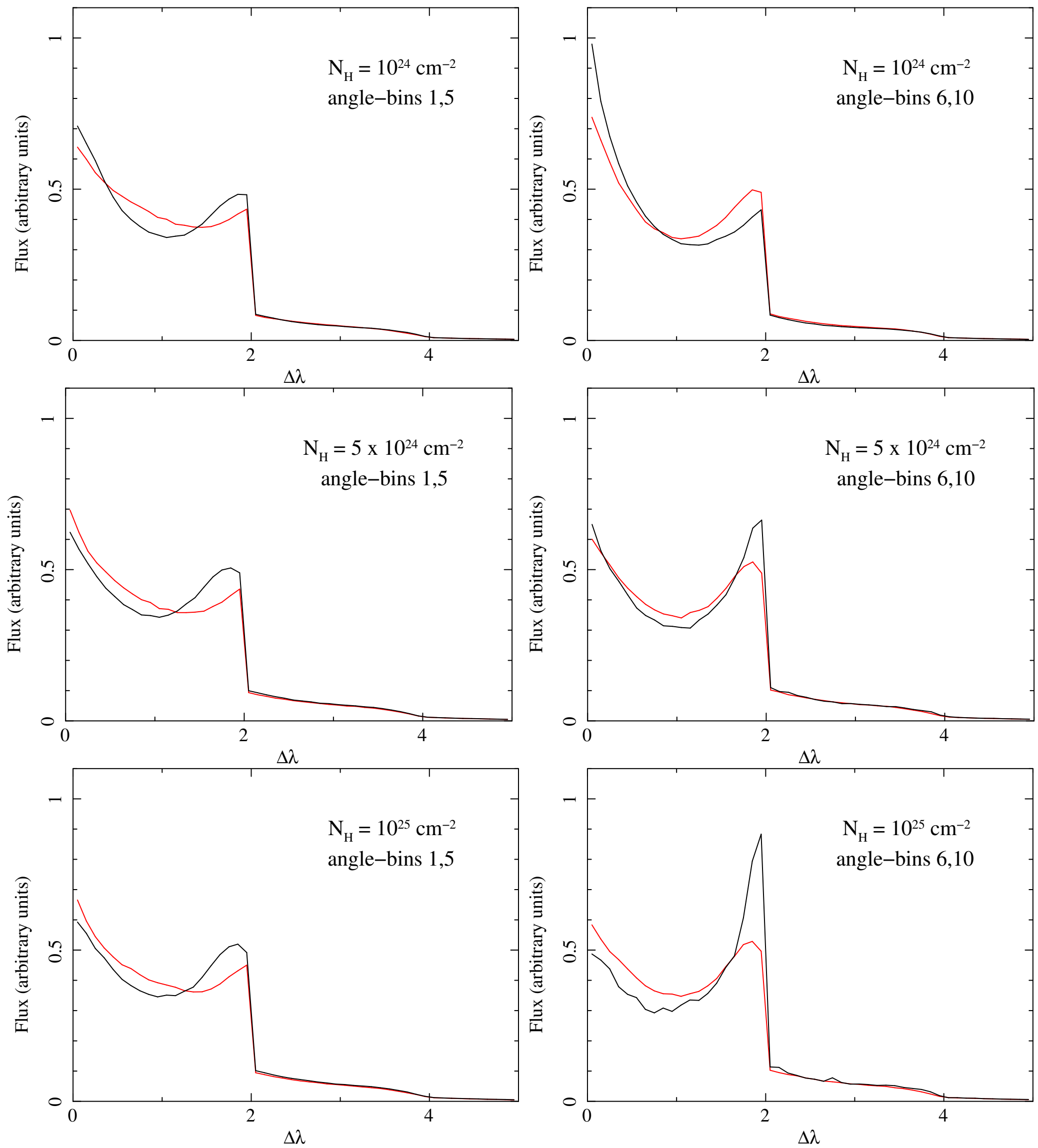

Figure 7.13: Fig. 7.12 *continued*.

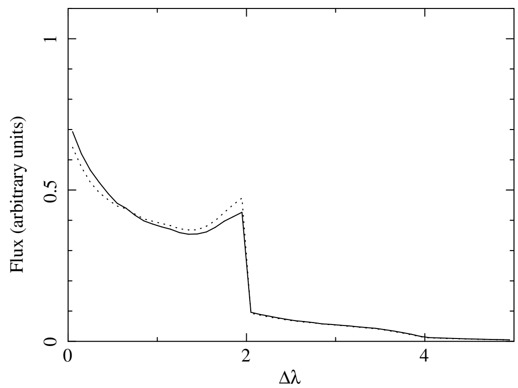

Figure 7.14: The Fe Kα emission-line Compton shoulders for $N_{\rm H} = 10^{25}\ {\rm cm}^{-2}$ and a power-law incident continuum with $\Gamma = 1.5$ (solid), and $\Gamma = 2.5$ (dotted). The *left-hand* panel shows the face-on angle bin and the *right-hand* panel shows the edge-on angle bin. No velocity broadening had been applied. *Note that in order to directly compare the Compton shoulder shapes, the total flux for each shoulder has been renormalized to the same value*. The line flux (in arbitrary units) is plotted against the Compton wavelength shift with respect to the zeroth-order rest-frame energy of the emission line, $\Delta\lambda = (511\ {\rm keV}/E) - (511\ {\rm keV}/E_0)$ (see §7.2.6).

7.3 Implementation as a spectral-fitting model

In this section we describe specific choices and methods employed to implement the fluorescent-line Monte Carlo results as part of a spectral-fitting model. The first major decision is whether the spectral-fitting implementation should calculate integrated spectra "on the fly" from the "raw" Monte Carlo results or whether it should interpolate on pre-calculated spectra. The former would allow the use of arbitrary input spectra but the latter would not. However, calculation of integrated spectra "on the fly" is much slower than interpolation of pre-calculated spectra. Eventually, the MYTORUS model will be implemented with both options but for the current release we chose the method of interpolation of pre-calculated spectra for the sake of fast run-times for the spectral-fitting and error analysis.

The interpolation of pre-calculated spectra could be implemented either as a code or directly as an interpolation table, such as an XSPEC "`atable`" model. The latter has faster run times and this is the form of the implementation in the current release of MYTORUS.

No matter which of the above methods is actually used in the implementation, there are several important issues that are common to any method and these are discussed in turn below.

7.3.1 Splitting of Fe Kα into Fe Kα_1 and Fe Kα_2

As described in §7.2.1 the Fe Kα line flux from the Monte Carlo results is divided amongst the two Fe Kα_1 and Fe Kα_2 components, with the correct branching ratio. This splitting is applied to both the zeroth-order flux *and* the scattered line spectrum (Compton shoulder).

7.3.2 Energy offset

No instrument has a perfectly calibrated energy scale. Therefore, the emission-line centroid energies in MYTORUS need to have some freedom to allow for energy offsets. If the spectral-fitting model is implemented as a code the energy offset can be applied as a function of one or more additional model parameters. However, if the model is implemented as an interpolation of pre-calculated spectra then an energy offset has to be included as another dimension of the interpolation table, or else different tables must be made for different offsets.

There are other reasons why an energy offset is needed. That is, the emission-line centroid energies in the data may not in fact correspond to the rest-frame energies used in the Monte Carlo calculations. Our Monte Carlo results were calculated assuming strictly neutral material. In reality the material may be mildly ionized, resulting in slightly different emission-line centroid energies. Doppler and/or gravitational shifts can also change the emission-line centroid energies, as can asymmetry of the line profiles. Obviously, in any of these scenarios, the physics in the model is no longer appropriate and the allowance of an energy shift in the line spectrum is simply an empirical compensation. It is *your* responsibility to determine whether the errors incurred in the process are tolerable, given the statistical quality of the data, the particular application, and any other relevant factors.

7.3.3 Velocity broadening and the composite line spectrum

The spectra for each included emission line (both zeroth-order and scattered components) are combined into one summed spectrum. As already mentioned, the Monte Carlo results do not include kinematic information so this is implemented in an empirical fashion by convolving the emission-line spectrum with a velocity-broadening function. This is of course not physical but this does not compromise the application for which MYTORUS is designed. This is because it is unlikely that even *Astro-H*, which will have the best spectral resolution for Fe Kα line spectroscopy in the foreseeable future, will be able to distinguish different geometries of the distant-matter Fe Kα line in AGN from its velocity profile (e.g. see Yaqoob *et al.* 1993). In the current implementation of the MYTORUS model we use a Gaussian line-broadening function, even though the line profile is unlikely to be Gaussian, and may even be double-peaked.

If the spectral-fitting model is implemented as a code, the velocity-broadening could be calculated "on the fly" with a function included in the code. If the spectral-fitting model is implemented as an interpolation on pre-calculated spectra, the velocity-broadening could either be included in the pre-calculated spectra, or it could be applied using a convolution function that is intrinsic to the spectral-fitting package.

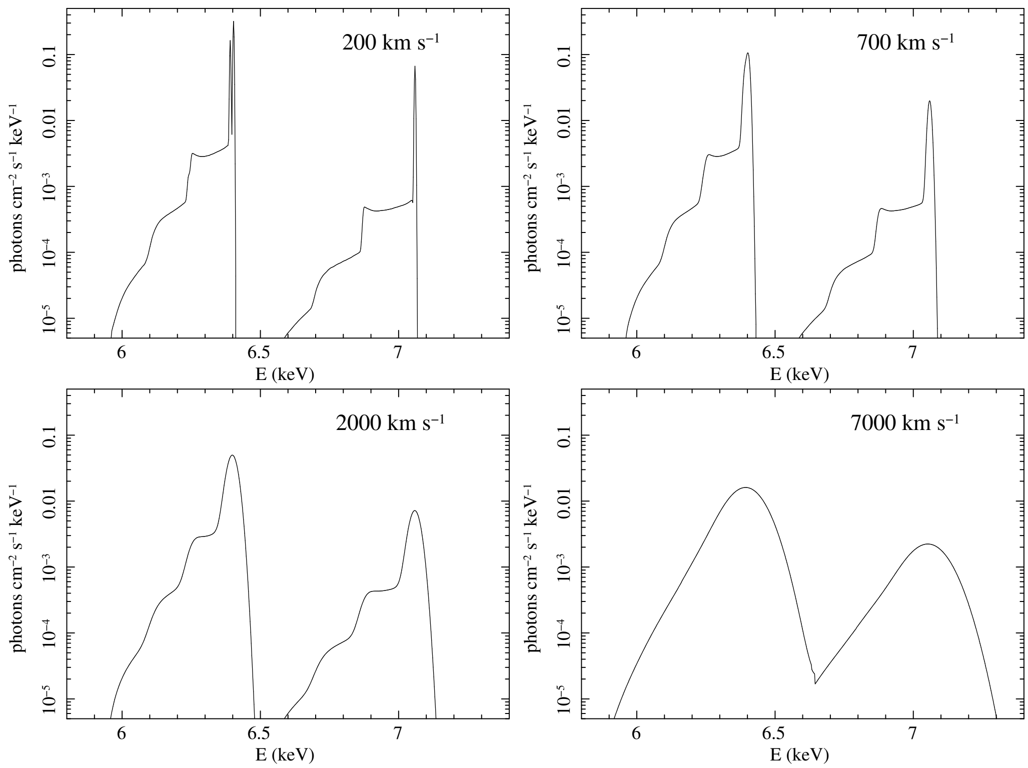

Figure 7.15: Effect of velocity broadening on the fluorescent emission-line spectra consisting of the Fe Kα_1, Fe Kα_2, and Fe Kβ lines. A Gaussian convolution function was applied to the Monte Carlo results for a toroidal X-ray reprocessor with $N_{\rm H} = 10^{24}\ {\rm cm}^{-2}$ (viewed *face-on*), illuminated by a power-law continuum with a photon index of $\Gamma = 1.9$. Four emission-line spectra are shown with a FWHM of 200, 700, 2000, and 7000 $\rm km\ s^{-1}$. *Note the logarithmic flux axis: the narrower core of the line for the smaller velocities makes the flux per keV in the core much higher than that in the Compton shoulder*.

The effect of velocity broadening on the fluorescent line spectrum (composed of the Fe Kα_1, Fe Kα_2, and Fe Kβ lines) is illustrated in Fig. 7.15 ($N_{\rm H} = 10^{24}\ {\rm cm}^{-2}$, face-on), Fig. 7.16 ($N_{\rm H} = 10^{24}\ {\rm cm}^{-2}$, edge-on), Fig. 7.17 ($N_{\rm H} = 10^{25}\ {\rm cm}^{-2}$, face-on), and Fig. 7.18 ($N_{\rm H} = 10^{25}\ {\rm cm}^{-2}$, edge-on). A simple Gaussian function has been employed for convolving emission-line profiles, with a FWHM velocity that is constant with respect to energy. For each column density and inclination-angle pair in Figs. Fig. 7.15 to Fig. 7.18, emission-line spectra are shown for four values of the FWHM, namely $200\ {\rm km\ s^{-1}}$, $700\ {\rm km\ s^{-1}}$, $2000\ {\rm km\ s^{-1}}$, and $7000\ {\rm km\ s^{-1}}$. The value of $200\ {\rm km\ s^{-1}}$ is approximately the velocity resolution that will be achieved in the Fe K band by the calorimeters aboard *Astro-H*. The value of $700\ {\rm km\ s^{-1}}$ is in the regime expected from the classical, parsec-scale torus. The value of 2000 km s^{-1} is approximately the velocity resolution of the *Chandra* high energy grating (HEG) spectrometer in the Fe K energy band. The value of 7000 km s^{-1} is approximately the velocity resolution of CCD detectors in the Fe K band. All emission-line spectra in Fig. 7.15 to Fig. 7.18 were calculated for an incident power-law spectrum with $\Gamma = 1.9$. Note that in some situations velocity broadening can mask the Compton shoulders as distinguishing features of the emission-line spectra even when the X-ray reprocessor is Compton-thick. In fact, at a FWHM of 7000 km s^{-1} *there is no shoulder to the line profile* and the only trace of it is a slight asymmetry in the line profile. An obvious implication of this is that *the Compton shoulder cannot be resolved with CCD detectors* (despite some claims in the literature to the contrary). Also notice that the zeroth-order cores for the Fe Kα_1 and Fe Kα_2 components cannot be distinguished as separate components even for a FWHM as low as 700 km s^{-1} (this has already been pointed out in Yaqoob *et al.* 2001).

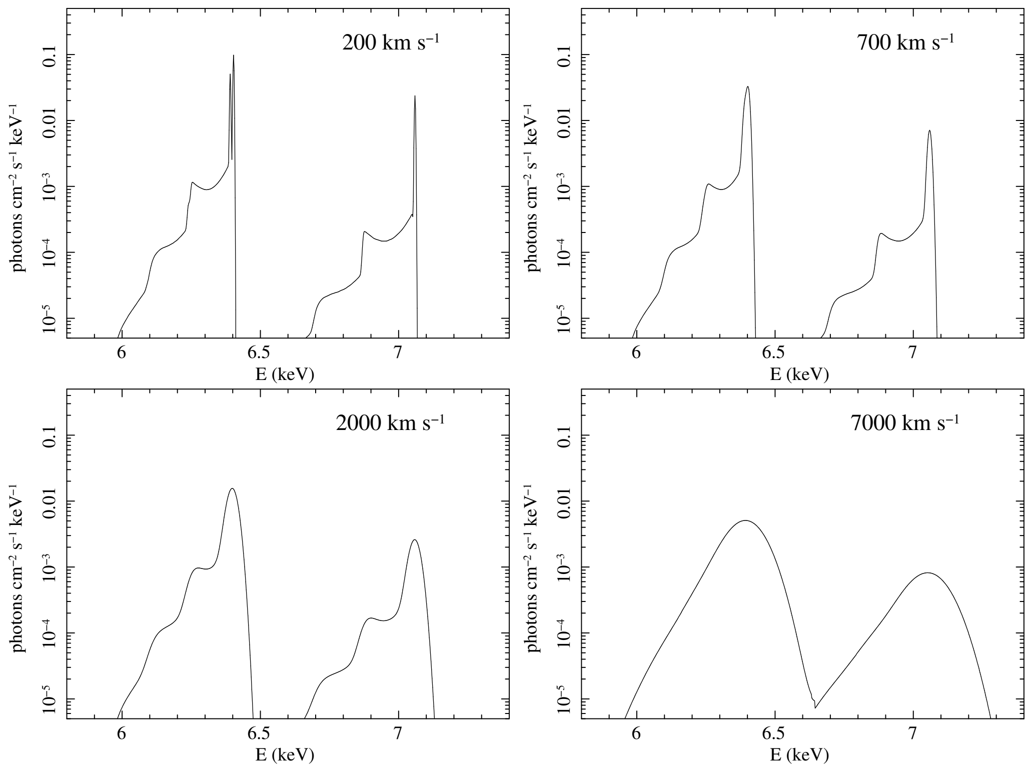

Figure 7.16: Effect of velocity broadening on the fluorescent emission-line spectra consisting of the Fe Kα_1, Fe Kα_2, and Fe Kβ lines. A Gaussian convolution function was applied to the Monte Carlo results for a toroidal X-ray reprocessor with $N_{\rm H} = 10^{24}$ cm^{-2} (viewed *edge-on*), illuminated by a power-law continuum with a photon index of $\Gamma = 1.9$. Four emission-line spectra are shown with a FWHM of 200, 700, 2000, and 7000 $\rm km\,s^{-1}$. *Note the logarithmic flux axis: the narrower core of the line for the smaller velocities makes the flux per keV in the core much higher than that in the Compton shoulder*.

7.3.4 Relative normalization of the emission-line spectrum

The fluxes of the fluorescent emission lines depend, amongst other things, on the torus half-opening angle (or covering factor) and element abundances. The abundances of elements other than the element producing a particular emission line can also affect the flux of that line. The flux of every emission line is of course also directly related to the normalization of the intrinsic, incident continuum. Indeed, in a self-consistent model, the absolute flux of every fluorescent line is *determined* by the incident continuum normalization (amongst other things) and has

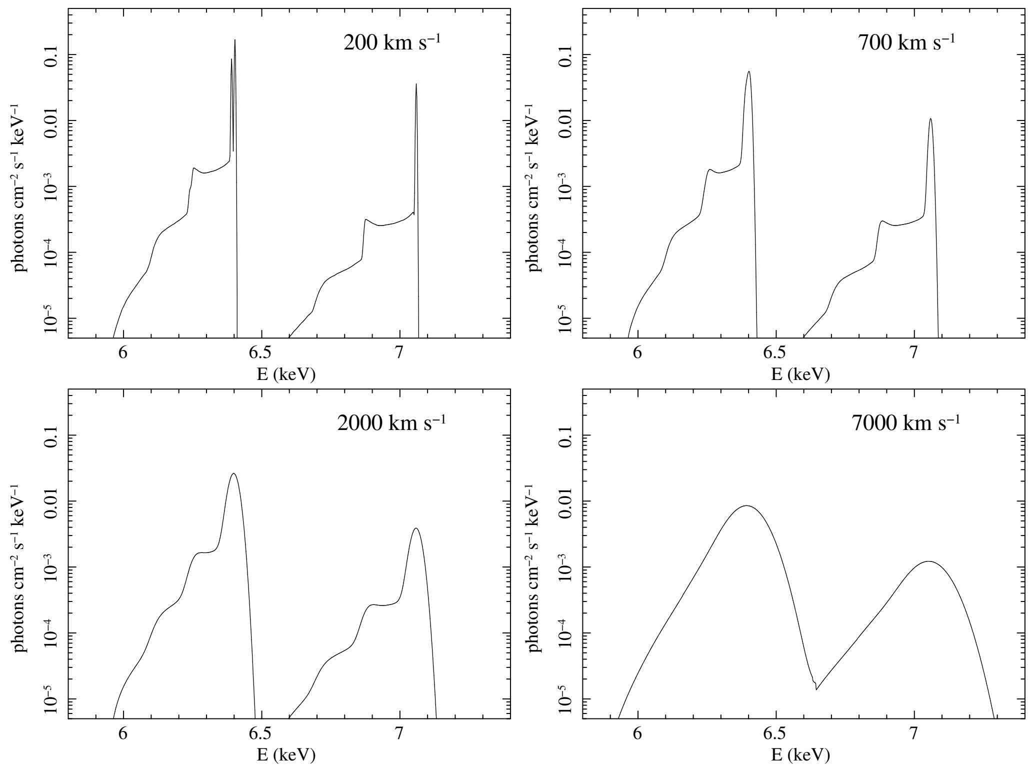

Figure 7.17: Effect of velocity broadening on the fluorescent emission-line spectra consisting of the Fe Kα_1, Fe Kα_2, and Fe Kβ lines. A Gaussian convolution function was applied to the Monte Carlo results for a toroidal X-ray reprocessor with $N_{\rm H} = 10^{25}\ {\rm cm}^{-2}$ (viewed *face-on*), illuminated by a power-law continuum with a photon index of $\Gamma = 1.9$. Four emission-line spectra are shown with a FWHM of 200, 700, 2000, and 7000 ${\rm km\ s}^{-1}$. *Note the logarithmic flux axis: the narrower core of the line for the smaller velocities makes the flux per keV in the core much higher than that in the Compton shoulder.*

no degrees of freedom. In practice, real data from a real source of course will not correspond to the exact assumptions that went into the model, including the exact toroidal geometry (see also §2.6). In particular, literal use of our Monte Carlo results would implicitly assume a steady-state situation so that there are no time lags affecting the fluorescent-line fluxes relative to the incident continuum normalization. Therefore an extra degree of freedom is needed to fit real data. For this purpose, we use a free parameter which is a scalar that is a multiplicative factor *applied to the composite fluorescent-line spectrum*. Throughout this manual we refer to this relative normalization factor for the fluorescent-line spectrum as A_L. Further discussion of how the fluorescent-line fluxes change for departures

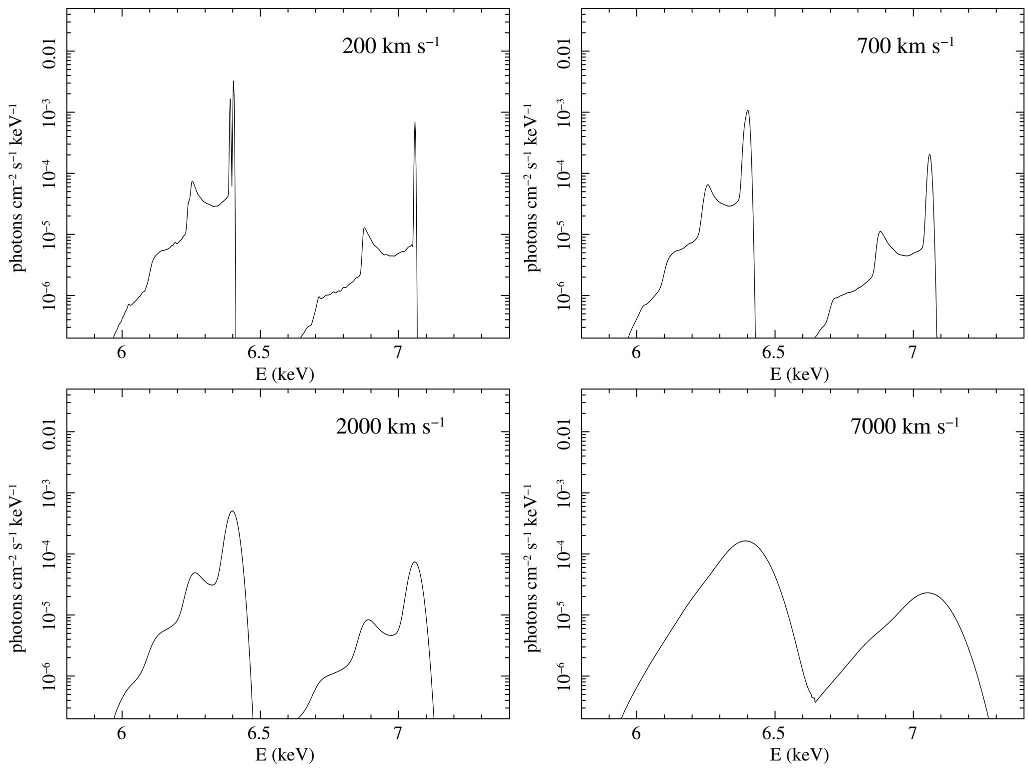

Figure 7.18: Effect of velocity broadening on the fluorescent emission-line spectra consisting of the Fe Kα_1, Fe Kα_2, and Fe Kβ lines. A Gaussian convolution function was applied to the Monte Carlo results for a toroidal X-ray reprocessor with $N_{\rm H} = 10^{25}\ {\rm cm}^{-2}$ (viewed *edge-on*), illuminated by a power-law continuum with a photon index of $\Gamma = 1.9$. Four emission-line spectra are shown with a FWHM of 200, 700, 2000, and 7000 ${\rm km\ s}^{-1}$. *Note the logarithmic flux axis: the narrower core of the line for the smaller velocities makes the flux per keV in the core much higher than that in the Compton shoulder*.

from the default assumptions in the MYTORUS model can be found in Chapter 9. Future enhancements to MYTORUS will include extension of the parameter space for the toroidal opening angle and element abundances. However, even with such extensions, time delays between continuum and line flux variations in real data may affect the relative normalization, A_L. Such time delays are not known *a priori* and cannot be determined from a single time-averaged spectrum. Time delays between continuum and emission-line variations can only be determined by time-resolved spectroscopy of extensive data sets from targeted monitoring campaigns, and these are extremely rare.

In summary, the relative normalization parameter A_L embodies a wealth of unknown and degenerate information in a single scalar value. The interpretation of any derived range for A_L from spectral-fitting to real data is therefore highly non-trivial. It is *your* responsibility to carefully interpret the meaning of A_L taking due consideration of all relevant information pertaining to the data and to the astrophysics of the source in question. In particular, *under no circumstances should the parameter A_L be interpreted directly as a measure of the covering factor or relative element abundance*. Review the analogous discussion of the relative normalization of the scattered continuum (A_S) in §6.2.3. In most cases a unique interpretation of A_L will not be possible without other supporting evidence and you should not hesitate to say so in a paper.

7.3.5 Table-model implementation (power-law continuum)

In this section we describe the table-model implementation of the fluorescent-line spectrum (currently the only implementation). The implementation is in the form of XSPEC "`atables`" which contain pre-calculated spectra for a power-law incident continuum. The intrinsic velocity width is 10 km s^{-1} FWHM (i.e. essentially zero) so the table model must be combined with the XSPEC gaussian convolution model GSMOOTH to produce a final model in which the line width is a free parameter. The relative normalization parameter, A_L, is implemented using the XSPEC model component CONSTANT, applied as a multiplicative factor. A set of tables are available for a range of values for the energy offset, between -100 eV and $+100$ eV, with the incident power-law continuum extending to 500 keV (i.e. $E_T = 500$ keV). The dependence of the fluorescent line spectrum on the termination energy, E_T, of the incident continuum can be evaluated for an energy offset of zero, for which several tables are available with different values of E_T. It is important to realize that for the purpose of interpolation of the spectra, the midpoints of the cosines of the $\theta_{\rm obs}$ angle bins are used, and this involves special treatment of the boundaries of the first and last angle bins (see §3.1.1). The full set of emission-line tables currently available is given in Table 7.2.

Symbolically, the fluorescent line spectrum in the tables will be represented throughout this manual as

Table 7.2: Fluorescent line spectrum XSPEC tables

Name	Energy Offset (eV)	Termination Energy[a] (keV)	V^{b}_{FWHM} ($\mathrm{km\ s^{-1}}$)
mytl_V000010nEp000H500_v00.fits	0.0	500	10
mytl_V000010nEp100H500_v00.fits	−100	500	10
mytl_V000010nEp090H500_v00.fits	−90	500	10
mytl_V000010nEp080H500_v00.fits	−80	500	10
mytl_V000010nEp070H500_v00.fits	−70	500	10
mytl_V000010nEp060H500_v00.fits	−60	500	10
mytl_V000010nEp050H500_v00.fits	−50	500	10
mytl_V000010nEp040H500_v00.fits	−40	500	10
mytl_V000010nEp030H500_v00.fits	−30	500	10
mytl_V000010nEp025H500_v00.fits	−25	500	10
mytl_V000010nEp020H500_v00.fits	−20	500	10
mytl_V000010nEp015H500_v00.fits	−15	500	10
mytl_V000010nEp010H500_v00.fits	−10	500	10
mytl_V000010nEp005H500_v00.fits	−5	500	10
mytl_V000010pEp100H500_v00.fits	+100	500	10
mytl_V000010pEp090H500_v00.fits	+90	500	10
mytl_V000010pEp080H500_v00.fits	+80	500	10
mytl_V000010pEp070H500_v00.fits	+70	500	10
mytl_V000010pEp060H500_v00.fits	+60	500	10
mytl_V000010pEp050H500_v00.fits	+50	500	10
mytl_V000010pEp040H500_v00.fits	+40	500	10
mytl_V000010pEp030H500_v00.fits	+30	500	10
mytl_V000010pEp020H500_v00.fits	+20	500	10
mytl_V000010pEp025H500_v00.fits	+25	500	10
mytl_V000010pEp015H500_v00.fits	+15	500	10
mytl_V000010pEp010H500_v00.fits	+10	500	10
mytl_V000010pEp005H500_v00.fits	+5	500	10
mytl_V000010nEp000H400_v00.fits	0.0	400	10
mytl_V000010nEp000H300_v00.fits	0.0	300	10
mytl_V000010nEp000H200_v00.fits	0.0	200	10
mytl_V000010nEp000H160_v00.fits	0.0	160	10
mytl_V000010nEp000H100_v00.fits	0.0	100	10

[a] The termination energy of the incident power-law continuum.

[b] The intrinsic gaussian velocity width already applied to the table spectrum data.

$$\mathrm{MYTL}(z, A_i, \Gamma_i, N_{\mathrm{H}}, \theta_{\mathrm{obs}}, E) \tag{7.1}$$

where z is the cosmological redshift, N_{H} is the equatorial column density, θ_{obs} is the inclination angle, and E is the energy (in keV). The incident continuum could be in principle be composed of more than one power-law spectrum and $A_i E^{-\Gamma_i}$ is the $i\mathrm{th}$ continuum component. If A_i is in units of $\mathrm{photons\ cm^{-2}\ s^{-1}\ keV^{-1}}$ the fluorescent line spectrum will have the same units. In other words, if A_i in the fluorescent line spectrum is forced to be the same parameter as the normalization of the incident power-law continuum component, the *integrated* flux for each line in MYTL (i.e. the model tables) will be correctly normalized for that continuum. In XSPEC language, the parameter A_i in the incident continuum model component must be tied together with the parameter A_i that is the fluorescent line table model normalization.

If we apply velocity broadening to the fluorescent line spectrum with a gaussian convolution function, we can write the resulting spectrum as

$$L(z, A_i, \Gamma_i, N_{\mathrm{H}}, \theta_{\mathrm{obs}}, \sigma_{\mathrm{L}}, E) = \int_{-\infty}^{+\infty} \exp\left[(E-x)^2/2\sigma_{\mathrm{E}}^2\right] \mathrm{MYTL}(z, A_i, \Gamma_i, N_{\mathrm{H}}, \theta_{\mathrm{obs}}, x)\ dx \tag{7.2}$$

where σ_E is a linear function of E in order that the velocity width is independent of energy (since v/c is proportional to σ_E/E). In XSPEC the gaussian convolution function, GSMOOTH, has

$$\sigma_E = \sigma_L \left(\frac{E}{6\ \mathrm{keV}}\right)^{\alpha} \tag{7.3}$$

where σ_L and α are parameters of the model. Therefore we must keep α fixed at 1.0, leaving σ_L as the basic line-width parameter of the XSPEC table-model implementation of MYTORUS. The parameter itself has units of keV but we can convert it to a velocity width using

$$V_{\mathrm{FWHM}} = 2.354c \left(\frac{\sigma_L(\mathrm{keV})}{6\ \mathrm{keV}}\right) \tag{7.4}$$

$$= 117.7\sigma_L(\mathrm{eV}) \quad \mathrm{km\ s^{-1}}. \tag{7.5}$$

Note that the units of σ_L are different in the above two equations. Similarly, the conversion from velocity-width to σ_L is given by

$$\sigma_L = 0.850 \left(\frac{V_{\mathrm{FWHM}}}{100\ \mathrm{km\ s^{-1}}}\right) \quad \mathrm{eV} \tag{7.6}$$

(but note that the XSPEC parameter σ_L must be entered in units of keV).

The table model with the gaussian velocity-broadening, plus the relative normalization parameter can be set in XSPEC as follows.

```
XSPEC>mo constant*gsmooth( atable{mytl_V000010nEp000H500_v00.fits} )
```

Here the XSPEC `atable` `mytl_V000010nEp000H500_v00.fits` is used as an example (see Table 7.2). A more detailed and practical description of how to set up the model with other model components is given in Chapter 8.

7.3.5.1 Energy resolution

The bin widths in various energy ranges in the fluorescent line model tables are given in Table 7.3, from which it can be seen that in the 5.8–7.2 keV band, the bin width over-samples the best spectral resolution that will be available from X-ray instrumentation in that band in the foreseeable future.

Table 7.3: Emission-line table energy bin widths

Energy Range (keV)	Bin Width (eV)
0.5–4.0	one bin
4.0–5.8	20 eV
5.8–7.2	0.4 eV
7.2–9.0	20 eV
9.0–500	one bin

However, the energy resolution of the MYTORUS fluorescent emission-line model is not simply a matter of examining the energy bin widths in the `atables`.

Rather, the energy resolution depends on the details of the original Monte Carlo calculations that were used to make the tables. The effective energy resolution trades off against the desired statistical accuracy and is a complex relationship. Obviously, one could increase statistical accuracy by sacrificing energy resolution. The worst-case scenario for both energy resolution and statistical accuracy is that of a torus with an edge-on inclination, with a column density of $10^{25}\ \mathrm{cm}^{-2}$. In that case the statistical accuracy is 3% or better for an energy resolution of ~ 8 eV for the Fe Kα line Compton shoulder, comparable to the resolution achievable by calorimeters to be flown on *Astro-H*. Even if the data have better resolution than 8 eV, they must have sufficiently small statistical errors on the counts per resolution element before they become comparable with the statistical accuracy of the model and this will not happen for most AGN. We point out that for column densities less than $10^{25}\ \mathrm{cm}^{-2}$ and lower inclination angles, the statistical accuracy of MYTORUS can be an order of magnitude or more *better* than the worst-case scenario outlined above. The energy resolution of the scattered *continuum* in the MYTORUS model is different to that of the emission-line spectrum and has been discussed in §6.2.5.1.

7.3.5.2 Emission lines that are not included

The implementation of the MYTORUS spectral-fitting model does not yet include the Ni Kα emission line, and nor does it include fluorescent emission lines from any other element aside from Fe. Some other lines may be implemented in the future but for the moment if such lines are observed in data they will have to be fitted with ad hoc model components. Such additional components should not be placed "behind" any absorber, but "in front", unless you really are including an absorber component that lies further from the central engine than the torus. (see discussion in §7.1.4). Even then, if the absorber is Compton-thick the physics of the final model will not in general be correct. Further discussion on including additional model components (that are not included in MYTORUS) can be found in Chapter 8.

7.3.5.3 Fluorescent line flux calculation

As explained in §7.1.4.2 emission-line fluxes are not free parameters in a self-consistent model and therefore must be explicitly calculated. In the table-model implementation the most straight-forward way to calculate an emission-line flux is to delete all model components except for the emission-line spectrum and use, for example, the "flux" command in XSPEC. You must of course manually specify the appropriate energy band over which to calculate the flux and you can get the energy boundaries from visual inspection of the model (it obviously depends on the relative strength of the Compton shoulder and the velocity width). Alternatively, you could use the convolution model CFLUX in XSPEC but it involves the same amount of work. Either way, the line fluxes thus obtained will be observed-frame quantities in the observed energy band between the two energies that you specified even though all the line parameters are in the rest frame. This observed-frame energy band is what you see in the XSPEC model plot in terms of the boundaries of the emission-line of interest. Observed-frame integrated fluxes are a factor of $(1 + z)$ smaller than fluxes in the rest-frame values (see also §8.3.1). Statistical errors on an emission-line flux can be obtained by obtaining statistical errors on A_L and scaling the best-fitting line flux with these. Alternatively, the statistical errors can be obtained directly if you use the XSPEC model CFLUX.

It is important to note that the MYTORUS emission-line fluxes will include the scattered components of the lines (Compton shoulders) even at the line cores. This is another reason for exercising caution when comparing line fluxes obtained using MYTORUS with corresponding line fluxes in the literature that were obtained by fitting ad hoc models. Empirical fits with single, Gaussian model components may under-estimate the observed line flux. Spectral fits that attempted to model the Compton shoulder with an ad hoc Gaussian component are not comparable because the Compton shoulder never even resembles a Gaussian shape.

7.3.5.4 Fluorescent line EW calculation

The facility to calculate the EW of a fluorescent emission line in the MYTORUS model is not provided because in a typical application there will be more than one choice about the continuum component to use for the EW calculation. You must be clear about which continuum component you want to use and you must measure that continuum using the spectral-fitting package that you are using. You must also be clear about whether you are measuring fluxes in the observed frame or the rest frame of the source - you must be adopt one or the other for *both* line and continuum. Express the continuum (at the line centroid of the line core) in units of $\mathrm{photons\,cm^{-2}\,s^{-1}\,keV^{-1}}$. Then take the measured line flux in units of $\mathrm{photons\,cm^{-2}\,s^{-1}}$ (not $\mathrm{ergs\,cm^{-2}\,s^{-1}}$) and divide it by the above monochromatic continuum flux (the EW will then be in units of keV). The observed-frame EW is a factor of $(1 + z)$ smaller than the rest-frame EW of an emission line (see also §8.3.1). The $(1 + z)$ factor does *not* cancel out in the calculation of EW because the denominator in the expression for the EW has a continuum in units of $\mathrm{photons\,cm^{-2}\,s^{-1}\,keV^{-1}}$ so that the compression of the continuum in energy space exactly balances the time dilation factor for that continuum. Be aware that if you measure the continuum from an XSPEC model plot, the plot will show you the observed-frame spectrum even though the model parameters are rest-frame quantities, and you must correct for this accordingly.

Note that the "eqw" command in XSPEC cannot be used because there is more than one emission line in the composite line spectrum table. Even if there were only one line, it could not be used because XSPEC finds the centroid energy of the emission-line model component and uses that energy to calculate the continuum, but the centroid energy may not be the energy you want for an EW calculation if the line is asymmetric (e.g. due to a Compton shoulder). You might use the "eqw" for lines that are not part of MYTORUS. Remember that the XSPEC "eqw" command gives EWs that are in the observed frame, even if all the other model parameters are rest-frame quantities.

It is not possible to directly calculate the statistical errors on the EW. However, it may be sufficiently accurate for some applications to simply scale the best-fitting line EW by the statistical errors on the line flux (see discussion in Yaqoob 1998). Finally, we note that whilst the EW may be a useful parameter when fitting ad hoc, non-physical models, for a self-consistent model such as MYTORUS, the EW is *not* a particularly useful parameter.

Chapter 8

Spectral Fitting with the MYTorus Model

8.1 General Issues

In this chapter we assume that you are already familiar with X-ray spectral fitting procedures and we will not explain such details or the various subtleties and issues associated with spectral fitting and statistical error analysis. Rather, we will demonstrate only how to set up the models since you could easily obtain incorrect results if you make mistakes at this stage. We will also point out important caveats and issues that may not be so familiar. We assume that you have read all the preceding chapters in this manual. Again, there are very important issues, definitions, and procedural points that were explained in previous chapters, and erroneous results could be obtained if you have not familiarized yourself with the material in previous chapters.

You will inevitably need to include model components in addition to the MYTorus model. In a future release of MYTorus we hope to include an implementation that can operate with arbitrary input spectra. In that case adding additional emission components that interact with the torus will be simple. However, in the table-model implementation, adding additional model components that are not part of the torus model must be done with great care and it can break the self-consistency of the model. Regardless of the particular implementation of the MYTORUS model, adding additional absorption components requires an even more careful approach. All of the principal issues involved with including additional model components that are not part of MYTORUS (corresponding to emission or absorption) are discussed in detail in §8.4.

8.1.1 General fitting procedure

The MYTORUS model is sufficiently complex that you will not in general be able to fit blindly, in the sense of starting with an arbitrary set of initial model parameters and letting the spectral-fitting package simply find the best fit. *It will help you immensely if you always keep in mind a physical picture of what you are attempting to model.* You must first understand what it is in your data that will drive various components and parameters of the model. For example, what aspect of your data will constrain the zeroth-order continuum if any? What aspect of your data will constrain the scattered continuum? How well can your data constrain the Fe Kα fluorescent line emission? You can do this preliminary work by manually (and iteratively) changing the parameters of the model and finding an approximate solution. You must then decide which parameters to freeze initially, bearing in mind that the scattered continuum changes only slowly with inclination angle when the line-of-sight does not intercept the torus. Recall that for arbitrary values of $\theta_{\rm obs}$ the scattered continuum and fluorescent emission-line spectra are interpolated using midpoints of the cosines of the angle-bin boundaries (Table 3.1). This necessitates that no interpolation is performed for values of $\theta_{\rm obs}$ less than the bin center of the first angle bin or for values of $\theta_{\rm obs}$ greater than the bin center of the last angle bin (this was discussed in §3.1.1). Thus, you should exercise caution when $\theta_{\rm obs}$ is allowed to be a free parameter and interpret statistical error ranges on $\theta_{\rm obs}$ with great care.

You will also usually need to initially set the relative normalizations of the scattered continuum and emission-line spectrum (A_S and A_L respectively) equal to unity. The emission-line velocity width is another parameter that you might need to initially freeze. After some preliminary fitting you may then "thaw" parameters as demanded by the data. If you allow both A_S and A_L to float we recommend that you first "tie" them together (i.e. force $A_S = A_L$) and only allow them to be independent of each other if the data demand it. Physically, we do not expect A_S

and A_L to be equal in general because the spatial distribution of scattering sites and line-emitting sites is not the same. However, the *macroscopic* characteristic size scales of the scattering sites and line-emitting sites *are* similar so we do not expect A_S and A_L to be too different from each other. In particular, the integrated temporal delay factors (with respect to the intrinsic continuum) that A_S and A_L embody will be of the same order. The interpretations of the relative normalization parameters (A_S and A_L) are not at all simple and their meaning has already been discussed throughout the preceding chapters (in particular see §2.6, §6.2.3, and §7.3.4). The relative normalization parameters encapsulate a wealth of unknown information, including information about the temporal transfer functions for the scattered continuum and the fluorescent-line spectrum. It is your responsibility to carefully interpret the meaning of A_S and A_L, taking due consideration of all relevant information pertaining to the data and to the astrophysics of the source in question. We reiterate here that *under no circumstances should the parameters* A_S and A_L *be interpreted directly as measures of the covering factor or relative element abundances*. In most cases a unique interpretation of A_S and A_L will not be possible without other supporting evidence and you should not hesitate to say so in a paper. Recall that in some situations in which the data do not harbor sufficient information about the intrinsic continuum there will be too many normalization parameters, leading to degeneracies that may prevent convergence of the spectral fit if one or more of the relative normalization parameters is not frozen (see §6.2.4).

All of the examples in this manual refer to XSPEC (Arnaud 1996) but they can in principle be adapted for other spectral-fitting packages. Table 8.1 to Table 8.3show screen output from XSPEC for the three examples in this Chapter. However, they do not depict what you will actually see on the screen because they have been annotated for clarity. Different versions of XSPEC will in fact exhibit different screen output for the same models and the examples here are meant to be generic and the annotation is designed to clearly depict the relations between different parameters. In particular, the examples are designed to show which parameters in the various model components are tied together, as well as the correspondence between the XSPEC parameters and the physical parameters that they represent.

You should also be cognizant of the valid ranges of the parameters where appropriate. In particular, you should be aware that in the process of deriving statistical error ranges on the model parameters, if a parameter boundary is encountered, the statistical error on that parameter will not be valid. Refer to Table 3.2 for a summary of the MYTORUS model parameters and their ranges. You should also be aware of the soft and hard bounds on parameters that are set and you should change them if it is appropriate. The default bounds are set in the XSPEC table model files themselves. *However, the bounds on* Γ *in the table models are overridden by the bounds on the power-law model in XSPEC so you must manually change these to match the bounds in Table 3.2.* In the example `.xcm` files that are provided with the MYTORUS model this has already been taken care of.

There are many different ways in which the different components of the MYTORUS model could be used and it is beyond the scope this manual to give an exhaustive exposition. By means of a few examples, we will demonstrate how to set up the model in the context of the most common likely scenarios.

Note that in all of the examples we will include a Galactic absorption component since this will nearly always be included in the model. It is modeled with the `phabs` component in XSPEC and the one parameter, the column density, is set to a value in the examples that has no particular significance: you must set it a value appropriate for your source. We also include in the examples a redundant `constant` model component (i.e. a simple scalar) that is useful when fitting data from more than one data file (e.g. from a different instrument) simultaneously. We denote this constant by C_k, where $k = 1, 2, 3..$ is the data file number label. If a model is set up correctly for one instrument, reading another data file into XSPEC will then correctly repeat the set up for the second data file. One then manually sets the initial value of C_2, allowing it to float, ensuring that C_1 is frozen at unity. The processes can be repeated for more data files. The C_k would then represent cross-normalization factors between the different data files.

In each example discussed below we will give symbolic expressions for the model in addition to the notation used by the XSPEC spectral-fitting package. The symbolic representations of the various components of MYTORUS have already been discussed in Chapters 5– 7 and will not be discussed again here.

8.2 Table model (power-law continuum)

The MYTORUS table model files can be downloaded from

`http://www.mytorus.com/`

under the "downloads" link. The basic model is contained in the file `mytorus_basic_v00.tar` and has the minimum number of tables necessary for spectral fitting. The tar file opens to a directory called `mytorusfiles/` and contains three tables that can be used, for example, with the `etable` and `atable` functions in XSPEC. The three tables correspond to the zeroth-order continuum component, the scattered continuum, and the fluorescent emission-line spectrum. The termination energy of the power law is 500 keV in the latter two tables, and the energy offset is zero for all the tables. Additional tables for the `mtable` version of the zeroth-order continuum, the scattered continuum for different termination energies (see Table 6.1), and for the emission-line spectra for different energy offsets and different termination energies (see Table 7.2) are available from the above URL. The details pertaining to all of the tables have been discussed extensively in Chapters 5–7. You will select not more than one table from each of the three groups of tables for a particular application. Also included in the basic tar file are three `.xcm` files that correspond to three specific examples that we discuss below. The `.xcm` files can be loaded into XSPEC in the usual way and will automatically set up the model for each example. To familiarize yourself with how to set up and use MYTORUS you should follow each of the three examples in turn, since the first one is the simplest, and the third is the most complex. Pay particular attention to which model parameters are tied together for the different components because the same physical parameter may appear in more than one of the separate model components, a situation that is forced by the particular method of implementation. In all of the examples, the input power-law continuum is symbolically represented by $A_i\, E^{-\Gamma_i}$ $\rm photons\, cm^{-2}\, s^{-1}\, keV^{-1}$, where A_i is the normalization (photon flux at 1 keV), and Γ_i is the photon index. Both the normalization A_i, and Γ_i, need to be communicated to the scattered continuum and emission-line model components because each of those table model components depend on *both* parameters of the input spectrum.

8.2.1 Example 1: continuum-only model

The XSPEC model file for this example is

```
myt_example_tablemodel_01.xcm
```

which models only the zeroth-order continuum and the scattered continuum, and no emission lines. The details of the zeroth-order continuum and the scattered continuum models have been discussed in Chapter 5 and Chapter 6 respectively. In this example we use the table `mytorus_scatteredH500_v00.fits` for the scattered continuum. Symbolically, the spectrum is given by

$$\begin{aligned} N(E) &= C_k\, e^{-\sigma_{\rm abs}(E) N_{\rm H,Gal}}([f(z)\, A_i\, [(1+z)E]^{-\Gamma_i} \\ &\times\ \mathrm{MYTZ}(z, N_{\rm H}, \theta_{\rm obs}, E)] \\ &+\ A_S\, [\mathrm{MYTS}(z, A_i, \Gamma_i, N_{\rm H}, \theta_{\rm obs}, E)]\,) \\ &\quad \mathrm{photons\ cm^{-2}\ s^{-1}\ keV^{-1}} \end{aligned} \tag{8.1}$$

where $f(z) = 1$ because for the units of $N(E)$ here, the time dilution and energy compression factors of $(1 + z)$ cancel out. The actual expression that sets up the XSPEC model in this particular example is

```
model constant*phabs(
( zpowerlw )etable{mytorus_Ezero_v00.fits} +
constant( atable{mytorus_scatteredH500_v00.fits} ) ).
```

In XSPEC this will be displayed as

```
constant<1>*phabs<2>( ( zpowerlw<3> )MYtorusZ<4> +
constant<5>( MYtorusS<6> ) )
```

(or an equivalent, similar expression).

The relationship between the XSPEC expression and the symbolic model components is illustrated in Fig. 8.1, whilst a plot of the model spectrum is shown in Fig. 8.2. Table 8.1 shows the correspondence between the model parameters as displayed by XSPEC, and the symbolic representation of the parameters.

Table 8.1: XSPEC parameters for example 1 (§8.2.1)

Model par #	Fit par #	Mod comp	Component	Parameter	Value	Property	Symbol
1	1	1	constant	factor	1.00000	frozen	C_k
2	2	2	phabs	nH 1e22	1.790000E-02	frozen	$N_{\rm H,Gal}$
3	3	3	zpowerlw	PhoIndex	1.90000		Γ_i
4	4	3	zpowerlw	Redshift	3.300000E-03	frozen	z
5	5	3	zpowerlw	norm	2.700000E-02		A_i
6	6	4	MYtorusZ	NH 1e24	2.00000		N_H
7	7	4	MYtorusZ	IncAng Degrees	90.0000	frozen	$\theta_{\rm obs}$
8	4	4	MYtorusZ	Redshift	3.300000E-03	$=$ par 4	z
9	8	5	constant	factor	1.00000		A_S
10	6	6	MYtorusS	NH 1e24	2.00000	$=$ par 6	N_H
11	7	6	MYtorusS	IncAng Degrees	90.0000	$=$ par 7	$\theta_{\rm obs}$
12	3	6	MYtorusS	PhoIndx	1.90000	$=$ par 3	Γ_i
13	4	6	MYtorusS	Redshift	3.300000E-03	$=$ par 4	z
14	5	6	MYtorusS	norm	2.700000E-02	$=$ par 5	A_i

```
Files being used for table models:
Model comp      File
 4              mytorus_Ezero_v00.fits
 6              mytorus_scatteredH500_v00.fits
```

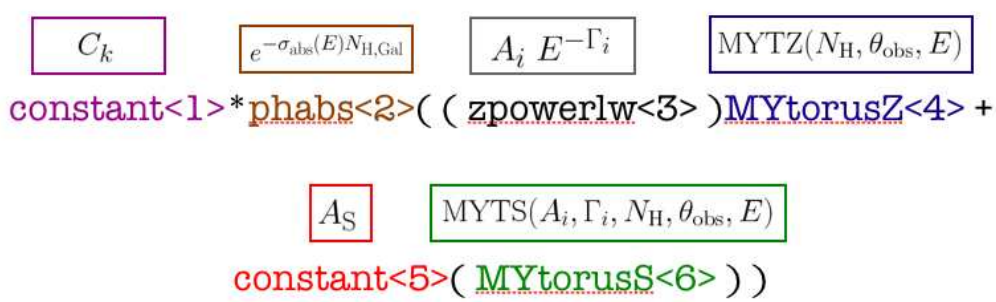

Figure 8.1: Schematic illustration showing how to set up the MYTORUS model in XSPEC for the continuum-only example discussed in §8.2.1. The relationship between the symbolic representation of the different model components and corresponding XSPEC model notation is shown. The complete set of parameters for this example is shown in Table 8.1.

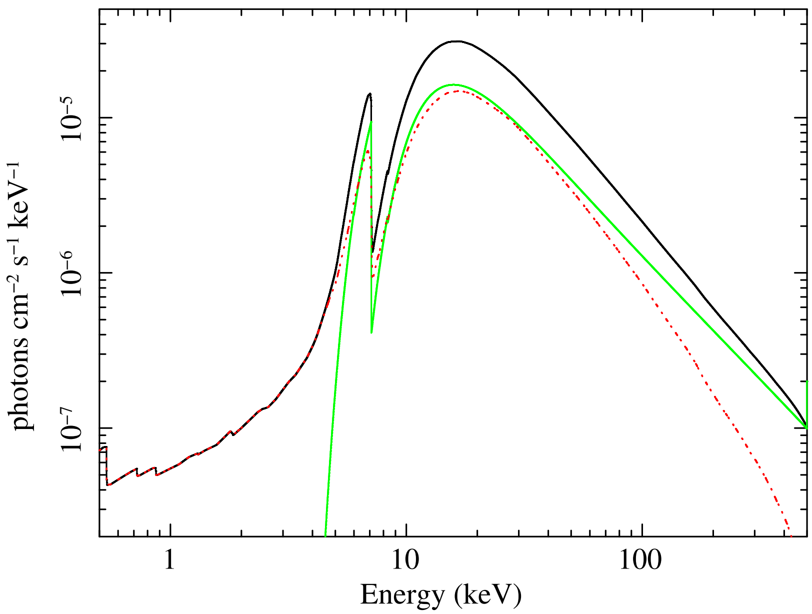

Figure 8.2: An XSPEC plot showing the MYTORUS model for the parameters shown in Table 8.1 for example 1. The black, solid curve is the total model, the green curve is the zeroth-order continuum, and the red, dotted curve is the model spectrum.

Some particular points that you should be most aware of, in this and similar applications are as follows.

- The units of column density in the MYTORUS model are 10^{24} cm^{-2}, *not* 10^{22} cm^{-2} (which are the units of "regular" column densities in other XSPEC models). You should *never* link a column density from MYTORUS with the column density of any other model in the spectral-fitting package. The different units serve as a means of discouraging any temptation to do so.

- The scattered continuum should not be placed in a position where it is absorbed or attenuated by any other model component. In particular, the scattered component is *not* absorbed by the zeroth-order table (but see §8.4.6 and §8.4.7).

- The normalization parameter of the scattered continuum table must be tied to the normalization of the intrinsic power-law continuum.

- The relative normalization of the scattered continuum, A_S, is modeled by a `constant` model component that is intrinsic to the spectral-fitting package.

- Absorption components, such as the Galactic absorber in this example, must have photoelectric cross sections and abundances set so that they are consistent with those used in the particular MYTORUS model components being used (see Chapters 3 and 4).

8.2.2 Example 2: continuum plus Fe Kα and Fe Kβ line model

The XSPEC model file for this example is

`myt_example_tablemodel_02.xcm`

in which we add the Fe Kα and Fe Kβ fluorescent emission-line spectrum to the continuum-only spectrum in example 1.

The details of the fluorescent emission-line model were discussed extensively in Chapter 7. As in example 1, we use `mytorus_scatteredH500_v00.fits` for the scattered continuum. Symbolically, the spectrum is given by

$$\begin{aligned} N(E) &= C_k\, e^{-\sigma_{\rm abs}(E) N_{\rm H,Gal}}([f(z)\; A_i\; [(1+z)E]^{-\Gamma_i} \\ &\times\; \mathrm{MYTZ}(z, N_{\rm H}, \theta_{\rm obs}, E)] \\ &+\; A_S\; [\mathrm{MYTS}(z, A_i, \Gamma_i, N_{\rm H}, \theta_{\rm obs}, E)] \\ &+\; A_L\; L(z, A_i, \Gamma_i, N_{\rm H}, \theta_{\rm obs}, \sigma_{\rm L}, E)\;) \\ &\quad\;\mathrm{photons\ cm^{-2}\ s^{-1}\ keV^{-1}} \end{aligned} \tag{8.2}$$

where $L(z, A_i, \Gamma_i, N_{\rm H}, \theta_{\rm obs}, \sigma_{\rm L}, E)$ is the fluorescent emission-line spectrum (see Eq. 7.2 and the associated discussion in §7.3.5). The actual expression that sets up the XSPEC model in this particular example is

```
model constant*phabs(
( zpowerlw )etable{mytorus_Ezero_v00.fits} +
constant( atable{mytorus_scatteredH500_v00.fits} ) +
constant*gsmooth( atable{mytl_V000010nEp000H500_v00.fits} ) ).
```

In XSPEC this will be displayed as

```
constant<1>*phabs<2>( ( zpowerlw<3> )MYtorusZ<4> +
constant<5>( MYtorusS<6> ) +
constant<7>*gsmooth<8>( MYtorusL<9> ) )
```

(or an equivalent, similar expression).

The relationship between the XSPEC expression and the symbolic model components is illustrated in Fig. 8.3, whilst a plot of the model spectrum is shown in Fig. 8.4. Table 8.2 shows the correspondence between the model parameters as displayed by XSPEC, and the symbolic representation for the parameters.

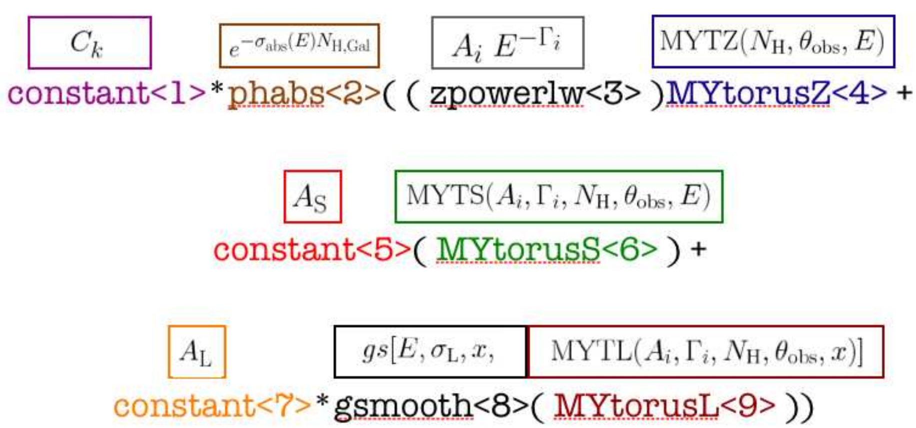

Figure 8.3: Schematic illustration showing how to set up the MYTORUS model in XSPEC for the continuum plus emission-line spectrum in example 2, discussed in §8.2.2. The relationship between the symbolic representation of the different model components and corresponding XSPEC model notation is shown. The complete set of parameters for this example is shown in Table 8.2.

Table 8.2: XSPEC parameters for example 2 (§8.2.2)

Model par #	Fit par #	Mod comp	Component	Parameter	Value	Property	Symbol
1	1	1	constant	factor	1.00000	frozen	C_k
2	2	2	phabs	nH 1e22	1.790000E-02	frozen	$N_{\rm H,Gal}$
3	3	3	zpowerlw	PhoIndex	1.90000		Γ_i
4	4	3	zpowerlw	Redshift	3.300000E-03	frozen	z
5	5	3	zpowerlw	norm	2.700000E-02		A_i
6	6	4	MYtorusZ	NH 1e24	2.00000		N_H
7	7	4	MYtorusZ	IncAng Degrees	90.0000	frozen	$\theta_{\rm obs}$
8	4	4	MYtorusZ	Redshift	3.300000E-03	= par 4	z
9	8	5	constant	factor	1.00000		A_S
10	6	6	MYtorusS	NH 1e24	2.00000	= par 6	N_H
11	7	6	MYtorusS	IncAng Degrees	90.0000	= par 7	$\theta_{\rm obs}$
12	3	6	MYtorusS	PhoIndx	1.90000	= par 3	Γ_i
13	4	6	MYtorusS	Redshift	3.300000E-03	= par 4	z
14	5	6	MYtorusS	norm	2.700000E-02	= par 5	A_i
15	9	7	constant	factor	1.00000		A_L
16	10	8	gsmooth	Sig@6keV keV	4.248000E-03		σ_L
17	11	8	gsmooth	Index	1.00000	frozen	α
18	6	9	MYtorusL	NH 1e24	2.00000	= par 6	N_H
19	7	9	MYtorusL	IncAng Degrees	90.0000	= par 7	$\theta_{\rm obs}$
20	3	9	MYtorusL	PhoIndx	1.90000	= par 3	Γ_i
21	4	9	MYtorusL	Redshift	3.300000E-03	= par 4	z
22	5	9	MYtorusL	norm	2.700000E-02	= par 5	A_i

```
Files being used for table models:
Model comp     File
 4             mytorus_Ezero_v00.fits
 6             mytorus_scatteredH500_v00.fits
 9             mytl_V000010nEp000H500_v00.fits
```

Some important points that you should be aware of (in addition to those described for example 1) are listed below.

- The normalizations of the scattered continuum and emission-line *table models* are both tied to the normalization of the intrinsic power-law continuum. This is necessary for correctly setting up the absolute normalizations of the different components. In addition, the column densities of all three table models are tied together. Again, this is necessary because there is physically only one column density in the MYTORUS model, even though the model is implemented with three separate tables.

- The emission-line table should NOT be attenuated by the zeroth-order continuum component.

- In this example, velocity broadening is applied only to the emission lines. It could be applied to the scattered continuum if desired (see discussion in §6.2.2).

- Details of the velocity broadening function (and the parameter α) were given in §7.3.5. The Gaussian velocity width in keV, σ_L (in keV), can be obtained for a given FWHM (in $\mathrm{km\ s^{-1}}$) using Eq. 7.6.

- You cannot use the "eqw" command in XSPEC. You must calculate the Fe Kα and Fe Kβ emission-line fluxes using the "flux" command in XSPEC or the CFLUX model in XSPEC (refer to the detailed discussions in §7.1.4 and §7.3.5.3). Then use the line flux for a given emission line, measure the relevant continuum manually, and thus obtain the line EW (see §7.3.5.4).

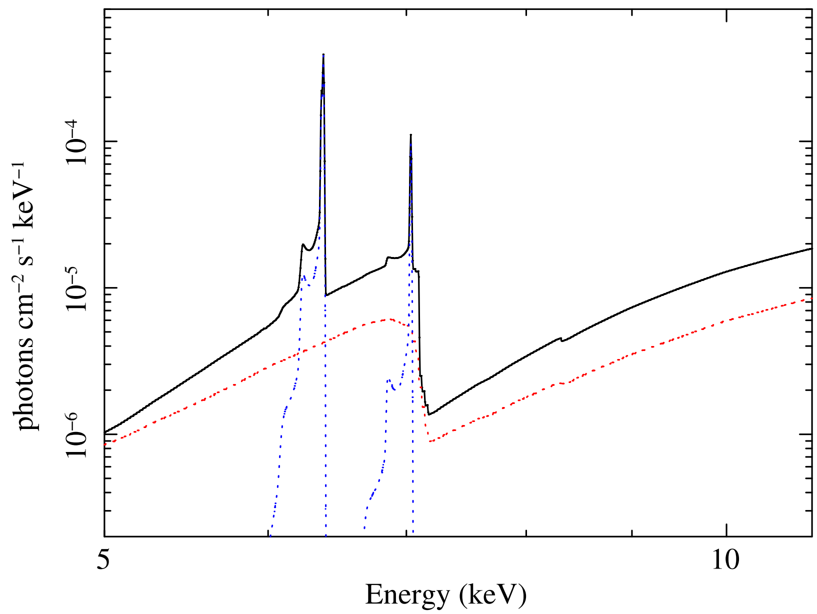

Figure 8.4: An XSPEC plot showing the MYTORUS model for the parameters shown in Table 8.2 for example 2. Since the model is the same as that in example 2 except for the Fe Kα and Fe Kβ emission lines, we show a zoom of the spectrum in the 5–10 keV band and omit the zeroth-order continuum for clarity. The black, solid curve is the total spectrum. The red, dotted curve is the scattered continuum. The emission lines are shown in blue, dotted curves.

8.2.3 Example 3: continuum, Fe Kα & Fe Kβ lines, plus optically-thin scattered continuum

In this example we add a continuum component to example 2 that is *not* part of the MYTORUS model. This additional component is commonly observed in obscured AGN in the form of a rise in the X-ray spectrum towards low energies above that expected from obscuration alone. Such a continuum component is thought to be due to electron scattering of the intrinsic continuum in an ionized (warm/hot) zone surrounding the central engine, and extended on a size scale that is larger than the obscuring structure (putative toroidal reprocessor). If the scattering zone is highly ionized and has a small enough column density that all absorption opacities can be neglected and that the Thomson depth is $\ll 1$, the scattered spectrum will have approximately the same shape as the intrinsic X-ray spectrum. In other words, a power-law intrinsic continuum will give approximately a power-law scattered spectrum. The fraction of the intrinsic X-ray continuum that is scattered into the line-of-sight is, under these circumstances, $\sim [\Delta\Omega/(4\pi)]\tau_s$, where $[\Delta\Omega/(4\pi)]$ is the fractional solid angle subtended by the scattering material at the X-ray source, and τ_s is its average Thomson depth. Using such a simple prescription, the scattered fraction has been estimated to be a few percent or less (Turner *et al.* 1997 estimated $\sim 0.02 - 5\%$ for a sample of Seyfert galaxies; see also Ueda *et al.* 2007, and references therein).

In principle, the optically-thin scattered spectrum should be calculated by properly taking into account the ionic absorption opacities, and Compton scattering on the appropriate Maxwellian distribution of warm/hot electrons (as well the geometry and other details). However, the total optical depths are small enough that the data do not yet warrant such a sophisticated treatment, and a power-law continuum approximation for the scattered spectrum is likely to be satisfactory. Often optically-thin thermal emission (likely from the same warm/hot zone) is also required but such a component is not included in this example for clarity (but see §8.4.2).

We denote the fraction of the intrinsic X-ray continuum that is scattered in the optically-thin zone by f_j, and in this this example we implement f_j with the `constant` model component in XSPEC. The scattered power-law continuum is denoted by $A_j E^{-\Gamma_j}$, with A_j tied to the A_i (the normalizations of the intrinsic power-law continuum components). The use of f_j as the variable parameter rather than A_j is a matter of convenience because it is more useful that the scattered fraction is a fit parameter rather than the absolute normalization of the scattered power law. It is unlikely that the data will be able to constrain any differences between Γ_i and Γ_j (which may in any case be negligible) so in this example we force Γ_j to be equal to Γ_i.

The XSPEC model file for this example is

```
myt_example_tablemodel_03.xcm
```

and the model can be symbolically represented as

$$
\begin{aligned}
N(E) &= C_k \, e^{-\sigma_{\rm abs}(E) N_{\rm H,Gal}} ([f(z) \; A_i \; [(1+z)E]^{-\Gamma_i} \\
&\times \; {\rm MYTZ}(z, N_{\rm H}, \theta_{\rm obs}, E)] \\
&+ \; A_S \; [{\rm MYTS}(z, A_i, \Gamma_i, N_{\rm H}, \theta_{\rm obs}, E)] \\
&+ \; A_L \; L(z, A_i, \Gamma_i, N_{\rm H}, \theta_{\rm obs}, \sigma_{\rm L}, E) \\
&+ \; f_s \; [f(z) \; A_j \; [(1+z)E]^{-\Gamma_j} \;) \\
& \quad {\rm photons \; cm^{-2} \; s^{-1} \; keV^{-1}}
\end{aligned} \tag{8.3}
$$

and the actual expression that sets up the XSPEC model is

```
model constant*phabs(
( zpowerlw )etable{mytorus_Ezero_v00.fits} +
constant( atable{mytorus_scatteredH500_v00.fits} ) +
constant*gsmooth( atable{mytl_V000010nEp000H500_v00.fits} ) +
constant( zpowerlw ) ).
```

In XSPEC this will be displayed as

```
constant<1>*phabs<2>(
( zpowerlw<3> )MYtorusZ<4> +
constant<5>( MYtorusS<6> ) +
constant<7>*gsmooth<8>( MYtorusL<9> ) +
constant<10>( zpowerlw<11> ) )
```

(or an equivalent similar expression).

The relationship between the XSPEC expression and the symbolic model components is illustrated in Fig. 8.5, whilst a plot of the model spectrum is shown in Fig. 8.6. Table 8.3 shows the correspondence between the model parameters as displayed by XSPEC, and the symbolic representation for the parameters. In this example, $f_j = 0.0013$, corresponding to 0.13% of the intrinsic continuum scattered into the line-of-sight.

Table 8.3: XSPEC parameters for example # 3 (§8.2.3)

Model par #	Fit par #	Mod comp	Component	Parameter	Value	Property	Symbol
1	1	1	constant	factor	1.00000	frozen	C_k
2	2	2	phabs	nH 1e22	1.790000E-02	frozen	$N_{\rm H,Gal}$
3	3	3	zpowerlw	PhoIndex	1.90000		Γ_i
4	4	3	zpowerlw	Redshift	3.300000E-03	frozen	z
5	5	3	zpowerlw	norm	2.700000E-02		A_i
6	6	4	MYtorusZ	NH 1e24	2.00000		N_H
7	7	4	MYtorusZ	IncAng Degrees	90.0000	frozen	$\theta_{\rm obs}$
8	4	4	MYtorusZ	Redshift	3.300000E-03	$=$ par 4	z
9	8	5	constant	factor	1.00000		A_S
10	6	6	MYtorusS	NH 1e24	2.00000	$=$ par 6	N_H
11	7	6	MYtorusS	IncAng Degrees	90.0000	$=$ par 7	$\theta_{\rm obs}$
12	3	6	MYtorusS	PhoIndx	1.90000	$=$ par 3	Γ_i
13	4	6	MYtorusS	Redshift	3.300000E-03	$=$ par 4	z
14	5	6	MYtorusS	norm	2.700000E-02	$=$ par 5	A_i
15	9	7	constant	factor	1.00000		A_L
16	10	8	gsmooth	Sig@6keV keV	4.248000E-03		σ_L
17	11	8	gsmooth	Index	1.00000	frozen	α
18	6	9	MYtorusL	NH 1e24	2.00000	$=$ par 6	N_H
19	7	9	MYtorusL	IncAng Degrees	90.0000	$=$ par 7	$\theta_{\rm obs}$
20	3	9	MYtorusL	PhoIndx	1.90000	$=$ par 3	Γ_i
21	4	9	MYtorusL	Redshift	3.300000E-03	$=$ par 4	z
22	5	9	MYtorusL	norm	2.700000E-02	$=$ par 5	A_i
23	12	10	constant	factor	1.300000E-03		f_j
24	3	11	zpowerlw	PhoIndex	1.90000	$=$ par 3	Γ_j $(=\Gamma_i)$
25	4	11	zpowerlw	Redshift	3.300000E-03	$=$ par 4	z
26	5	11	zpowerlw	norm	2.700000E-02	$=$ par 5	A_j $(=A_i)$

```
Files being used for table models:
Model comp     File
 4             mytorus_Ezero_v00.fits
 6             mytorus_scatteredH500_v00.fits
 9             mytl_V000010nEp000H500_v00.fits
```

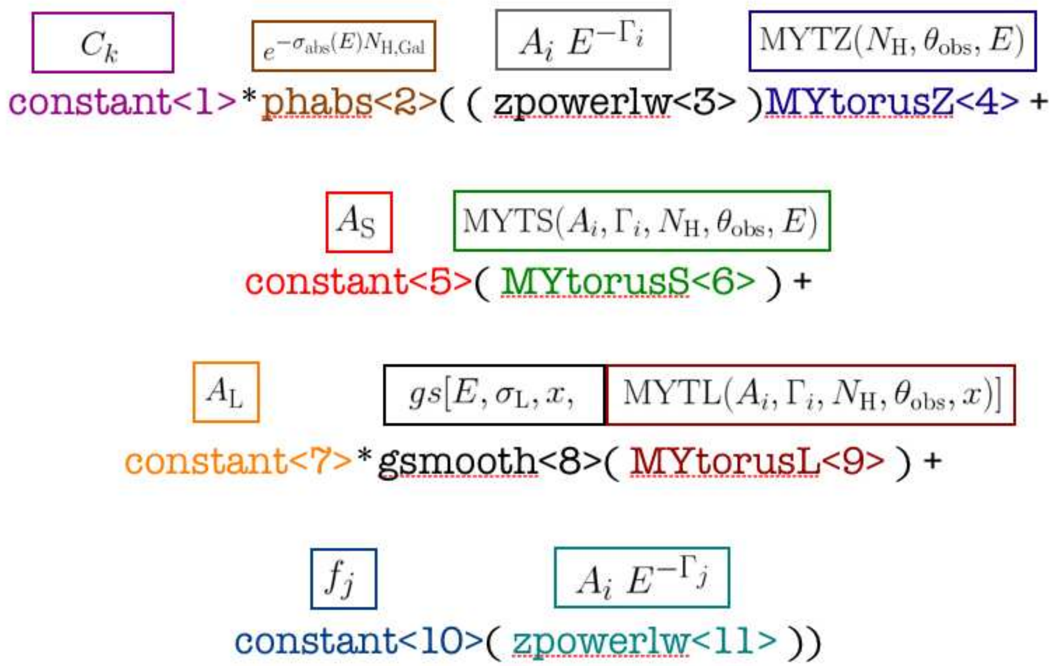

Figure 8.5: Schematic illustration showing how to set up the MYTORUS model in XSPEC for example 3, which includes the reprocessed spectrum plus an optically-thin scattered continuum (see §8.2.3 for details). The relationship between the symbolic representation of the different model components and corresponding XSPEC model notation is shown. The complete set of parameters for this example is shown in Table 8.3.

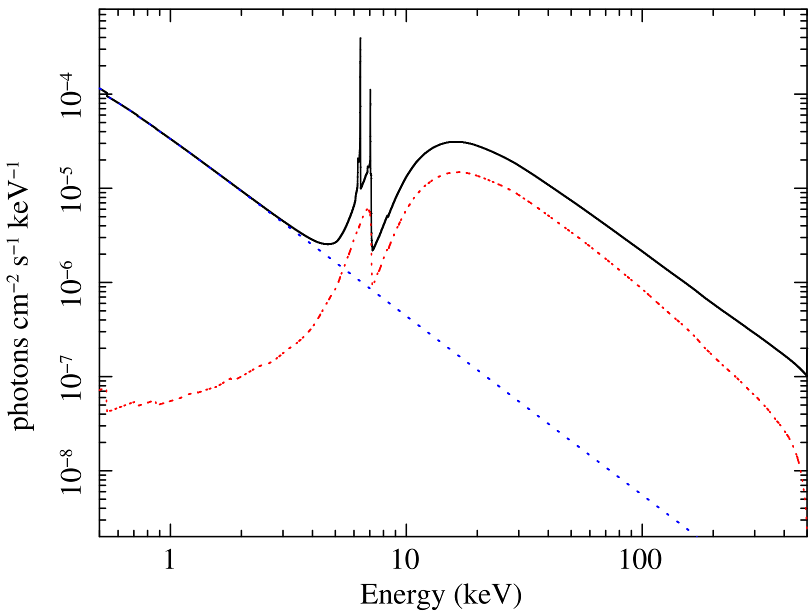

Figure 8.6: An XSPEC plot showing the MYTORUS model (plus an optically-thin scattered continuum) for the parameters shown in Table 8.3 for example 3. The black, solid curve shows the total spectrum. The scattered continuum component from the torus is shown as a red, dotted curve, and the optically-thin scattered continuum is shown as a blue, dotted curve. For clarity, the separate contributions from the zeroth-order continuum and the emission lines are not shown.

8.2.4 Fluxes and Luminosities

Fluxes and luminosities in specified energy bands can be obtained in the usual way. With the full model in place these fluxes and luminosities will of course correspond to observed quantities. In order to obtain *intrinsic* continuum fluxes and luminosities you must remove *ALL* three components of the MYTORUS model (including scattered continua and emission lines), and any other absorption components. You must of course also remove any other continuum components that you are not seeking the flux or luminosity for (e.g. components that may be due to some other type of reprocessing, such as the optically-thin scattered continuum discussed in §8.2.3). You must also correctly account for the source redshift (see §8.3.1).

8.3 Modeling high-redshift sources

Since the MYTORUS model is calculated up to a certain energy, E_T (the termination energy), an astrophysical source with a cosmological redshift of z will produce a spectrum that extends only up an energy of $E_T/(1+z)$ in the observer's frame. If the energy range (or bandpass) of the data (which measures the observed-frame spectrum) extends beyond $E_T/(1+z)$ the resulting spectral fit will be invalid. Aside from the fact that the scattered continuum does not extend beyond E_T in the rest frame, the zeroth-order continuum table ends at 500 keV in the rest frame, and XSPEC will simply use a multiplicative factor of unity since a value in the table will not be available. This produces an anomalous "jump" in the spectrum at $500/(1+z)$ keV in the observed frame. Therefore you should *manually* restrict the upper energy of the data to $E_T/(1+z)$ in order to avoid problematic or erroneous spectral fits.

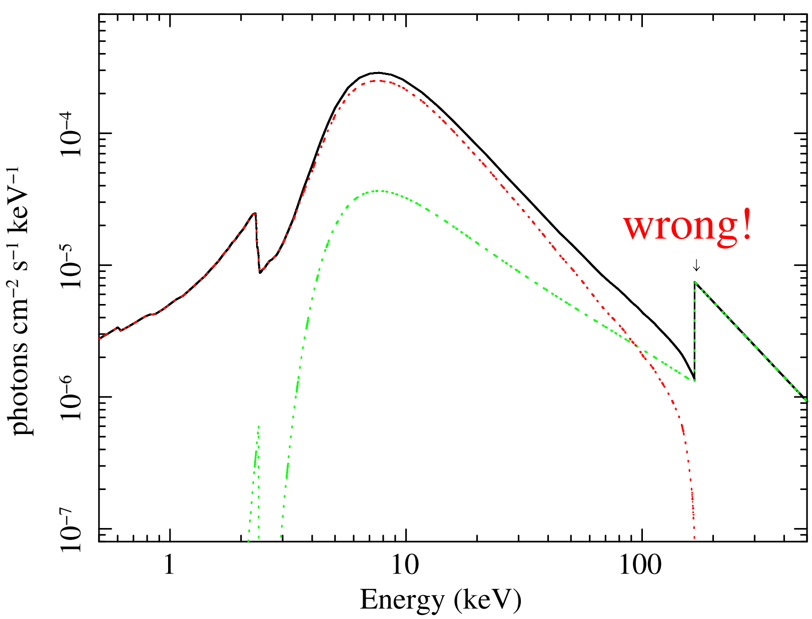

Figure 8.7: A plot from XSPEC of the MYTORUS model spectrum for $z = 2$, illustrating that the model is only valid below $[E_T/(1+z)]$ in the observed frame. In this example, the data above $[500\ \mathrm{keV}/(1+z)]$ should be discarded before fitting. The other parameters of the model are $\Gamma = 1.9$, $N_H = 5 \times 10^{24}\ \mathrm{cm}^{-2}$, and $\theta_{\rm obs} = 90°$. See §8.3 for details.

Fig. 8.7 shows a model plot from XSPEC illustrating what happens when you don't manually restrict the energy band. In this example the the source redshift is

2.0 (the figure caption gives the other parameters of the model). Recall that in the table model implementation of MYTORUS, different scattered continuum tables have been calculated for different values of E_T (see Table 6.1). One can obtain the maximum redshift of a source that the model is applicable to, given the upper limit on the energy spanned by the data, say E_U:

$$z_{\max} = \left(\frac{E_T}{E_U}\right) - 1. \tag{8.4}$$

Conversely, for a source with redshift z, you should restrict the data to energies

$$E < \frac{E_T}{(1+z)} \tag{8.5}$$

8.3.1 Fluxes, luminosities, and equivalent widths

XSPEC gives fluxes that are observed-frame quantities, in an energy band that is specified by energy boundaries in the observed frame. Luminosities are calculated by XSPEC at the specified value of z, using energy boundaries that are specified in the rest frame. All model parameters, including line intensities, displayed by XSPEC are rest-frame quantities. HOWEVER, if you calculate the flux of an emission-line that is part of the MYTORUS model (see §7.1.4, §7.3.5.3, and §7.3.5.4), that line flux will be an *observed-frame* quantity. To convert an observed-frame line flux that is in units of $\mathrm{photons\ cm^{-2}\ s^{-1}}$ to a flux in the rest frame of the source, you must multiply the observed flux by $(1+z)$. To calculate the EW of an emission line in the rest frame, you must use the rest-frame line flux and the rest-frame continuum at the line center. Recall that the EW of an emission line in the observed frame is smaller than that in the rest frame by a factor $(1+z)$. It is important to note, however, that the XSPEC "eqw" command gives the EW in the *observed frame* even though all the model parameters are rest-frame quantities (but recall that you will not be using the "eqw" command for calculating EWs of lines that are intrinsic to the MYTORUS model).

8.4 Including additional model components

In most situations you will inevitably need to include model components that are not part of MYTORUS and these will unavoidably be ad hoc components. Great care must be exercised when combining MYTORUS with other model components because it is possible to obtain results that are either not what you intended, or results that are not meaningful. In some situations the self-consistency of the MYTORUS model will be destroyed, in which case you are responsible for determining whether the particular application can tolerate such a compromise. We recommend that you always keep in mind a physical picture of the situation you are trying to model because it is easy to lose sight of it when using ad hoc model components. If you add model components simply for the sake of obtaining a good fit to the data, without proper regard for the physical interpretation of the ad hoc components, there is no purpose in using the MYTORUS model. Your entire model may as well be ad hoc.

We discuss below the most common situations that are likely to arise for including additional model components.

8.4.1 Power-law continua

Since the current table-model implementation of the MYTORUS model is calculated for an incident power-law continuum, you may add as many additional power-law continuum components as you wish, without destroying the self-consistency of the model. Each power-law continuum may have its normalization and photon index independent of every other power-law component. However, for every power-law component that has an independent normalization or photon index (or both), *you must include a separate scattered continuum component and a separate emission-line component for each intrinsic continuum component*. In the table-model implementation this means that each power-law component is associated with its own scattered continuum `atable`. There would still be only one value of $N_{\rm H}$ and $\theta_{\rm obs}$. On the other hand, you can apply the zeroth-order multiplicative model (e.g. an `etable`) to the sum of all the power-law continua. For example, for a double power-law we would have, in symbolic notation

$$
\begin{aligned}
N(E) &= [(A_1 E^{-\Gamma_1}) + (A_2 E^{-\Gamma_2})]\mathrm{MYTZ}(z, N_{\mathrm{H}}, \theta_{\mathrm{obs}}, E) \\
&+ [(A_1 E^{-\Gamma_1})\mathrm{MYTS}(z, A_1, \Gamma_1, N_{\mathrm{H}}, \theta_{\mathrm{obs}}, E)] \\
&+ [(A_2 E^{-\Gamma_2})\mathrm{MYTS}(z, A_2, \Gamma_2, N_{\mathrm{H}}, \theta_{\mathrm{obs}}, E)]. \qquad (8.6)
\end{aligned}
$$

Strictly speaking the above expression is valid only for $z = 0$ because we have omitted cosmological factors involving z for the sake of clarity of presentation since it is the *form* of the expression that is important here. In analogy to Eq. 8.6, if you use the fluorescent emission-line spectrum of the MYTORUS model you will need a separate MYTORUS emission-line component for each independent power-law continuum component. For the table-model implementation this means that you need a separate MYTL table for every power-law continuum component, with various parameters tied together following the example above for the MYTS components.

Implicit in all of the above discussion is of course that *all of the power-law intrinsic (or incident) continuum source components are located at the center of the torus and that they are all emitting isotropically*, because those were the assumptions that the original Monte Carlo calculations were based on. If you want to model power-law continuum components that are *not* tied to these two assumptions you *can* include such components *but* you cannot then include the MYTORUS scattered continuum and emission-line spectrum. You *can*, however, include the zeroth-order multiplicative component for MYTORUS, if the line-of-sight between the additional power-law continuum source and the observer intercepts the torus. In other words, you will be forced to neglect the Compton-scattered continuum and fluorescent line emission associated with your additional power-law source. It is your responsibility to determine whether the resulting compromise is tolerable.

In §8.2.3 we gave an example of an additional power-law component for which the approximation of neglecting all three MYTORUS components (MYTZ, MYTS, and MYTL) *was* acceptable. In that case the additional power-law modeled optically-thin electron scattering in a zone that was extended on a size-scale larger than the torus. The absorption and scattering optical depth of the zone was so small that the fraction of the intrinsic continuum scattering in that zone *and then scattering back from the torus* was negligible. The fluorescent line emission from the already small fraction of the intrinsic continuum returning to the torus could also be neglected. The source of the additional power-law component had a physical location such that X-rays from it could reach the observer without intercepting the torus, so the zeroth-order component of MYTORUS (MYTZ) was not needed either. Although in that example it is possible that some of the optically-thin zone scatters X-rays that then do intercept the torus, they would be further attenuated by the torus and rendered undetectable compared to the reprocessed X-rays from the primary power-law continuum.

8.4.2 Non-power-law continua

As explained above in §8.4.1, if you include additional continuum components that are not power laws you will not be able to include the associated Compton-scattered continuum and fluorescent line emission from the MYTORUS model. If the additional continuum source is located at the center (origin) of the torus then you can still use the zeroth-order multiplicative component of MYTORUS (MYTZ). In situations that correspond to the additional power-law continuum source being located in positions for which the line-of-sight does not intercept the torus, you will not of course need a zeroth-order continuum attenuation factor from MYTORUS. Recall from Chapter 5 that the MYTZ `etable` values are identically equal to zero (optical depth) for lines-of-sight that do not intercept the torus (and the corresponding `mtable` values are identically equal to unity). This facilitates a seamless transition from the intrinsic (unobscured) continuum to the attenuated continuum for the full range of model inclination angles.

Clearly, the location of the additional continuum source relative to the torus determines how the zeroth-order MYTORUS component is set up. Suppose the additional continuum component is denoted by $J(E, x_n,\ n = 1, 2, ..)$ (where the x_n are the model parameters). Symbolically, the model would be set up as

$$\begin{aligned} N(E) &= [(A_i E^{-\Gamma_i}) + J(E, x_n)]\mathrm{MYTZ}(E) \\ &+ (\text{remaining model components}) \end{aligned} \tag{8.7}$$

if $J(E, x_n)$ is located in a position for which the line-of-sight between it and the observer could intercept the torus, or

$$\begin{aligned} N(E) &= [(A_i E^{-\Gamma_i})]\mathrm{MYTZ}(E) + J(E, x_n) \\ &+ \text{(remaining model components)} \end{aligned} \quad (8.8)$$

if $J(E, x_n)$ is located where no interception of the additional emission components by the torus is possible. Here, we have omitted other model components, the units, and abbreviated the notation for clarity.

In many situations the lack of a mechanism to include the Compton-scattered continuum and fluorescent line emission from additional continuum components that are not power laws will not be a problem. For example, if the additional continuum is thermal with a temperature less than ~ 1 keV or so, both Compton scattering and Fe Kα fluorescent line emission in the torus due to that continuum will be negligible. Compton scattering will be negligible because the absorption opacity at the relevant energies is much greater than the electron-scattering optical depth. Fluorescent line emission due to Fe Kα will be negligible because the continuum flux above the Fe K absorption edge will be negligible for a low-temperature thermal continuum. On the other hand, fluorescent line emission due to the lighter elements may potentially be important, but these are not yet included in MYTORUS anyway.

An optically-thin soft X-ray thermal continuum (with $kT \sim 0.5 - 0.7$ keV) is sometimes observed in AGN, originating in the extended warm/hot zone surrounding the putative torus and central engine. Such a continuum component would likely be placed in a location for which the emitted radiation does not intercept the torus before reaching the observer. On the other hand, a thermal (possibly optically-thick) continuum component (manifesting itself as a "soft excess" in the observed X-ray spectrum) might originate in an accretion disk, in which case it would be placed in a location for which the radiation could intercept the torus before reaching the observer. However, in such situations, a soft continuum component may only be observable for unobscured lines-of-sight. Placing such a component in a position in the XSPEC model expression that allows it to be obscured by the torus is still correct because the MYTZ component does not require *a priori* knowledge of the inclination angle.

8.4.3 High-energy exponential cutoff

If you have a deficit in the data at high energies compared to the best-fitting model, you may be tempted to include an exponential cutoff model component in order to make the high-energy continuum fit the data. We have discussed at length in this manual the reasons why applying an exponential cutoff to the continuum is not physical (e.g. see §3.2.3 and §6.1.3). Here we point out that in addition to the reasons already given, modifying the continuum with an exponential cutoff destroys the self-consistency of the MYTORUS model. Applying a high-energy exponential cutoff to the continuum will yield no new physical information. Therefore one must question the value of applying a high-energy cutoff simply for the sake of obtaining a good fit to the data without learning anything new. If the spectral fit really is so poor that it is not tolerable then you should use a MYTORUS scattered continuum model with a different termination energy (E_T–see §6.2.5). In addition, it is important to remember that *you can already use any arbitrary physical continuum model with the zeroth-order* MYTORUS *component* (MYTZ). For example, a variety of thermal Comptonization models are available in XSPEC and these have intrinsic high-energy turn-overs that are physical and not ad hoc. You may approximate the corresponding scattered continuum with MYTS using judiciously chosen values of the normalization, photon index, and E_T. *You* are responsible for determining whether such approximations are tolerable for your application. In the future we may also make available pre-calculated MYTS tables for thermal, Comptonized continua.

In summary, *do not apply a high-energy exponential cutoff to the continuum*. Instead, use models with different values of E_T or construct an approximation using a physically motivated intrinsic continuum.

8.4.4 Additional "narrow" emission lines

There are two distinct situations in which you may want to include additional emission lines, modeled for example, with Gaussian components. One is to model fluorescent line emission from the torus that is not yet included in MYTORUS (for example, the Ni Kα line), and the other is to include emission lines from physical locations other than the torus. In the former case, the emission-line component should NOT be attenuated by MYTZ because the fitted model should correspond to the *observed* line. Recall that in the case that an emission line is associated with an absorber in which it is created, there is no such thing as the "absorption-corrected" flux. Only the observed flux has a physical meaning. The measured line flux (or EW) can then be compared with theoretical predictions. If you are modeling the Ni Kα fluorescent emission line you can use the theoretical results in §7.2.4 to determine whether the measured line flux is consistent with the other parameters of the MYTORUS model.

In the second case, that you want to model line emission from a location other than the torus, you must first specify whether the physical situation requires that any of the lines-of-sight between the observer and the line-emitting region intercept the torus. If not, then no zeroth-order continuum multiplicative factor is needed, otherwise it is. Setting up the model components is then simply a matter of following the examples in Eq. 8.7 or Eq. 8.8 by analogy. In the particular situation described here you cannot expect the MYTZ component to automatically determine the line-of-sight attenuation from $\theta_{\rm obs}$ alone because you may locate the source of additional emission at a position that has a different line-of-sight attenuation compared to the primary X-ray continuum source.

Modeling emission lines from the torus or elsewhere in an ad hoc manner means that Compton scattering of those emission lines in the torus is neglected so you will not be able to model the Compton shoulder created by the ad hoc emission lines. Compton scattering will occur whether or not the emission line is formed in the torus or not. The zeroth-order attenuation, where relevant (for emission lines not created in the torus), will however be correct. The magnitude of the Compton-scattered component relative to the core of an emission line depends principally on the column density of the torus and its orientation, and the single-scattering albedo at the line energy. Refer back to §7.1.2 for a detailed discussion of the properties of the Compton-shoulder. Although most of that discussion refers to the Fe Kα line, some general principles are relevant for any emission line.

We strongly recommend that you do *not* model the Compton shoulder with a Gaussian model component because you will not derive any physically-meaningful information from doing so. The Compton shoulder is not Gaussian in shape. Having said that, it is very unlikely that your data will give you unambiguous, statistically significant evidence of a Compton shoulder on any line other than the Fe Kα emission line for at least a few years yet.

8.4.5 Accretion disk spectra

Most of the preceding discussions in §8.4.1–§8.4.4 are also relevant for continuum and emission-line components originating in the putative accretion disk. We include here a separate section on the accretion disk components in case some issues are not obvious. If one of the standard assumptions about AGN geometry is correct, the accretion disk can be assumed to be coincident with the center of the torus. Indeed, the monte-carlo calculations for MYTORUS were based on that assumption. We take this opportunity to remind you that the torus in MYTORUS need not be the parsec-scale structure that is usually referred to as "the torus". The torus in MYTORUS can correspond to *any* toroidal distribution of matter, including the BLR, or even (albeit approximately) part of the very outer accretion disk.

The inclusion of any continuum emission from the accretion disk along with the MYTORUS model, whether it is thermal or non-thermal, can be done by following the discussions in §8.4.1 and §8.4.4. The same principles also apply to any reflection continuum from the disk, whether or not it is ionized, and whether or not it is affected by relativistic distortion due to the putative black hole. The discussions in §8.4.4 apply to any line emission from the disk, whether or not it is relativistically broadened.

The current implementation of the MYTORUS model can only treat Compton-scattering of disk emission components that are power laws (and this is described in §8.4.1). This means that Compton-scattering of the *X-ray disk-reflection continuum and disk emission lines in the torus* is neglected. Such "double-reflection" may in fact *not* be negligible for unobscured lines-of-sight. Future enhancements of the MYTORUS model may be able to treat such a scenario. We note that ad hoc models that are currently widely used cannot treat this "double-reflection" correctly, even in principle.

Although Compton-scattering of the disk-reflection and emission-line spectrum by the torus cannot yet be handled by MYTORUS, if the line-of-sight to the observer intercepts the torus, the zeroth-order attention by MYTORUS *will* be correct. The zeroth-order multiplicative component of the MYTORUS model (MYTZ) should be employed for all disk continuum and line emission components and should be applied to the disk spectra that already have relativistic effects applied (if required).

8.4.6 Cold/neutral absorber components

Including additional absorber components with the MYTORUS model will, in general, break the self-consistency of the model. Compton scattering is not treated at all in most "regular" absorption models. If it is treated, the treatment is very simple and may be inadequate (if it is not simple then the model is not an absorption model). The absorption model will also not include the fluorescent line emission that would be produced by the absorber.

Having said that, you may include *uniform* column densities less than $\sim 10^{22}\ \mathrm{cm}^{-2}$ without concern about the treatment of Compton scattering and fluorescent line emission (unless any of the element abundances are significantly higher than solar). Thus, Galactic absorption and absorption by the AGN host galaxy may be included quite trivially, as in the examples in §8.2.1– §8.2.3. Obviously, both Galactic and host galaxy absorption must be applied to *all* model components. When including *any* additional absorber components with MYTORUS, you must remember to set the photoelectric absorption cross sections to those of Verner *et al.* (1996), and the elements abundances to be consistent with those used by MYTORUS (Anders & Grevesse 1989 for the current implementation).

For column densities higher than $\sim 10^{22}\ \mathrm{cm}^{-2}$, if the absorber is modeling a component in the central engine, you must first establish whether your data really require additional absorption or whether your assumptions about the continuum are inadequate. For example, what do the residuals around the Fe K absorption edge (after fitting the MYTORUS model) tell you about the requirement for extra absorption? Then you must establish what physical scenario you are trying to model, bearing in mind that "regular" absorption models are *one dimensional* in the sense that they only provide extinction in the line-of-sight.

Are you trying to model additional absorption farther out from the center than the torus? If so, is the size of the additional absorber much smaller than the size of the torus? If so, the additional absorption must be applied only to the MYTORUS zeroth-order (attenuated) continuum, and not the MYTORUS Compton-scattered continuum (MYTS) or the emission-line spectrum (MYTL). In that case both the Compton-scattered continuum and fluorescent line emission from the additional absorber may be small enough to be negligible. On the other hand, if you envisage an additional absorber that is of comparable size to the torus (or larger), the additional absorber component must be applied to all model components (just like Galactic absorption). In that case your model will be missing the Compton-scattered continuum and fluorescent line spectrum from the additional absorber. In either case, it will be more accurate to use another MYTZ component for the additional absorber rather than a "regular" absorber component because the former includes a better treatment of Compton-thick line-of-sight attenuation.

Alternatively, an additional absorber component may be required to compensate for the fact that the distant-matter reprocessor in AGN is unlikely to be an exact torus. Again, it is more accurate to use another MYTZ component rather than "regular" absorption (although MYTZ does not yet allow element abundances to be free parameters). If the column density is much greater than $10^{22}\ \mathrm{cm}^{-2}$ you will lose the self-consistency of the MYTORUS model.

If you are trying to model additional absorption located between the accretion disk and the torus the self-consistency of the MYTORUS model will be broken. Such a scenario requires a specific, three-dimensional model and a full Monte Carlo treatment to calculate the spectra correctly. Therefore, placing an additional absorber in between the X-ray continuum source and the torus is strongly discouraged. In fact XSPEC, with the current table-model implementation of MYTORUS does not allow you to do this anyway.

It is important to bear in mind that even if the self-consistency of the MYTORUS model is lost by including additional absorber components, it is still better than the current practice of using completely ad hoc models consisting of simple attenuation plus disk-reflection. Such models are not physical and do not yield physically-meaningful parameters in the context that they are applied. On the other hand, using the MYTORUS model plus some additional ad hoc model components builds upon a *baseline* that is physical and self-consistent. Results from fitting data can then serve as a basis for eventually improving the baseline model.

8.4.6.1 Partial covering models

So far we have discussed including additional *uniform* absorber components. Partial covering models apply absorption to only a fraction of the spectrum. The fraction that is absorbed is then numerically added to the unabsorbed fraction of the spectrum. Mathematically, partial covering models are equivalent to a fully covering absorber with some of the unabsorbed continuum being scattered into the line-of-sight without a change in the spectral shape. The literature is very confused on the application and interpretation of partial covering models. Like the simple uniform absorbers, partial covering models are *one-dimensional*. A physical interpretation requires additional assumptions. If the partial covering is interpreted literally, it means that the covering factor refers only to fraction of the source covered in the line-of-sight. That covering factor tells us nothing about the global covering factor of the absorber (i.e. the solid angle of the absorber subtended at the source). Including partial covering model components with MYTORUS is problematic because it could be applied to the zeroth-order continuum, the scattered continuum, the fluorescent line spectrum, or any combination of these. No matter how the partial covering is applied, the physical meaning of the final model and derived parameters may not be clear or even physically-meaningful. Rather than use a partial covering model that has a line-of-sight covering factor as one of the parameters, it is better to separate the continuum components into those that are absorbed (uniformly) and unabsorbed, since this is mathematically equivalent. Interpretation of the resulting parameters is then less problematic, although it is still rather ad hoc. In summary, *you should not use partial covering models with* MYTORUS .

8.4.7 Warm absorbers

If your data require one or more photoionized (or "warm") absorber components, the least complicated situation is one in which the warm absorber is not obscured by the torus. In that case it is simply applied to the intrinsic X-ray continuum, or the X-ray intrinsic continuum plus scattered torus emission (MYTS) if you think the warm absorber has a size that is larger than the torus. Symbolically this scenario can be written in abbreviated form as

$$N(E) \quad = \quad \mathrm{WARM}(E)[A_1 E^{-\Gamma_1} + (A_S \mathrm{MYTS}(A_1, \Gamma_1, E))] \tag{8.9}$$

where $\mathrm{WARM}(E)$ is the warm absorber model. An implicit assumption in the above procedure is that the MYTS component has little effect on the ionization state of the warm absorber (which may not be true). Placing a warm absorber in between the X-ray source and the torus is problematic for the same reasons that were discussed above (§8.4.6) for a cold/neutral absorber placed in between the X-ray source and the torus. As for the case of the cold/neutral absorber, XSPEC does not actually allow you to do this with the current implementation of the MYTORUS model. Placing a warm absorber farther from the X-ray source than the torus is also problematic, unless you produce warm absorber models using the MYTORUS spectra as inputs to a photoionization code, but the best-fitting MYTORUS spectrum is not known *a priori*. In any case, the latter is an unlikely scenario in AGN because the continuum from the Compton-thick reprocessor will not be able to ionize the warm absorber sufficiently to produce the usual observed warm absorber features. It is possible to approximate a scenario in which the warm absorber is identified with a wind on the surface of the torus by splitting the intrinsic X-ray continuum into a portion that is absorbed by a warm absorber and a portion that is reprocessed by the torus. In abbreviated notation, this can be written as

$$\begin{aligned} N(E) &= [A_1 E^{-\Gamma_1}]\mathrm{WARM}(E) + \\ & \quad [(A_2 E^{-\Gamma_1})\mathrm{MYTZ}(E) + (A_S \mathrm{MYTS}(A_2, \Gamma_1, E))]. \end{aligned} \tag{8.10}$$

The cost of this procedure is an extra ad hoc normalization.

8.5 WARNING: "plot model" anomaly

We reiterate here something that was mentioned in §5.4.3 and §6.2.6. That is, the "plot model" command in XSPEC may plot a model outside of the energy range covered by the data and/or outside of the energy range covered by a table model. The valid energy range of the MYTORUS model is currently 0.5 keV up to E_T (and the energy range of the data should of course never lie outside these bounds). This "plot model" anomaly can result in model plots that are incorrect. Moreover, if an energy bin is so coarse that it crosses one of the boundaries of the valid energy range, the model plot *inside the valid energy range can be incorrect*. This can happen, for example, when simultaneously fitting *Suzaku* XIS and HXD data. The problem affects only the plot and does not affect the spectral fitting itself. Other plot commands in XSPEC such as "plot data" and "plot ufspec" do not exhibit the anomalous behavior.

Chapter 9

Effects of Different Opening Angles, Element Abundances, & Geometry

As described throughout this manual, the MYTORUS model is based on a number of fixed assumptions. Moreover, it is not possible to allow all of the physical parameters to be free in a spectral-fitting context. In future enhancements we intend to expand the capabilities of the MYTORUS spectral-fitting model. However, the Monte Carlo simulations on which the model results are based are extremely CPU-intensive in order to achieve a statistical precision that is high enough for spectral-fitting purposes, with the desired energy resolution. Expanding the parameter space of MYTORUS will therefore require significantly more labor and CPU time. From the perspective of modeling AGN X-ray spectra, it would be most useful to allow the torus opening angle (or, equivalently the covering factor), and the Fe abundance to be free parameters for spectral-fitting purposes. Quantitative results and extension of the MYTORUS model will be presented in future work, but in the meantime we provide here only some general indications of how the reprocessed spectra would change with departure from some of the default assumptions.

We again emphasize the fact that even with the current default assumptions, it is still better to use the MYTORUS model than an ad hoc combination of model components that result in a model that is not physical. For example, simple line-of-sight attenuation combined with disk reflection is not a physical model of the circumnuclear matter in AGN and such a model cannot yield physically meaningful parameters. On the other hand, the MYTORUS model provides a *physical and self-consistent baseline* as a starting point. Real AGN will not conform to all of the assumptions in the model but the results of fitting data with MYTORUS will serve as quantitative indicators of how the model should be extended in a physical and self-consistent manner. Such an approach is *not possible* with models that are completely ad hoc.

9.1 Covering factor

If the covering factor is changed (or equivalently, if the torus opening angle is changed), the change in the scattered spectrum is not trivial. Both the *shape and magnitude* of the scattered spectrum change as a function of covering factor. The same is true for fluorescent line fluxes and EWs. The continuum and line spectra must be calculated using full Monte Carlo simulations.

For both the scattered continuum and the fluorescent emission-line spectrum there are two opposing effects. One effect is the increase in the fraction of the X-rays from the central source that are intercepted by the torus as the covering factor is increased. The other effect is the increasing amount of self-shielding of the scattered continuum and the fluorescent line as the covering factor increases. The self-shielding results from photons that emerge from the surface of the torus and then re-enter it. There is thus a value of the covering factor that yields the maximum scattered continuum level, and the maximum fluorescent emission-line flux. In the MYTORUS geometry the value of the covering factor that maximizes the reprocessed flux is in the range $\sim 0.4 - 0.6$ (it depends on the inclination angle as well). Some more general aspects of the effect of the covering factor on the reprocessed spectrum can be found in Ikeda *et al.* (2009), albeit for a different toroidal geometry than that adopted for MYTORUS.

We repeat here something that we have already pointed out in Chapter 6 and Chapter 7 because it is so important. That is, the relative normalization factors for the scattered continuum and for the fluorescent line spectrum, A_S and A_L respectively (see Table 3.2), should *never* be interpreted simply as covering factors.

9.2 Element abundances

The single-scattering albedo is a function of photon energy, element abundances, the photoelectric absorption cross sections, and the Compton scattering cross section (see §2.3 and Eq. 2.5). It has a value between 0 and 1, the former corresponding to pure absorption, the latter corresponding to pure scattering. For the cosmic abundances of Anders & Grevesse (1989), and the Verner *et al.* (1996) absorption cross sections adopted for MYTORUS, the albedo has a value of 0.90 at ~ 25 keV. If the element abundances are reduced, this energy becomes lower (Compton scattering then dominates over absorption at lower energies). Since the absolute energy shifts due to Compton scattering become less and and less at lower and lower energies, the reprocessed soft X-ray spectrum then rises and becomes more and more like the intrinsic (incident) X-ray continuum as the element abundances are decreased. The high-energy spectrum still steepens due to Compton downscattering but the Compton-hump becomes less and less prominent because absorption no longer produces the flux deficit that forms the low-energy side of the Compton hump. The details of course depend on which element abundances are reduced. Fe has the greatest effect on the shape and relative magnitude of the Compton hump.

If the element abundances are increased relative to the cosmic values, the energy at which the albedo is 0.90 increases to values higher than 25 keV. The Compton hump becomes more prominent and its peak energy moves higher. Below the Compton hump the reprocessed spectrum becomes more and more diminished as the element abundances increase. Again, the detailed shape of the spectrum depends on which element abundances are increased.

9.2.1 Fe abundance and the Fe Kα line

The dependence of the Fe Kα fluorescent emission-line flux and EW on the Fe abundance is of particular interest but it is not a simple relationship. There are two opposing effects. A change in the Fe abundance changes the fraction of the continuum that is absorbed by the Fe K shell but it also changes the optical depth for the line photons to escape the medium. The effect of changing the Fe abundance also depends on the inclination angle of the reprocessor. The detailed behavior of the Fe Kα fluorescent emission-line flux and EW must be obtained by full Monte Carlo calculations. The relative normalization of the fluorescent emission-line spectrum, A_L (see Table 3.2), should not be interpreted simply as a relative Fe abundance.

9.3 Geometry

Due to the strong angular dependence of the differential Klein-Nishina Compton scattering differential cross section, and geometry-dependent optical depth effects, the shape of the reprocessed spectrum and its relative magnitude compared to the intrinsic incident continuum depends on the geometry of the reprocessor. We do not know the exact geometry of the circumnuclear matter distribution in AGN. However, the geometry and other assumptions adopted for MYTORUS serve as a baseline for a self-consistent model that we can start applying to real data and use the results to deduce how the model should be refined to reflect the true properties of the reprocessor.

Ghisellini *et al.* (1994) and Ikeda *et al.* (2009) have studied the X-ray reprocessing properties of a toroidal geometry that corresponds to a sphere with a bi-cone removed from it. Photons from the X-ray source impinge on the reprocessor with a different range of angles compared to the toroidal geometry in MYTORUS . The angle-dependencies of the optical depths for escaping the medium are also different for the two geometries. Therefore the scattered continuum and fluorescent emission-line spectrum are different for the geometries, even for the same covering factor.

A clumpy, or patchy toroidal matter distribution would again produce different scattered and emission-line spectra. The most significant difference would come from the fact that the observed spectrum would consist of a complex composition of reprocessed emission covering a larger range of incident and emergent angles than the "uniform" toroidal distribution (e.g. see Nandra & George 1994; Miller *et al.* 2009).

A fully covering spherical distribution of matter surrounding an X-ray source gives yet another set of characteristics for the reprocessed emission (e.g. see Leahy & Creighton 1993; Yaqoob 1997). Notably, the soft X-ray spectrum would be diminished much more than any of the geometries discussed above because the soft X-ray flux in those geometries preferentially comes from parts of the matter distribution that have the smallest optical depths in the line-of-sight. The symmetry of a spherical geometry does not provide any preferred directions for photon escape. For the same reason, the Fe Kα line will not be observed from the same surface as the X-ray continuum illumination so its flux and EW will more closely resemble values obtained for the edge-on torus.

The fully-covering spherical geometry actually gives a lower limit on the level of the soft X-ray continuum (below ~ 10 keV) relative to any other geometry. All other geometries give a larger and softer low-energy X-ray continuum because of the smaller optical depths near the physical boundaries of the circumnuclear matter. This sensitivity of the scattered X-ray continuum to the particular geometry of surface of the reprocessor must be borne in mind when interpreting the results of spectral fits with the MYTORUS model (this was also discussed in §6.1.1).

Chapter 9. Effects of Different Opening Angles, Element Abundances, & Geometry

References

Anders E., Grevesse, N., 1989, Geochimica et Cosmochimica Acta 53, 197

Arnaud, K. A., 1996, in Astronomical Data Analysis Software and Systems V, ed. Jacoby, G., Barnes, J. (Astronomical Society of the Pacific), Conference Series, Vol. 101, p. 17

Asplund, M., Grevesse, N., Sauval, A. J., Scott, P., 2009, ARA&A, 47, 481

Dadina M., 2008, A&A, 485, 417

Gaskell C. M., Goosmann R. W., Klimek E. S., 2008, MmSAI, 79, 1090

Ghisellini G., Haardt F., Matt G., 1994, MNRAS, 267, 743

Ikeda S., Awaki H., Terashima Y., 2009, ApJ, 692, 608

Leahy D. A., Creighton J., 1993, MNRAS, 263, 314

Matt, G. 2002, MNRAS, 337, 147

Miller, L., Turner, T. J., Reeves, J., 2009, MNRAS, 399, L69

Murphy, K. D., Yaqoob, T., MNRAS, 397, 1549

Nandra, K., George, I. M., 1994, MNRAS, 260, 504

Pozdnyakov L. A., Sobol I. M., Sunyaev R. A., 1983, ASPRv, 2, 189

Shu, X. W., Yaqoob, T., Wang, J. X., 2010, ApJS, 187, 581.

Turner, T. J., George, I. M., Nandra, K., Mushotzky, R. F., 1997, ApJ, 488, 164

Ueda, Y., Eguchi, S., Terashima, Y., Mushotzky, R. F., Tueller, J., Markwardt, C., Gehrels, N., Hashimoto, Y., Potter, S. 2007, ApJ, 664, 79

Verner D. A., Ferland G. J., Korista K. T., Yakovlev D. G., 1996, ApJ, 465, 487

Verner D. A., Yakovlev D. G., 1995, A&AS, 109, 125

Yaqoob T., 1997, ApJ, 479, 184

Yaqoob, T., 1998, ApJ, 500, 893

Yaqoob, T., George, I. M., Nandra, K., Turner, T. J., Serlemitsos, P. J., Mushotzky, R. F., 2001, ApJ, 546, 759

Yaqoob T., McKernan, B., Done, C., Serlemitsos, P. J., Weaver, K. A. 1993, ApJ, 416, L5

Yaqoob T., Murphy, K. D., Miller, L., Turner, T. J., 2010, MNRAS, 401, 411